TÉCNICO LISBOA

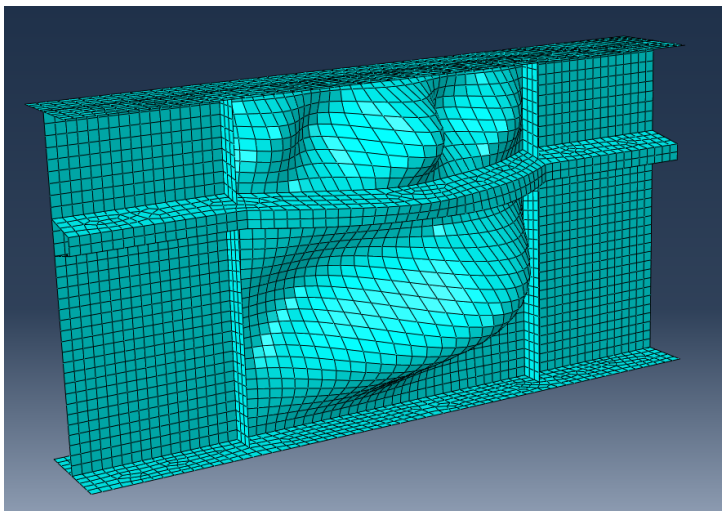

Design of High Strength Steel Longitudinal Stiffened Plate Girders Loaded with combined Bending, Shear and Compression

Filipa Alexandra Clemente Ribeiro Baguinho

Thesis to obtain the Master of Science Degree in

Civil Engineering

Supervisor
Professor Doctor José Joaquim Costa Branco de Oliveira Pedro

Júri

Chairperson: Professor Doctor Orlando José Barreiros D'Almeida Pereira

Supervisor: Professor Doctor José Joaquim Costa Branco de Oliveira Pedro

Member of Committee: Professor Doctor João Pedro Simões Cândido Martins

October 2021

Declaration:

I declare that this document is an original work of my own authorship and that it fulfils all the requirements of the Code of Conduct and Good Practices of the Universidade de Lisboa.

Acknowledgements

Ao meu orientador José Oliveira Pedro, pela constante disponibilidade e dedicação demonstrada e pela confiança que me proporcionou em todos os momentos desde as aulas, a horários de dúvidas, até à dissertação de mestrado. A ele, os meus sinceros agradecimentos, que mais do que um orientador, sempre o guardarei como um pilar da minha formação académica.

Ao Eng. André Biscaya, pela orientação e paciência ao longo deste trabalho, disponibilizando-se sempre mesmo quando o tempo era escasso (recém-nascidos dão trabalho).

Aos Eng. Sérgio Nascimento e Luís Vieira, pelas constantes sugestões e ideias nas reuniões, assim como a constante demonstração de interesse no meu trabalho.

Aos meus pais e irmãos, a minha profunda e sincera gratidão pelo apoio e o amor incondicional, sem eles nada era possível. Com um especial agradecimento à minha irmã que partilhou esta caminhada comigo e pela mútua motivação nos serões a trabalhar.

Ao meu namorado Bruno Carvalho pela paciência e apoio ao longo dos momentos mais stressantes assim como as maiores demonstrações de orgulho nos momentos mais gloriosos.

Finalmente, a todos os meus colegas e amigos que partilharam esta jornada comigo, tornaram estes últimos 5 anos os mais memoráveis.

Abstract

This study presents the numerical analysis of slender S690 high-strength steel plate girders, with welded sections and longitudinal stiffeners, loaded under combined bending, shear and compression.

The ultimate strength of steel plate girders is evaluated using the formulations according with the recent prEN 1993-1-5 regarding both methods proposed in the standard, the Effective Width Method (EWM) and the Reduced Stress Method (RSM).

Using the EWM, the global safety verification of the plate girders loaded with combined bending, shear and compression is performed adopting the interaction formulation proposed by Biscaya. These results are compared to the ultimate resistances of plate girders computed using numerical models using a geometrically and materially non-linear analysis with imperfections.

When using the RSM, the global safety of the plate girders loaded with combined bending, shear and compression is performed adopting the standard procedure and a new feature of considering the RSM formulation with some possible stress shedding from the web to the flanges (RSM+S).

A parametric study is carried out to compare the ultimate resistances of a set of plate girder geometries given by the EWM, RSM and RSM+S with the results provided by the numerical models, for a plate girder geometry with and without flanges, and considering one longitudinal closed stiffener placed at several different positions along the compressed part of the web.

Keywords: Plate girder, N-M-V interaction, prEN 1993-1-5, high strength steel S690, longitudinal stiffener

Resumo

Este trabalho apresenta a análise numérica de vigas esbeltas de secção soldada em aço de alta resistência S690, com reforços longitudinais, submetidos a esforços combinados de flexão, esforço transverso e compressão.

A resistência das vigas de aço de secção soldada é avaliada utilizando as formulações de acordo com a recente prEN 1993-1-5 no que diz respeito a ambos os métodos propostos na norma, o Método de Largura Efetiva (EWM) e o Método da Tensão Reduzida (RSM).

Utilizando o Método de Largura Efetiva, é feita a verificação global da segurança das vigas de aço de secção soldada submetidas a esforços combinados utilizando a formulação de interação proposta por Biscaya. As resistências últimas são comparadas com as obtidas por modelos numéricos de elementos finitos usando uma análise geométrica e materialmente não linear com imperfeições.

Ao utilizar o Método da Tensão Reduzida, é avaliada a segurança global das vigas de secção soldada submetidas a esforços combinados adotando o procedimento definido no código e uma nova possibilidade de considerar uma certa redistribuição de tensões normais da alma da viga para os banzos (RSM+S).

É realizado um estudo paramétrico para comparar as resistências últimas de um conjunto de geometrias de vigas de secção soldada obtidas pelos métodos EWM, RSM e RSM+S com os resultados fornecidos pelos modelos numéricos, para uma geometria da viga de uma placa de alma com e sem banzos, e considerando um reforço longitudinal de secção fechada colocado em várias alturas da parte comprimida da alma da viga.

Palavras-chave: Viga de secção soldada, Interação N-M-V, prEN 1993-1-5, aço de alta resistência S690, reforço longitudinal.

Contents

List of Figures

List of Tables

List of Abbreviations

EC3-1-5	Eurocode 3 – Part 1-5
EWM	Effective Width Method
RSM	Reduced Stress Method
RSM + S	Reduced Stress Method with Stress Shedding
EBP	EBPlate software (*Elastic Buckling of Plates*)
GMNIA	Geometrically and Materially Nonlinear Analysis with Imperfections
LPF	Load Proportion Factor
IMP	Equivalent geometric imperfection
FEM	Finite Element Method
HSS	High Strength Steel

List of Symbols

The following list is not exhaustive. Other notations may be introduced in the text.

Chapter 1

N	Axial force
M	Bending moment
V	Shear force

Chapter 2

a	Length of a stiffened or unstiffened plate
b	Width of a stiffened or unstiffened plate
h	Total height of the beam cross-section
l	Span
h_w	Height of the web
t_w	Thickness of the web
t_f	Thickness of the flanges
b_f	Width of the flanges
b_{fs}	Width of the top flange

b_{fi}	Width of the bottom flange
C_s	Width "in cantilever" of the top flange
C_i	Width "in cantilever" of the bottom flange
λ	Slenderness
A	Cross-sectional area of the structural steel section
A_w	Web area
A_f	Flange area
I_y	Second moment of area, relative to the out-of-plane bending of the plate
W_y	Elastic section modulus
ε	Material parameter dependent of f_y
f_y	Steel yield stress

Chapter 3

$\sigma_{cr,loc}$	Local sub-panel elastic critical direct stress
k_σ	Local buckling of sub-panels coefficient
v	Poisson´s coefficient
b_i	Height of sub-panel
E	Modulus of elasticity of structural steel
γ	Relative bending stiffness of longitudinal stiffener
D	Flexural stiffness of plate
δ	Relative axial stiffness of longitudinal stiffener
A_{sl}	Cross-sectional area of stiffener
I_{sl}	Second moment of area of the gross cross-section of the stiffener
$\bar{\lambda}_{loc}$	Relative slenderness associated with local buckling mode between stiffeners
ρ_{loc}	Reduction factor associated with local buckling mode between stiffeners
$\sigma_{cr,loc}$	Local sub-panel elastic critical direct stress
ψ	Correction factor
$\sigma_{cr.sl}$	Elastic critical column buckling stress
$A_{s\ell,1}$	Gross cross-sectional area of the stiffener and the adjacent parts of the plate
$I_{sl.1}$	Second moment of area of the gross cross-section of the stiffener and the adjacent parts of the plate, relative to the out-of-plane bending of the plate
b_1	Gross length of first sub-panel
b_2	Gross length of second sub-panel
b_c	Gross length of compressed panel
$\sigma_{cr,c}$	Global column-like elastic critical direct stress
$b_{sl.1}$	Distance between the longitudinal stiffener and neutral axis
$\bar{\lambda}_c$	Global column-like buckling relative slenderness
χ_c	Reduction factor associated with global column buckling mode

ϕ	Auxiliar parameter
α_c	Imperfection factor
$\bar{\alpha}$	Generalized imperfection factor
i	Radius of gyration of the longitudinal stiffener
$\sigma_{cr,p}$	Global plate-like elastic critical direct stress
b_I	Distance between the superior longitudinal edge of the place to the centre of the longitudinal stiffener
b_{II}	Distance between the inferior longitudinal edge of the place to the centre of longitudinal stiffener
a_c	Auxiliar parameter
$\bar{\lambda}_p$	Relative slenderness associated with global stiffened plate mode
ρ_c	Reduction factor associated with interpolation between plate-like and column-like global buckling modes
ξ	Auxiliar parameter
$N_{b.Rd}$	Design axial force resistance
$A_{c.eff}$	Effective cross-sectional area of the compression zone of a section
$A_{c.eff.loc}$	Effective cross-sectional area for local buckling
$b_{edge.eff}$	Length of the effective parts supported on the longitudinal edges
$A_{sl.eff}$	Effective cross-sectional area of longitudinal stiffener
b_{eff}	Effective width
N_y	Yielding axial force
$N_{cr.c}$	Critical axial force associated with the global column-like buckling mode
$N_{cr.p}$	Critical axial force associated with the global plate-like buckling mode
A_c	Gross cross-sectional area
$\beta_{A.c}$	Correction factor
$M_{eff.y}$	Bending moment of resistance of the cross section consisting of the effective area of the flanges and the fully effective web irrespective of its section class
$W_{el.eff.y}$	Effective elastic section modulus
$I_{eff.y}$	Second moment of effective cross-section, relative to the out-of-plane bending of the plate
y_{sup}	Position of the neutral axis with respect the top fibre of the cross-section
y_{inf}	Position of the neutral axis with respect the bottom fibre of the cross-section
η	Shear area factor
k_τ	Shear buckling coefficient
$V_{b.Rd}$	Design resistance for shear
$V_{bw.Rd}$	Contribution of the web for the design resistance for shear
$V_{bf.Rd}$	Contribution of the flanges for the design resistance for shear
$V_{plw.Rd}$	Plastic design shear resistance

χ_w	Shear reduction factor
$\bar{\lambda}_w$	Shear relative slenderness
f_{yw}	Steel yielding stress of the web
f_{yf}	Steel yielding stress of the flange
τ_{cr}	Critical shear stress
σ_E	Euler stress
β_{sl}	Correction factor
$I_{sl.V}$	Sum of second moment of longitudinal stiffeners
$k_{\tau sl}$	Corrective parameter for the calculation of the buckling coefficient
M_{Ed}	Design bending moment
$M_{f.Rd}$	Design value of the plastic resistance moment of a cross-section consisting of the flanges only
c	Distance between the plastic hinges and transversal stiffeners
V_{Ed}	Design shear force
η_1	Ratio between applied bending moment and resistance to bending moment
η_2	Ratio between applied force and ultimate resistance of web to concentrated load
$\bar{\eta}_3$	Ratio between shear load and resistance of web to shear
η_4	Ratio between axial load and effective resistance to axial force
$\eta_{1.f}$	Ratio between the flanges resistance to bending moment and the effective resistance to bending moment
μ	Auxiliar parameter
$\bar{\eta}_3^{máx}$	Maximum value of $\bar{\eta}_3$
$N_{f.Rd}$	Design axial force resistance of a cross-section consisting of the flanges only
β	Auxiliar parameter
σ_N	Normal stress due to compression
σ_M	Normal stress due to bending moment
τ_V	Shear stress
θ_1	Horizontal angle of the N-M plane
θ_2	Vertical angle
$\alpha_{ult,k}$	Lowest value of the load amplifier
α_{cr}	Elastic critical load amplifier
α_{rk}	Load amplifier to reach the characteristic resistance

Chapter 4

P_{Total}	Total load
LPF	Load proportionality factor
P_{Ref}	Initial reference load
f_y	Steel yielding stress

f_u	Ultimate steel stress
ε_y	Strain correspondent to the yielding stress
ε_u	Strain correspondent to the ultimate stress

Chapter 5

$N_{b,FEM}$	Resistance to axial force of a plate girder obtained by the finite element model
$M_{b,FEM}$	Resistance to bending moment of a plate girder obtained by the finite element model
$V_{b,FEM}$	Resistance to shear of a plate girder obtained by the finite element model
R_{FEM}	Distance from the origin to a point of the interaction surface N-M-V obtained by finite elements model
$R_{PROPOSTA}$	Distance from the origin to a point of the interaction surface N-M-V obtained by the proposed formulation

Chapter 6

N_{RSM}	Resistance to axial force of a plate girder obtained by the RSM
N_{EWM}	Resistance to axial force of a plate girder obtained by the EWM
M_{RSM}	Resistance to bending moment of a plate girder obtained by the RSM
M_{EWM}	Resistance to bending moment of a plate girder obtained by the EWM
V_{RSM}	Resistance to shear of a plate girder obtained by the RSM
V_{EWM}	Resistance to shear of a plate girder obtained by the EWM
τ_{cr}	Critical shear stress
$\sigma_{f,N}$, $\sigma_{f,M}$	Normal stress due to compression and bending moment on the flange
$\sigma_{w,N}$, $\sigma_{w,M}$	Normal stress due to compression and bending moment on the web
F_f	Applied force in the flange
$F_{f,sup,N}$, $F_{f,sup,M}$	Applied force due to N and M in the flange

1. Introduction

1.1. Background and Motivation

Over the last three decades, the construction of steel-concrete composite cable-stayed bridges has increased significantly given their high range of spans, from 600 m to over 1000 m [1]. Due to the high competitiveness and structural efficacy of these types of bridges, plate-girders are often adopted, commonly using I-girders and box-girders decks. In addition to being subjected to bending and shear, these beams are also subjected to high compression forces as the deck is suspended by inclined steel cables [Fig. 1]. Thus, to guarantee the structural safety of the plate girders adopted, the interaction of N-M-V forces must be verified, considering their plate buckling behaviour.

The development of high strength steels, namely the S690 steel, poses new challenges in design, as to take advantage of the material´s high strength it is necessary to adopt slender beams which may lead to the need of a greater number of stiffeners in the beam's web or the use of stronger closed stiffeners [4].

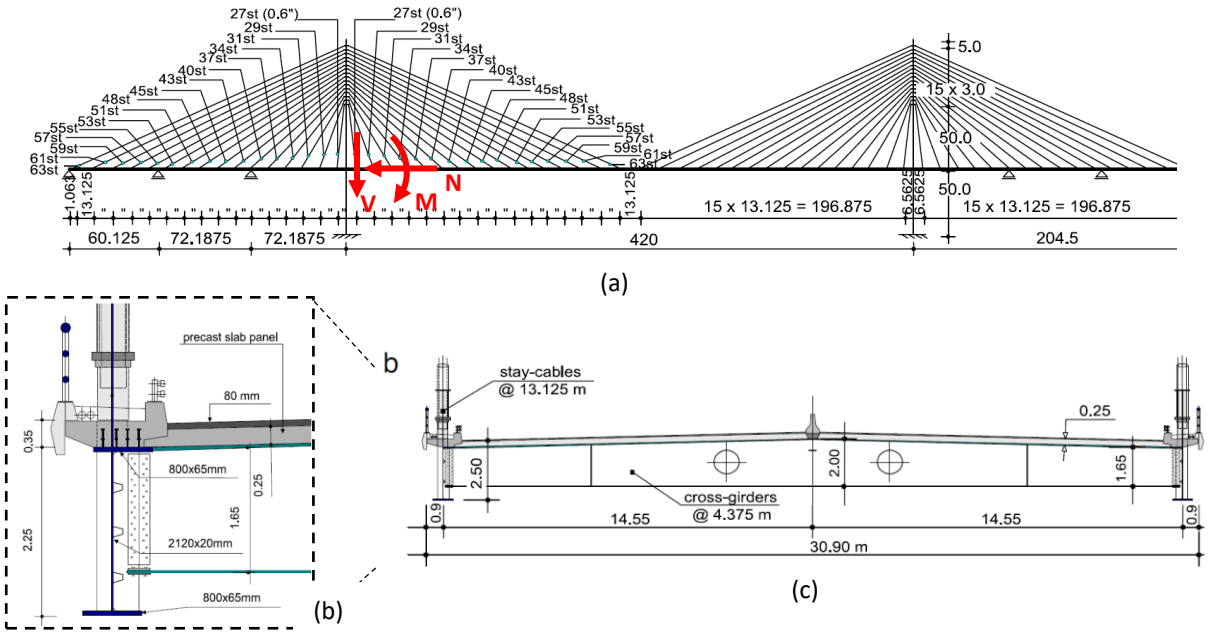

Figure 1.1: Steel-concrete composite cable-stayed bridge deck example: (a) N-M-V interaction at governing section, (b) I-girder cross-section and (c) deck cross-section [2, 3]

1.2. Objectives and Scope

The focus of this research work is the study of high strength steel plated I-girders with longitudinal stiffeners subjected to combined loads, namely compression, bending and shear. The N-M-V interaction can follow the formulations present in the current version of EN1993-1-5 [5].

However, it is known that this formulation does not give the best assessment of the real interaction of the forces. In that regard, it is worth noting the investigations conducted by Sinur and Beg [6,7], and Jáger and Kövesdi [8,9,10], who investigated numerically and experimentally the bending-shear interaction (M-V interaction) for a large range of stiffened and unstiffened I-girders, but without compression. Based on these studies some enhancements have been introduced in the prEN1993-1-5 [11], namely in the bending-shear interaction formulas.

Recently, Biscaya studied the behaviour of S355 steel plate girders submitted to the combined N-M-V forces [12,13] and proposed some improvements in the design N-M-V interaction formulation. This formulation has been tested for high strength steel S690 plate girders with only transverse stiffeners [14] and proved to give good results as well.

Therefore, the main goal of this study is to extend the application of the proposed formulation for the case of high strength steel S690 longitudinally stiffened slender plate girders. Indeed, it is intended to investigate the optimum position of the longitudinal closed stiffener when the girder is loaded under pure bending, shear, and compression, and when all three N-M-V internal forces are present.

Moreover, the results of the numerical investigation will be compared with the resistances obtained using the prEN1993-1-5[11] formulations, using the Effective Width Method and the Reduced Stress Method, which makes it possible to compare the efficiency of both methods. Finally, it is intended to extend the Reduced Stress Method formulation considering the possibility of some stress shedding from the web to the flanges, as proposed in reference [12], and evaluate the enhancements obtained with this procedure, still not possible in the frame of the prEN1993-1-5 [11] formulation.

1.3. Outline

After this chapter of general introduction to the background and identification of the objectives and scope of the present work, in Chapter 2 the pre-design rules for slender plated girders structures are introduced including for the longitudinal stiffeners.

Chapter 3 refers to the aspects of the behaviour of plate girders, regarding their different buckling modes, and presents the current methodologies for structural verification of plates and beams of welded sections proposed in prEN 1993-1-5 [11], namely according with the effective width method (EWM) and the reduced stress method (RSM).

Chapter 4 presents in detail the construction of the numerical models, referring in particular the proposed geometry of the model and different patterns of equivalent geometric imperfections to be considered in order to identify the imperfection that leads to the lowest ultimate resistance of longitudinally stiffened plates subjected to different loads.

Chapter 5 analyses and discusses the results obtained for the ultimate resistance of stiffened plates when subjected to axial forces, bending moments and shear forces, applied separately as well as combined. These results are compared with the resistances obtained by the new proposal developed for plate girder sections in [12], as well as by the formulation given in the prEN 1993-1-5 [11]. A study of the post maximum load behaviour of the plate girders for different loadings is also carried out in this chapter.

Chapter 6 presents a detailed study of the Reduced Stress Method (RSM) and its application for the safety verification of plate girders with one longitudinal stiffener placed at several positions along the web and loaded with different N-M-V loadings. A new proposal for the formulation of the RSM method that assumes the possibility of stress shedding from the webs to the flanges. These results are compared with those obtained applying the EWM and RSM with the formulations proposed in prEN 1993-1-5 [11].

Finally, in Chapter 7 the general conclusions of the present study are outlined, namely referring to the possible enhancements in the N-M-V design verification of slender plate girders made of HSS S690 in relation to the current standard formulations of the EWM and RSM, with the possibility of considering some stress shedding from the webs to the flanges. Further research works, identified during the development of the present study, are also proposed.

2. Pre-design of plate girders with longitudinal stiffeners

2.1. Introduction

In the field of steel and steel-concrete composite bridge decks, the structural capacity that is required sometimes leads to uneconomical solutions. To overcome this limitation, it is possible to adopt structural plated girder structures, formed by welding steel plates as presented in Figure 2.1.

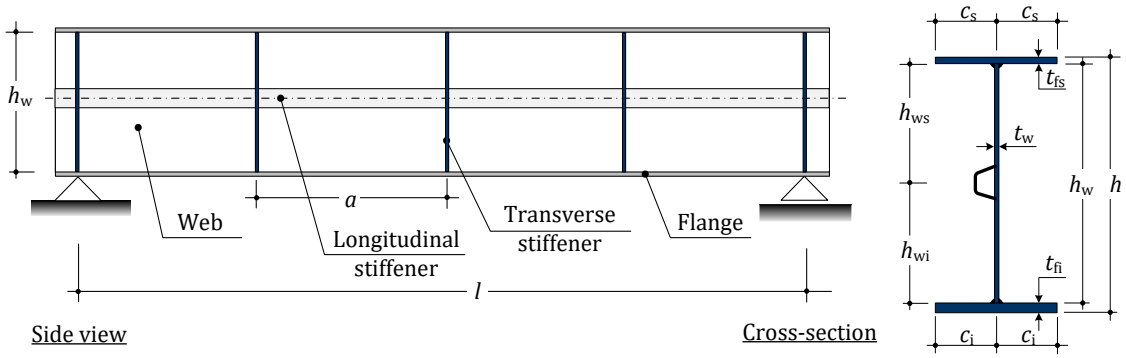

Figure 2.1: Plate girder – geometry and notation [adapted from ref. 15]

This solution allows the cross-section of a beam to be defined in a very efficient way, designing the plates in order to optimize the resistance/weight ratio; thus, welded section beams are a flexible solution in terms of structural design, because the cross-section of the beams (possibly variable) can be better adjusted to design requirements and conditioning (such as spans, applied loads, construction phasing, desired geometry for beams, etc.) as well as variations in calculation efforts over the spans.

In this chapter steel beams with section in `I` are considered. In terms of notation, the following is adopted with respect to the geometric variables:

b_{fs} , t_{fs}	width and thickness of the top flange
b_{fi} , t_{fi}	width and thickness of the bottom flange
h_w, t_w	height and thickness of the web
h_{ws}, h_{wi}	height of the top and bottom subpanels of the web, if a longitudinal stiffener is adopted
a	length of a web plate panel (corresponds to the distance between transverse stiffeners)
c	width "in cantilever" of a flange
h	total height of the beam cross-section ($h = h_w + t_{fs} + t_{fi}$)
l	span (distance between external supports)

2.2. Pre-design of a plate girder

Plated girder structures are designed using several standards that should consider specifically the features related to plate buckling. The prEN 1993-1-5 [11] is the most recent European standard for the design and safety check of steel plates and plate-girders with and without longitudinal stiffeners. Before stating this evaluation, plated girder structures should be designed following some simple guidelines, as reviewed next.

2.2.1. Plate girder slenderness

As it is adopted in most situations, the pre-design of this type of structures starts with the definition of the chosen slenderness, that is, the ratio between the beam height and the span length, $\lambda = \frac{h}{l}$. This slenderness is inherent to the type of application and adopted static system; for plate-girder beams with different applications, the indicative values in Table 2.1 can be referred to.

Table 2.1: Pre-design of plate-girders – Slenderness [15]

$\lambda = \frac{h}{l}$	**Simply supported spans**	**Continuous beams**
Industrial buildings	1/15 a 1/25	1/22 a 1/35
Road bridges	1/15 a 1/20	1/20 a 1/30
Railway bridges	1/10 a 1/15	1/12 a 1/20
cranes	1/7 a 1/12	1/10 a 1/18

2.2.2. Plate girder cross-section

Having defined the height of the beam, the next step is the pre-design of its cross section, defined by the web´s thickness t_w and the width and thickness of the upper and lower flanges, (b_{fs}, t_{fs}) and (b_{fi}, t_{fi}), respectfully. For the simple case of plate-girders with identical flanges the notation is simplified to (b_f, t_f). For this case of a bi-symmetric beam, the following relations can be written:

Web height	Web area	Flange area	Height of the section referred to the midline of the flanges
$h_w = h - 2t_f$	$A_w = h_w\, t_w$	$A_f = b_f\, t_f$	$d = h_w + t_f \approx h_w$

where the moment of inertia and section modulus with respect to the strong axis, y axis, are given by:

$$I_y = 2\left(\frac{b_f t_f^3}{12} + b_f t_f \left(\frac{h_w}{2}\right)^2\right) + \frac{t_w h_w^3}{12} \cong \frac{h_w^2}{2}\left(A_f + \frac{1}{6}A_w\right) \qquad W_y = \frac{I_y}{\frac{h_w}{2}} \cong h_w\left(A_f + \frac{1}{6}A_w\right) \qquad (2.1)$$

If no flange local buckling occurs, they should be limited to width/thickness ratios of Class 3 sections; knowing that these elements are subjected mainly to compression, it must be ensured for the flange under compression that:

$$\frac{c}{t_f} \leq 14\,\varepsilon \qquad \varepsilon = \sqrt{\frac{235}{f_y}} \text{ with } f_y \text{ in MPa} \qquad (2.2)$$

Where c is the "cantilever" part of the compressed flange, approximately equal to the half-width of the flange considered, as shown in Figure 2.1. However, if high-strength steels are adopted, the flanges can be designed to be Class 4, under compression.

According to EN 1993-1-5 [5], the web slenderness should be limited to the following limits, to avoid the design considering the local buckling induced by bending or shear:

$$\begin{aligned} &\frac{h_w}{t_w} \leq 124\,\varepsilon && \text{for part subjected to bending} \\ &\frac{h_w}{t_w} \leq 72\,\varepsilon && \text{for unstiffened webs subjected to shear and} \\ &\frac{h_w}{t_w} \leq 31\,\frac{\varepsilon}{\eta}\sqrt{k_\tau} && \text{for stiffened webs subjected to shear} \end{aligned} \qquad (2.3)$$

where k_τ represents the shear buckling coefficient and η is a coefficient that allows the reserve of plastic resistance to be considered in addition to the yield strength to shear, normally observed in slender webs. These coefficients are introduced in Chapter 3. However, many plate girders used in bridge decks have a slenderness higher than these limits, namely if high strength steel is adopted. To avoid a design using HSS plate girder with very slender web panels, one or more longitudinal stiffeners may be adopted. In that case, the slenderness limits introduced above are applied to each sub-panel.

2.2.3. Design of longitudinal and transverse stiffeners

The main purpose of using longitudinal and transverse stiffeners on steel plate girders is to increase their ultimate strength, fundamentally, by increasing the local stability of the web plates to N, M and V loadings. Transverse stiffeners are always adopted in plate girders used in bridge decks. They are usually composed by flat stiffeners, or T sections, spaced at distances a, usually not higher than h_w at support sections, and at the limit between 1.5 h_w to 2 h_w at span sections. For the special case of steel and steel-concrete composite cable-stayed decks, the high compression along the span regions leads to transverse stiffeners equally spaced along the spans; typically, spaces between 1/3 to 1/4 of the distance between stay-cables at the deck level are adopted.

Concerning the longitudinal stiffeners, when they are adopted, two main types can be selected:

- Open stiffener (typically single flat stiffeners)
- Closed stiffener (typically trapezoidal stiffeners)

For box-girder bridge decks, longitudinal stiffeners are placed inside the box section, usually at the bottom flange but also in the webs; as for I-girders, they are generally used in the inner side of the webs. However, in some cases, the closed stiffener can be located on the outside of the web´s girder, solving the problem of the intersection with the vertical stiffeners. The decision to stiffen the beam only on one side of the slab is purely for aesthetic purposes but, in some cases, it can be symmetrically welded to the plate, as shown in Figure 2.2. The number of stiffeners varies usually between 1, 2 or 3 open or closed sections.

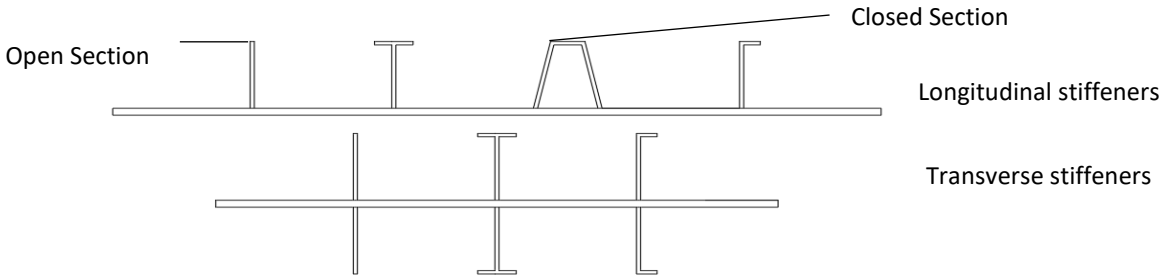

Figure 2.2: Types of longitudinal and transverse stiffeners

The position of the longitudinal stiffener depends mainly on the loads to which the beam is subjected. In the case of being subjected only to a bending moment, it makes sense to place the longitudinal stiffener in the compressed web area. However, if both M and V have significant values, it is not so clear where to place the longitudinal stiffeners. When a high value of N is also present, as it occurs in cable-stayed decks, perhaps distributing the stiffeners equidistant from the plate height will lead to better results. Given that it is not clear what is the best option, Chapter 5 will include a discussion of what is the most adequate position when one longitudinal closed stiffener is adopted.

The direction of the longitudinal stiffeners is usually horizontal. Recent studies have proposed placing the stiffeners along the tension or compression diagonal of each panel [16,17]. The structural advantages of such alternatives for slender longitudinal stiffened plate girders subjected to combined N-M-V loadings is still not clear.

In terms of the stiffener's slenderness, it is generally chosen to be Class 2 or 3, in order to avoid the local buckling of the stiffener that can aggravate the problem of stability of the panel. Considering the slenderness limits given by EN 1993-1-1 [18] for Class 3 sections, the following pre-design rules can be adopted:

- Open stiffener $\frac{b_s}{t_s} \leq 14\,\varepsilon$
- Closed stiffener $\frac{b_s}{t_s} \leq 42\,\varepsilon$ (2.4)

in which b_s and t_s are the width and the thickness of each panel that forms the longitudinal stiffener cross-section.

3. Behaviour of Plate Girders with Longitudinal Stiffeners

This chapter presents the main characteristics and structural behaviour of longitudinally stiffened steel plate girders. This refers to the types of global and local buckling of the panels or sub-panels, subjected to individual or combined loads, and the way the ultimate strength of stiffened panels is evaluated according to EN 1993-1-5 [5].

3.1. Plate Buckling Background

3.1.1. Local plate-like buckling between stiffeners

The local buckling mode of a longitudinally stiffened panels is shown in Figure 3.1, which illustrates a panel subjected to uniform compression. The buckling of the sub-panels is observed between the longitudinal stiffener and the longitudinal edges of the plate.

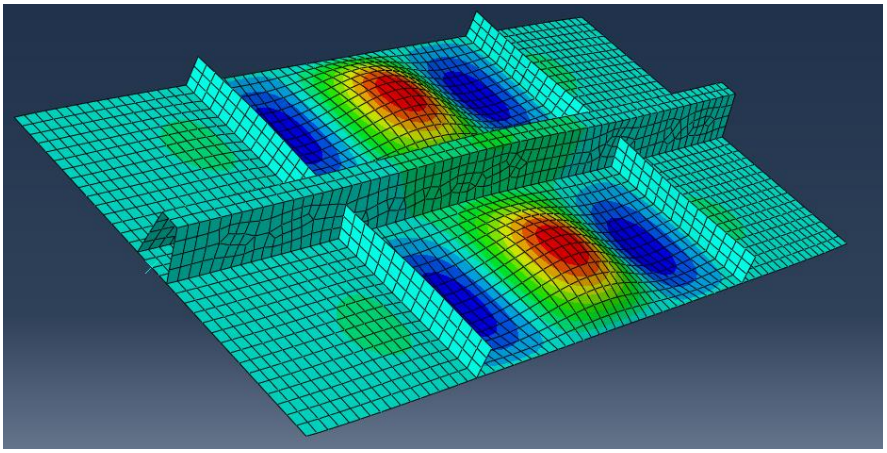

Figure 3.1: Local buckling mode between stiffeners of a stiffened plate under compression

The critical stress associated with the local buckling between stiffeners is given by:

$$\sigma_{cr.loc} = k_\sigma \times \frac{\pi^2 E}{12(1-v^2)} \times \left(\frac{t_w}{b_i}\right)^2 \tag{3.1}$$

where k_σ represents, in this case, the local buckling factor of the sub-panels, being dependent on the torsional stiffness of the longitudinal stiffeners. In order to comply with the provisions of EN 1993-1-5, if there is a uniform compression (ψ=1), the torsional stiffness effect of the longitudinal stiffeners should be neglected, considering $k_\sigma = 4$ to obtain the local critical load of the sub-plate.

However, although the contribution of the torsional rigidity of closed longitudinal stiffeners in the safety checks is usually neglected, it is clear that it exists if closed longitudinal stiffeners are adopted.

To analyse the buckling of plates with longitudinal stiffeners, two parameters are used:

$$\gamma = \frac{EI_{sl}}{h_w D}, \quad \text{with} \quad D = \frac{Et_w^3}{12(1-v^2)} \tag{3.2}$$

$$\delta = \frac{A_{sl}}{h_w t_w} \tag{3.3}$$

where γ is the relative bending stiffness of the longitudinal stiffener and δ its axial stiffness. The calculation of I_{sl} and A_{sl} should be based on the cross section of the stiffener, illustrated on Figure 3.2, being that the second moment of area of the whole stiffened plate should be calculated for bending about the z-axis and on the centre of gravity of the stiffener and the associated portion of plate.

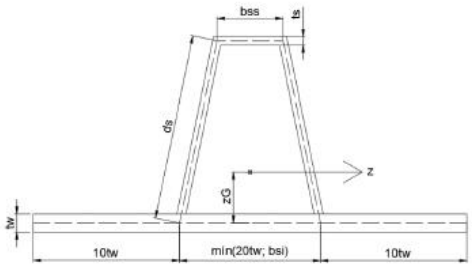

Figure 3.2: Transversal Section considered in the calculation of Isl and Asl

The next step is to determine $\bar{\lambda}_{loc}$, as well as ρ_{loc}, necessary to obtain the effective areas of the sub-panels and stiffeners. According to EN 1993-1-5, and based on the Winter's formula,

$$\bar{\lambda}_{loc} = \sqrt{\frac{f_y}{\sigma_{cr.loc}}} \tag{3.4}$$

- For internal compression elements

$$\begin{aligned} \rho_{loc} &= 1 && \bar{\lambda}_{loc} \leq 0.5 + \sqrt{0.085 - 0.055\psi} \\ \rho_{loc} &= \frac{\bar{\lambda}_{loc} - 0.055(3+\psi)}{\overline{\lambda_{loc}}^2} && \bar{\lambda}_{loc} > 0.5 + \sqrt{0.085 - 0.055\psi} \end{aligned} \tag{3.5}$$

- For outstand compression elements

$$\begin{aligned} \rho_{loc} &= 1 && \bar{\lambda}_{loc} \leq 0.748 \\ \rho_{loc} &= \frac{\overline{\lambda_{loc}} - 0.188}{\overline{\lambda_{loc}}^2} && \bar{\lambda}_{loc} > 0.748 \end{aligned} \tag{3.6}$$

3.1.2. Global column-like buckling behaviour

The global column-like buckling behaviour of a stiffened plate corresponds to the case in which the width of the plate is large, and thus the side boundary restraints along the longitudinal edges of the plate have small influence in the central area of the stiffened plate.

The elastic critical column buckling stress $\sigma_{cr.sl}$ is then determined by the following equation:

$$\sigma_{cr.sl} = \frac{\pi^2 E I_{sl,1}}{A_{sl,1} a^2} \tag{3.7}$$

where $A_{sl,1}$ and $I_{sl,1}$ correspond to, respectively, the gross cross-sectional area and the second moment of area of the stiffener and the adjacent parts of the plate. These values are determined accordingly to prEN 1993-1-5 [11] shown in Figure 3.3.

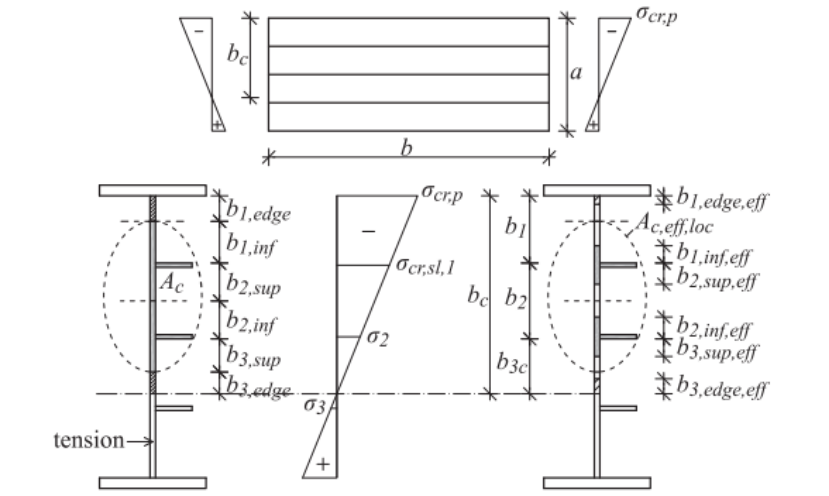

	Width for gross area	Width for effective[p] area	Condition for ψ_i
$b_{1,edge}$	$\frac{2}{5-\psi_1} b_1$	$\frac{2}{5-\psi_1} b_{1,eff}$	$\psi_1 = \frac{\sigma_{cr,sl,1}}{\sigma_{cr,p}} > 0$
$b_{1,inf}$	$\frac{3-\psi_1}{5-\psi_1} b_1$	$\frac{3-\psi_1}{5-\psi_1} b_{1,eff}$	$\psi_1 > 0$
$b_{2,sup}$	$\frac{2}{5-\psi_2} b_2$	$\frac{2}{5-\psi_2} b_{2,eff}$	$\psi_2 = \frac{\sigma_2}{\sigma_{cr,sl,1}} > 0$
$b_{2,inf}$	$\frac{3-\psi_2}{5-\psi_2} b_2$	$\frac{3-\psi_2}{5-\psi_2} b_{2,eff}$	$\psi_2 > 0$
$b_{3,sup}$	$0.4 b_{3c}$	$0.4 b_{3c,eff}$	$\psi_3 = \frac{\sigma_3}{\sigma_2} < 0$
$b_{3,edge}$	$0.6 b_{3c}$	$0.6 b_{3c,eff}$	$\psi_3 < 0$

Figure 3.3: Notations and effective widths for longitudinally stiffened plates [5].

If the compression varies linearly ($\psi \neq 1$), it is necessary to affect the equation by a scaling factor so that $\sigma_{cr.c}$ is relative to the most compressed fibre:

$$\sigma_{cr.c} = \sigma_{cr.sl} \times \frac{b_c}{b_{sl.1}} \tag{3.8}$$

This stress corresponds to a normalized column slenderness, λ_c, being the reduction factor χ_c given by:

$$\bar{\lambda}_c = \sqrt{\frac{f_y}{\sigma_{cr.c}}} \qquad \chi_c = \frac{1}{\phi + \sqrt{\phi^2 - \bar{\lambda}_c^2}} \qquad \phi = 0.5\left[\bar{\lambda}_c^2 + \alpha_c\left(\bar{\lambda}_c - 0.2\right) + 1\right] \tag{3.9}$$

where α_c is the equivalent column imperfection factor, given by

$$\alpha_c = \bar{\alpha} + \frac{0.09\ e}{i} \qquad \begin{matrix} \bar{\alpha} = 0.34 \text{ for closed section stiffeners (}b\text{ curve)} \\ \bar{\alpha} = 0.49 \text{ for open section stiffeners (}c\text{ curve)} \end{matrix} \qquad i = \sqrt{\frac{I_{sl,1}}{A_{sl,1}}} \tag{3.10}$$

and e is the largest distance from the centroids of the plating and the one-sided stiffener to the neutral axis of the effective column.

3.1.3. Global plate-like buckling behaviour

The global plate-like buckling corresponds to the joint buckling of the plate with the longitudinal stiffener as shown in Figure 3.4. The Annex A of EN 1993-1-5 gives different simplified formulas to calculate the critical stress associated with this global mode as a function of the number of longitudinal stiffeners available. As one longitudinal stiffener is adopted, only the corresponding formulas are introduced in the sequence.

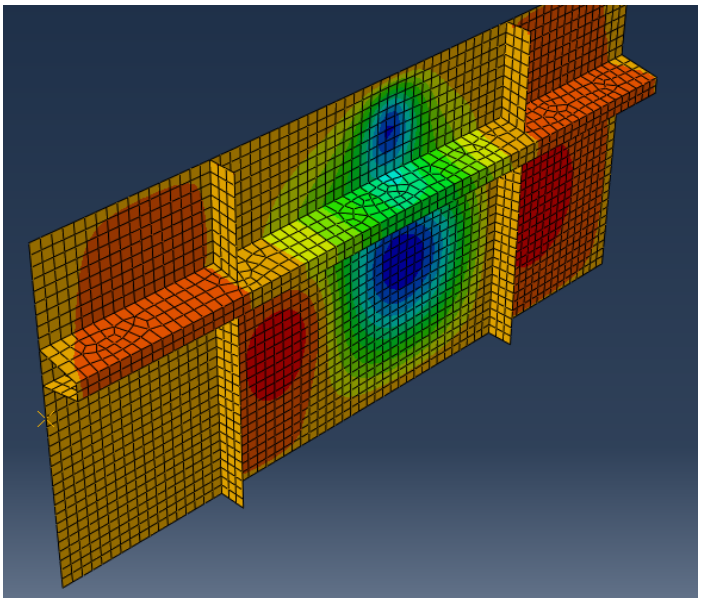

Figure 3.4: Global plate buckling of a stiffened plate

The critical stress for the global plate-like buckling of a plate with one stiffener is given by:

$$\sigma_{cr.p} = \sigma_{cr.sl} = \frac{1.05\ E}{A_{sl.1}} \times \frac{\sqrt{I_{sl.1}\ {t_w}^3 h_w}}{b_I\ b_{II}} \qquad for\ a \geq a_c$$

$$\sigma_{cr.p} = \sigma_{cr.sl} = \frac{\pi^2\ E\ I_{sl.1}}{A_{sl.1}\ a^2} + \frac{E\ t_w^3\ h_w\ a^2}{4\pi^2\ (1-\nu^2)\ A_{sl.1}\ b_I^2\ b_{II}^2} \qquad for\ a < a_c$$

$$a_c = 4.33 \times \sqrt[4]{\frac{I_{sl.1}\ b_I^2\ b_{II}^2}{t_w^3\ h_w}} \tag{3.11}$$

The critical stress of the stiffened plate is given by the lowest value between the critical stress associated with the buckling of each sub-panels and the global plate buckling.

If the compression varies linearly ($\psi \neq 1$), it is necessary to affect the equation by a scaling factor so that $\sigma_{cr.p}$ is relative to the most compressed fibre:

$$\sigma_{cr.p} = \sigma_{cr.sl} \times \frac{b_c}{b_{sl.1}} \tag{3.12}$$

It is verified that when the distance $b_{sl.1}$ from the stiffener to the neutral axis tends to zero, then $\sigma_{cr.p}$ tends to infinity, which corresponds to considering that global plate buckling does not occur because the stiffener is not fully compressed. In this case, the conditioning mode is the local buckling mode of the b_1 width sub-panel. The same happens if the width of the compressed sub-panel b_1 tends to zero. In this case, a_c would equally tend to zero and, consequently, $\sigma_{cr.sl}$ to infinity. This situation would correspond to not having a compressed web, in which case the buckling could not take place, which sometimes occurs in the cross sections of the span of the steel-concrete composite beams where the neutral line is sometimes located in the transition of the web with the upper flange.

As it was previously presented, for the normalized slenderness and for the reduction factor of the local buckling mode, the orthotropic stiffened plate has a critical tension given by $\sigma_{cr.p}$, which corresponds to a normalized slenderness defined by:

$$\bar{\lambda}_p = \sqrt{\frac{\beta_{A.c} f_y}{\sigma_{cr.p}}} \tag{3.13}$$

The adaptation of Winter's formula remains valid in this case according to Eqs. (3.5) and (3.6), replacing the parameters $\bar{\lambda}_{loc}$ and ρ_{loc} by $\bar{\lambda}_p$ and ρ, respectively.

3.1.4. Interpolation between plate-like and column-like buckling modes

There have been detailed studies based on the investigation of the interpolation between the different buckling modes of a longitudinally stiffened plates [19]. Currently, the design methodology for longitudinally stiffened plates is found in EN 1993-1-5 [5], where the existence of plate-like and column-like behaviour as well as an interactive behaviour is implicit. This distinction is based on the ratio $\frac{\sigma_{cr.p}}{\sigma_{cr.c}}$, wherein if the stress ratio is small, a column-like behaviour can be assumed therefore, no post-buckling reserve (normally exhibited when the aspect ratio is relatively small, $\frac{a}{b} < 1$). On the contrary, if the ratio is high enough, a plate-like behaviour can be assumed, consequently considering a significant post-buckling reserve.

Firstly, the reduction factors based on plate-like behaviour (ρ) and column-like behaviour (χ_c) are computed, as indicated in EN 1993-1-5 [5]. The actual behaviour is frequently somewhere in between these, as normally $\sigma_{cr.p} > \sigma_{cr.c}$, we can deduce that $\chi_c < \rho_c < \rho$ where ρ_c is the final reduction factor.

From this expression, in a very conservative way, it is possible to verify that the ultimate strength of the stiffened plate can always be determined using $\rho_c = \chi_c$. In this way the postcritical resistance of the longitudinally stiffened plate in global plate buckling is neglected, only remaining present the postcritical resistance of the sub-panels. To determine the actual reduction factor (ρ_c), the interpolation formula is given by:

$$\rho_c = (\rho - \chi_c)\, \xi\, (2 - \xi) + \chi_c \tag{3.14}$$

where ξ is a way to measure the distance between the elastic critical column and plate buckling stresses:

$$\xi = \frac{\sigma_{cr.p}}{\sigma_{cr.c}} - 1 \qquad 0 \leq \xi \leq 1 \tag{3.15}$$

The graphical interpretation of ρ_c is shown in Figure 3.5.

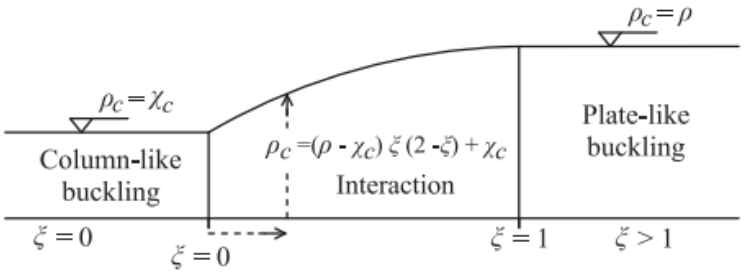

Figure 3.5: Interpolation between plate-like and column-like behaviour [20]

- If $\xi > 1$, we have $\rho_c = \rho$, which tends to happen for long and narrow plates where the ratio $\frac{\rho}{\chi_c} > 2$, meaning that the global column buckling behaviour can be neglected and the ultimate resistance of the panel is given by $\sigma_{cr.p}$.
- If $0 \leq \xi \leq 1$, usually the case of approximately square plates ($\frac{a}{b} \approx 1$), it is necessary to consider the interpolation between column and plate-like modes, obtaining the final reduction coefficient.
- Lastly if $\xi = 0$, in the case of shorter plates ($\sigma_{cr.p} \approx \sigma_{cr.c}$) corresponds to a reduction factor of $\rho_c = \chi_c$.

3.2. Resistance due to direct stresses – Different methods

In the next sections, it is intended to present in detail, the methodology for the ultimate strength of a longitudinally stiffened steel plate, submitted separately to compression, bending and shear, as per the prEN 1993-1-5 [11]. The structural design of these longitudinally stiffened slender beams is done according to this standard following two different methods:

I. Effective Width Method (EWM)
II. Reduced Stress Method (RSM)

In Portugal, the effective width method is preferred for evaluating the ultimate strength of stiffened plates however, for this work, the reduced stress method will be investigated as well.

The first method (EWM) is based on the calculation of an effective cross-section, referred in von Karman et al [21], and assumes that certain parts of the cross-section remain effective and other regions are ineffective. This method has the great advantage of considering the effect of non-linear stress redistribution that occurs after the web local buckling but imposes the need for a separate and global interaction check if different loads are applied to the plate girder.

The second method (RSM) has the advantage of determining the plate slenderness based on a linear (reduced) stress distribution, obtained by the complete stress field applied to the plate. This formulation thus avoids the need for plate interaction checks. The downside of this method is that is does not considers the stress shedding between the web and adjacent flanges, therefore neglecting the favourable contribution of the flanges to withstand part of the applied stresses once the web starts bucking.

3.3. Formulation based on the Effective Width Method (EWM)

3.3.1. Axial force (N) – Panels subjected to uniform compression

To determine the resistance of a class 4 cross section under direct stresses, all details are given in EN 1993-1-5 [5]. For the calculation of the design axial force resistance, $N_{b.Rd}$, the effective area should be considered, by using:

$$N_{b.Rd} = \frac{A_{c.eff}\, f_y}{\gamma_{M1}} \qquad A_{c.eff} = \rho_c\, A_{c.eff.loc} + \sum b_{edge.eff}\, t_w$$

$$A_{c.eff.loc} = \sum_i (A_{sl.eff} + \rho_{loc}\, b_{c.loc}\, t_w) \qquad A_{sl.eff} = \rho_{loc}\, A_{sl} \tag{3.16}$$

where $b_{edge.eff} = \frac{b_{eff}}{2}$, $A_{c.eff.loc}$ is the area composed of the effective sections of all the longitudinal stiffeners and sub-plates, except for the effective parts supported on the longitudinal edges, as shown in Figure 3.6, and $A_{sl.eff}$ is the sum of effective sections of all longitudinal stiffeners that are fully in the compression zone.

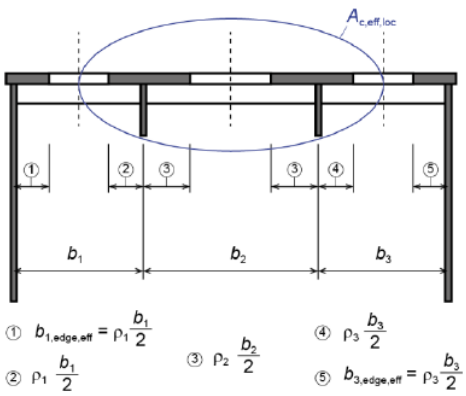

Figure 3.6: Stiffened plate submitted to uniform compression – effective widths

The normalized column slenderness and plate slenderness, respectively $\bar{\lambda}_c$ and $\bar{\lambda}_p$, are obtained from the equations (3.17) and **Erro! A origem da referência não foi encontrada.**). To consider the effective areas due to the local buckling of sub-panels, these normalized slendernesses are given by:

$$\bar{\lambda}_c = \sqrt{\frac{N_y}{N_{cr.c}}} = \sqrt{\frac{A_{c.eff.loc}\, f_y}{A_c\, \sigma_{cr.c}}} = \sqrt{\frac{\beta_{A.c}\, f_y}{\sigma_{cr.c}}} \tag{3.17}$$

$$\bar{\lambda}_p = \sqrt{\frac{N_y}{N_{cr.p}}} = \sqrt{\frac{A_{c.eff.loc}\, f_y}{A_c\, \sigma_{cr.p}}} = \sqrt{\frac{\beta_{A.c}\, f_y}{\sigma_{cr.p}}} \tag{3.18}$$

with

$$\beta_{A.c} = \frac{A_{c.eff.loc}}{A_c} \tag{3.19}$$

3.3.2. Bending moment (M) – Panels subjected to non-uniform compression

The ultimate strength of stiffened panels under variable compression, such as webs with longitudinal stiffeners in entire web beams when subjected to a bending moment, are calculated similarly to the previous section. Both the critical column stress, $\sigma_{cr.c}$ and the critical plate stress, $\sigma_{cr.p}$,are relative to the critical stress of the plate's most compressed edge.

To determining the panel's resistance to bending moment, only the area of the section located in the compressed zone is accounted for in the definition of the area A_c, from which the effective area $A_{c.eff.loc}$ is derived. In turn, obtaining the reduction coefficient ρ and the associated effective width of the compressed zone of the web, as well as distributing this effective width according to Figure 3.3, based on the standard EN 1993-1-5 [5], required for the calculation of the ultimate resistance to bending.

The corresponding resistant bending moment about the y direction of the longitudinally stiffened plate is given by:

$$M_{eff.y} = \frac{W_{el.eff.y} \times f_y}{\gamma_{M1}} \qquad \text{with} \qquad W_{el.eff.y} = \frac{I_{eff.y}}{\max\left(y_{sup}; y_{inf}\right)} \tag{3.20}$$

where $W_{el.eff.y}$ represents the effective elastic section modulus, $I_{eff.y}$ the second moment of area of the effective cross section with respect to the y direction, and finally y_{sup} and y_{inf} are the distances from the longitudinal edges to the centre of gravity of the effective transverse section.

3.3.3. Shear (V) – Panels subjected to pure shear

The ultimate resistance of longitudinally stiffened plates to shear has a calculation methodology based on the rotated stress field method, as defined in EN 1993-1-5 [5]. It should be noted that it is only necessary to assess the resistance of the web considering shear buckling if the plate slenderness is greater than:

Unstiffened Plates: $$\frac{h_w}{t_w} > 31\frac{\varepsilon}{\eta}\sqrt{k_\tau} \quad (3.21)$$

Stiffened Plates $$\frac{h_w}{t_w} > 72\frac{\varepsilon}{\eta} \quad (3.22)$$

The ultimate resistance to shear of these types of slender beams, regardless of whether they are stiffened or not, is fundamentally given by the ultimate resistance to shear, since the contribution of the flanges is relatively small, and often neglected in design practice.

If the plate has longitudinal stiffeners, there is a gain in the web´s resistance to shear due to the additional support given by these stiffeners that "delay" the buckling of the web, dividing them into two sub-panels. According to prEN 1993-1-5 [11], the ultimate design resistance of the web to shear is given by:

$$V_{b.Rd} = V_{bw.Rd} + V_{bf.Rd} \leq V_{plw.Rd} \quad \text{and} \quad V_{plw.Rd} = \eta \times \frac{h_w\, t_w\, f_y}{\sqrt{3} \times \gamma_{M1}} \quad (3.23)$$

where $V_{bw.Rd}$ represents the ultimate strength of the web plate, regardless of whether it is stiffened or not, and which includes the pre-critical and post-critical contributions associated with τ_{cr} and the diagonal tensile field, and $V_{bf.Rd}$ the contribution of the flanges, resulting from the formation of plastic hinges in the flanges.

$V_{plw.Rd}$ will always be limited to $V_{plw.Rd}$, the web plastic resistance to shear, where η indirectly takes into account the hardening of the steel in slightly slender plates, which translates into a substantial increase in the plastic resistance of the stiffened plate.

$$\eta = 1.2 \text{ for } f_y \leq 460\ MPa \qquad \eta = 1 \text{ for } f_y > 460\ MPa$$

In the present investigation, given that a high strength steel S690 is used, $\eta = 1.0$.

- **Contribution of the web**

The web's contribution considers both elastic and post-buckling resistance, and it is given by:

$$V_{bw.Rd} = \chi_w \times \frac{h_w\, t_w\, f_y}{\sqrt{3} \times \gamma_{M1}} \quad (3.24)$$

Where χ_w is the shear buckling factor, dependent on the web normalised slenderness $\overline{\lambda_w}$ and on the type of end post being used, according to Table 3.1. In the case of longitudinally stiffened web panels with closed section stiffeners, connected to the end stiffeners and the transversal stiffeners, the end support can always be considered as rigid. The difference between a rigid and a non-rigid end post is the way the diagonal stress field is anchored.

Table 3.1: Contribution from the web to the shear buckling resistance according to prEN 1993-1-5 [11]

$\overline{\lambda_w} = 0.76\sqrt{\frac{f_{yw}}{\tau_{cr}}}$	Non-rigid end post	Rigid end post
$\overline{\lambda_w} < \frac{0.83}{\eta}$	η	η
$\frac{0.83}{\eta} < \overline{\lambda_w} < 1.08$	$\frac{0.83}{\overline{\lambda_w}}$	$\frac{0.83}{\overline{\lambda_w}}$
$\overline{\lambda_w} > 1.08$	$\frac{0.83}{\overline{\lambda_w}}$	$\frac{1.37}{0.7 + \overline{\lambda_w}}$

For webs with lower slenderness, $\overline{\lambda_w} < 1.08$, the stiffness of the end stiffeners has no bearing on the coefficient χ_w. On the other hand, for slender webs, $\overline{\lambda_w} > 1.08$, the end support influences much the determination of χ_w since it is in these cases that the post-critical resistance to shear load is more significant.

To obtain the normalized slenderness, $\overline{\lambda_w}$, firstly, the elastic critical buckling stress, τ_{cr}, should be evaluated according to EN 1993-1-5 [5], given by:

$$\tau_{cr} = k_\tau \, \sigma_E \qquad \sigma_E = \frac{\pi^2 \, E \, t_w^2}{12(1-\upsilon^2) b_i^2} \tag{3.25}$$

being k_τ the buckling shear coefficient, dependent on the web panel´s aspect ratio and evaluated assuming simply supported edges, as given by prEN 1993-1-5 [11]:

i. For plates with one or two longitudinal stiffeners and $\frac{a}{h_w} < 3$

$$k_\tau = 4{,}1 + \frac{6{,}3 + 0.18 \times \frac{\beta_{sl} \, I_{sl.V}}{t_w^3 \, h_w}}{\alpha^2} + 2{,}2\sqrt[3]{\frac{\beta_{sl} \, I_{sl.V}}{t_w^3 \, h_w}} \tag{3.26}$$

ii. For plates without longitudinal stiffeners or with more than two longitudinal stiffeners

$$k_\tau = 5{,}34 + 4 \cdot \left(\frac{h_w}{a}\right)^2 + k_{\tau sl} \qquad \alpha \geq 1$$

$$k_\tau = 4 + 5{,}34 \cdot \left(\frac{h_w}{a}\right)^2 + k_{\tau sl} \qquad \alpha < 1$$

$$k_{\tau,sl} = max\left\{9\left(\frac{h_w}{a}\right)^2 \left(\frac{\beta_{sl} I_{sl}}{h_w t^3}\right)^{0.75} ; \frac{2.1}{t}\left(\frac{\beta_{sl} I_{sl}}{h_w}\right)^{\frac{1}{3}}\right\} \tag{3.27}$$

If using sub-panels, the shear buckling coefficient of longitudinal stiffeners is neglected, otherwise:

$\beta_{sl} = 1$ for open-section longitudinal stiffeners

$\beta_{sl} = 3$ for closed-section longitudinal stiffeners

and being I_{sl} the sum of the moment of inertia of the individual stiffeners with respect to the z-z axis according to Figure 3.7.

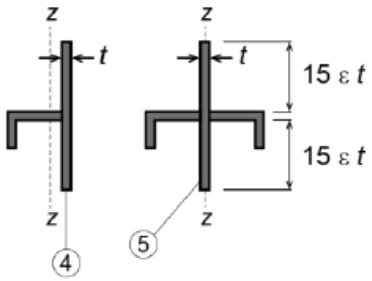

Figure 3.7: Calculation of I_{sl}

- **Contribution of the flanges**

As previously mentioned, the contribution of the flanges to the ultimate resistance is relatively small compared to the web and is often neglected, especially when the beam is subjected to high bending moments. The contribution of the flanges is linked to the formation of plastic hinges, located in the flanges, where the diagonal stress field is anchored, as illustrated in Figure 3.8.

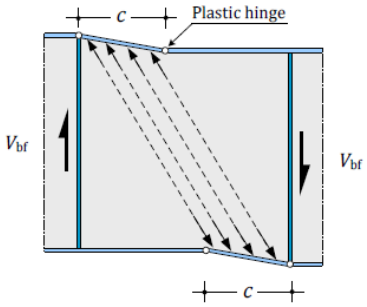

Figure 3.8: Plastic hinges in flanges

The contribution of the flanges, according to prEN 1993-1-5 [11] is given by:

$$V_{bf.Rd} = \frac{b_f\, t_f^2\, f_{yf}}{c\, \gamma_{M1}} \left[1 - \left(\frac{M_{Ed}}{M_{f.Rd}}\right)^2\right] \tag{3.28}$$

where b_f and t_f are the flange dimensions with the smallest area A_f, and b_f must not exceed $15\varepsilon t_w$ on each side of the web. The distance between the plastic hinges, *c*, is obtained by:

$$c = a\left(0.25 + \frac{1.6\, b_f\, t_f^2\, f_{yf}}{t_w\, h_w^2\, f_{yw}}\right) \tag{3.29}$$

Alternatively, although not in prEN 1993-1-5 [11], there have been several alternative proposals to evaluate this distance c [12], as a function of the web normalised slenderness, by:

André Reis $$c = a\left(0.25 + \frac{1.6 b_f t_f^2 f_{yf}}{t_w h_w^2 f_{yw}}\right)\left(2.8 - 0.6 \times \overline{\lambda_w}\right)$$

André Biscaya $$c = a\left(0.02 + \frac{20 b_f t_f^2 f_{yf}}{\overline{\lambda_w} t_w h_w^2 f_{yw}}\right)$$

(3.30)

In section 5.1, the differences obtained between these three ways of estimating the distance c are evaluated.

3.3.4. N-M-V interaction according to the prEN 1993-1-5

The interaction between loadings in stiffened plates subjected to combined N-M-V loadings and their ultimate strength following the EWM are determined according to the interaction equations given by the prEN 1993-1-5 [11]. Regarding the section where the verification of the interaction must be carried out, it is indicated that this must be done for the loads calculated at a distance corresponding to the min($0.5h_w$;$0.4a$) of the most loaded section, where a is the length of the plate panel between transverse stiffeners.

Before evaluating the safety for the interaction of N-M-V loadings, it is necessary to ensure that each strength ratio between the acting forces separately and the corresponding design resistances are $\frac{N_{Ed}}{N_{Rd}}, \frac{M_{Ed}}{M_{Rd}}, \frac{V_{Ed}}{V_{Rd}} \leq 1$.

In the presence of an compression force, and not considering the eccentricity with respect to the local buckling, e_N, the prEN 1993-1-5 [11] provides the relations between acting and resisting forces as $\eta_1 = \frac{M_{Ed}}{M_{eff.Rd}}$, $\eta_2 = \frac{F_{Ed}}{F_{Rd}}$, $\bar{\eta}_3 = \frac{V_{Ed}}{V_{bw.Rd}}$ and $\eta_4 = \frac{N_{Ed}}{N_{eff.Rd}}$, which separately must not be greater than 1.0.

According to EN 1993-1-5, the combined effects of N-M-V loadings in the web should satisfy:

$$\eta_1 + \eta_4 + \left(1 - \eta_{1.f}\right)\ (2\bar{\eta}_3 - 1)^{\mu} = 1 \qquad \eta_1 \geq \eta_{1.f} \tag{3.31}$$

$$\bar{\eta}_3 = \bar{\eta}_3^{máx} + \frac{V_{bf.Rk}}{V_{bw.Rk}} \left\{1 - \left[\frac{M_{Ed}}{M_{f.Rd}.\left(1 - \frac{N_{Ed}}{2.N_{f.Rd}}\right)}\right]^2\right\} \qquad \eta_1 < \eta_{1.f} \tag{3.32}$$

where $\bar{\eta}_3^{máx}$ corresponds to the maximum value of $\bar{\eta}_3$, obtained from Eq (3.30), and where $N_{f.Rd}$ includes only the ultimate compressive strength of a single flange, hence being multiplied by the factor 2.

The remaining parameters are given by:

- $\eta_{1.f} = \frac{M_{f.Rk}\left(1 - \frac{N_{Ed}}{2.N_{f.Rd}}\right)}{M_{eff.Rk}.(1-\eta_4)}$ if the web is not fully in compression
- $\eta_{1.f} = 0$ if the web is fully in compression
- $\mu = \left(\eta_{1.f} + 0.2\right)^{15} + 1$

(3.33)

When subjected to a large axial force and the entire web is compressed, the flange plastic bending resistance $M_{f.Rk} = 0$, resulting in the modified design equation:

$$\eta_1 + (2\bar{\eta}_3 - 1)^{\mu} = 1 \tag{3.34}$$

This different treatment between loading cases creates a drop on the interaction surface, making it discontinuous as shown in Figure 3.9.

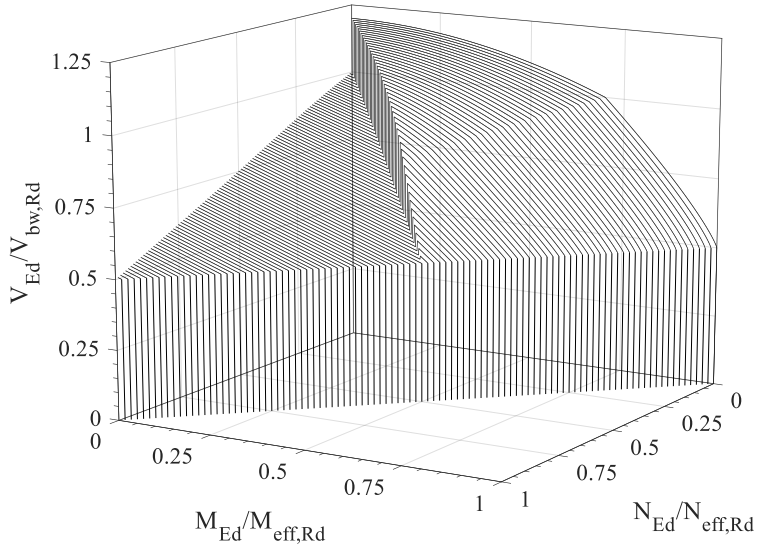

Figure 3.9: N-M-V interaction surface from the prEN1993-1-5 [11]

3.3.5. N-M-V interaction according to Biscaya's proposal

The behaviour of slender beams to the N-M-V interaction was investigated by Biscaya [12], who verified inconsistencies between the interaction surface defined in prEN 1993-1-5 [11] and the surface obtained through numerical and experimental trials. Thus, he developed and tested a new formulation using numerous case studies in S355 steel. In Chapter 5, the main objective is to compare results of the numerical model of a S690 high-strength steel beam, with longitudinal stiffeners in six different positions.

This new proposal for the design of plate girders subjected together to an axial force, a bending moment and a shear force considers the following ratios of active and resistant forces:

$$\eta_{1.M} = \frac{M_{Ed} + N_{Ed}.e_N}{M_{eff.Rd}} \qquad \bar{\eta}_3 = \frac{V_{Ed}}{V_{bw,Rd}} \qquad \eta_{1.N} = \frac{N_{Ed}}{N_{eff.Rd}} \tag{3.35}$$

that must never be higher than 1.0.

Considering an axial force in compression ($N_{Ed} > 0$) and $\bar{\eta}_3 \geq 0.5k$, the new surface that ensures the safety for the interaction N-M-V corresponds to the following expressions:

$$\eta_{1.M} + \eta_{1.N} + \left(1 - \frac{M_{\mathrm{f,N,Rk}}}{M_{\mathrm{eff,Rk}}} - \eta_{1.N}\right)\left(\frac{2\bar{\eta}_3}{k} - 1\right)^{\mu} \leq 1 \qquad \eta_{1.M} \geq \frac{M_{\mathrm{f,N,Rk}}}{M_{\mathrm{eff,Rk}}} \tag{3.36}$$

$$\bar{\eta}_3 \leq k + \frac{V_{\mathrm{bf,N,Rk}}}{V_{\mathrm{bw,Rk}}}\left[1 - \left(\frac{M_{\mathrm{Ed}}}{M_{\mathrm{f,N,Rd}}}\right)^2\right] \qquad \eta_{1.M} < \frac{M_{\mathrm{f,N,Rk}}}{M_{\mathrm{eff,Rk}}} \tag{3.37}$$

with k given by:

$$k = \begin{cases} 1 & \eta_{1.N} \leq \left(\frac{\mathrm{V_{b,Rk}}}{V_{\mathrm{bw,Rk}}} - 1\right)/i \\ \frac{V_{\mathrm{b,Rk}}}{V_{\mathrm{bw,Rk}}} - i \cdot \eta_{1.N} & \left(\frac{\mathrm{V_{b,Rk}}}{V_{\mathrm{bw,Rk}}} - 1\right)/i < \eta_{1.N} \leq \frac{N_{\mathrm{f,Rk}}}{N_{\mathrm{eff,Rk}}} \\ \sqrt{\frac{1-{\eta_{1.N}}^{\beta}}{\xi}} & \eta_{1.N} > \frac{N_{\mathrm{f,Rk}}}{N_{\mathrm{eff,Rk}}} \end{cases} \quad (3.38)$$

where:

$M_{\mathrm{f,N,Rk}}$ is the characteristic resistant bending moment of the effective flanges to take into account the axial force installed in the flanges: $M_{f,N,Rk} = M_{f,Rk}\left(1 - \frac{N_{Ed}}{N_{f,Rd}}\right)$, if $N_{Ed} \leq N_{f,Rd}$; otherwise, $M_{f,N,Rk} = 0$.

$$M_{eff,Rk} = W_{eff} \times f_y \qquad N_{f,Rk} = \left(A_{f1} + A_{f2}\right) \times f_{yf} \qquad \mu = \left(\frac{M_{\mathrm{f,N,Rk}}}{M_{\mathrm{eff,Rk}}} + 0.2\right)^{15} + 1 \quad (3.39)$$

$V_{bw,Rk}$ and $V_{bf,Rk}$ are calculated by Eq. (3.24) and Eq. (3.28) (considering $M_{Ed} = 0$, $\gamma_{M1} = 1$) and $V_{b,Rk}$ is obtained by Eq. (3.23)

$$V_{bf,N,Rk} = V_{b,Rk}(1 - i.\eta_{1.N}) - V_{bw,Rk} \geq 0 \qquad i = \frac{1}{2} - e^{-\bar{\lambda}} \geq 0 \quad (3.40)$$

$$\beta = 1 + \frac{1}{\bar{\lambda}^2} \leq 2 \qquad \xi = \frac{1 - \left(\frac{N_{f,Rk}}{N_{eff.Rk}}\right)^{\beta}}{\left(1 - i.\frac{N_{f,Rk}}{N_{eff.Rk}}\right)^2} \quad (3.41)$$

To apply this formulation, the slenderness should be $\bar{\lambda} = \bar{\lambda}_p = \sqrt{\frac{\beta_{A.c}\, f_y}{\sigma_{cr.p}}}$ in the case of non-stiffened plate-girders while, for longitudinally stiffened plates, the slenderness should be determined by $\bar{\lambda} = \max\left(\bar{\lambda}_{loc} = \sqrt{\frac{f_y}{\sigma_{cr.loc}}};\ \bar{\lambda}_p = \sqrt{\frac{\beta_{A.c}\, f_y}{\sigma_{cr.p}}}\right)$. The two normalised slendernesses are obtained considering the web in pure compression, given that they are based in the N-V interaction.

3.4. Formulation of the Reduced Stress Method (RSM)

The RSM is based on the von-Mises criterion; it allows to consider the effect of different loadings, without the need for an additional interaction verification [23,24].

To begin with, the minimum load amplifier for the design loads to reach the characteristic value of the resistance $\alpha_{ult,k}$ and the minimum load amplifier for the design loads to reach the elastic critical value of the plate α_{cr} are determined.

As shown in Figure 3.10, the web normal stresses due to the compression (σ_N) and the bending (σ_M) and the shear stress (τ_V) can be written as function of the load amplifier α $\left(\text{in } \frac{N}{mm^2}\right)$ and the interaction angles θ_1 and θ_2 by:

$$\begin{Bmatrix} \sigma_N = \alpha \times cos\theta_1 \times cos\theta_2 = \alpha c_{\theta,N} \\ \sigma_M = \alpha \times sen\theta_1 \times cos\theta_2 = \alpha c_{\theta,M} \\ \tau_V = \alpha \times sen\theta_2 = \alpha c_{\theta,V} \end{Bmatrix} \tag{3.42}$$

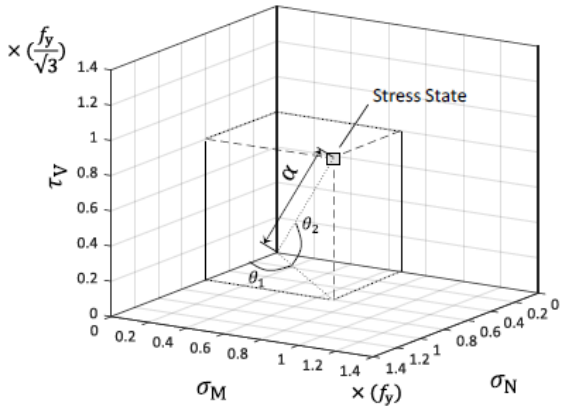

Figure 3.10: Graphical representation of stress amplifier α and interaction angles θ

Adopting the von-Mises criterion, the lowest value of the load amplifier, $\alpha_{ult,k}$, is then given by:

$$\alpha_{ult,k} = f_y \times \sqrt{\frac{1}{3\left(c_{\theta,V}\right)^2 + \left(c_{\theta,N} + c_{\theta,M}\right)^2}} \tag{3.43}$$

The values of the elastic critical load amplifier, α_{cr}, are obtained using the EBPlate software [25], introduced in detail in Chapter 6. Having this value for the different N-M-V loadings, the relative plate slenderness is given by:

$$\bar{\lambda}_p = \sqrt{\frac{\alpha_{ult,k}}{\alpha_{cr}}} \tag{3.44}$$

Finally, the load amplifier to reach the characteristic resistance, α_{rk}, is obtained by:

$$\alpha_{rk} = f_y \times \sqrt{\frac{1}{3\left(\frac{c_{\theta,V}}{\chi_w}\right)^2 + \left(\frac{c_{\theta,N} + c_{\theta,M}}{\rho}\right)^2}} \tag{3.45}$$

where the reduction factors of plate-like buckling due to normal stresses ($\rho_{x,c}$) and shear-like buckling (χ_w) are determined according to prEN 1993-1-5 [11], as summarised in Figure 3.11, with $\sigma_{x,Ed} = \sigma_N + \sigma_M$ and $\tau_{Ed} = \tau_V$, and $\sigma_{z,Ed} = 0$, as in all case studies no biaxial compression is applied.

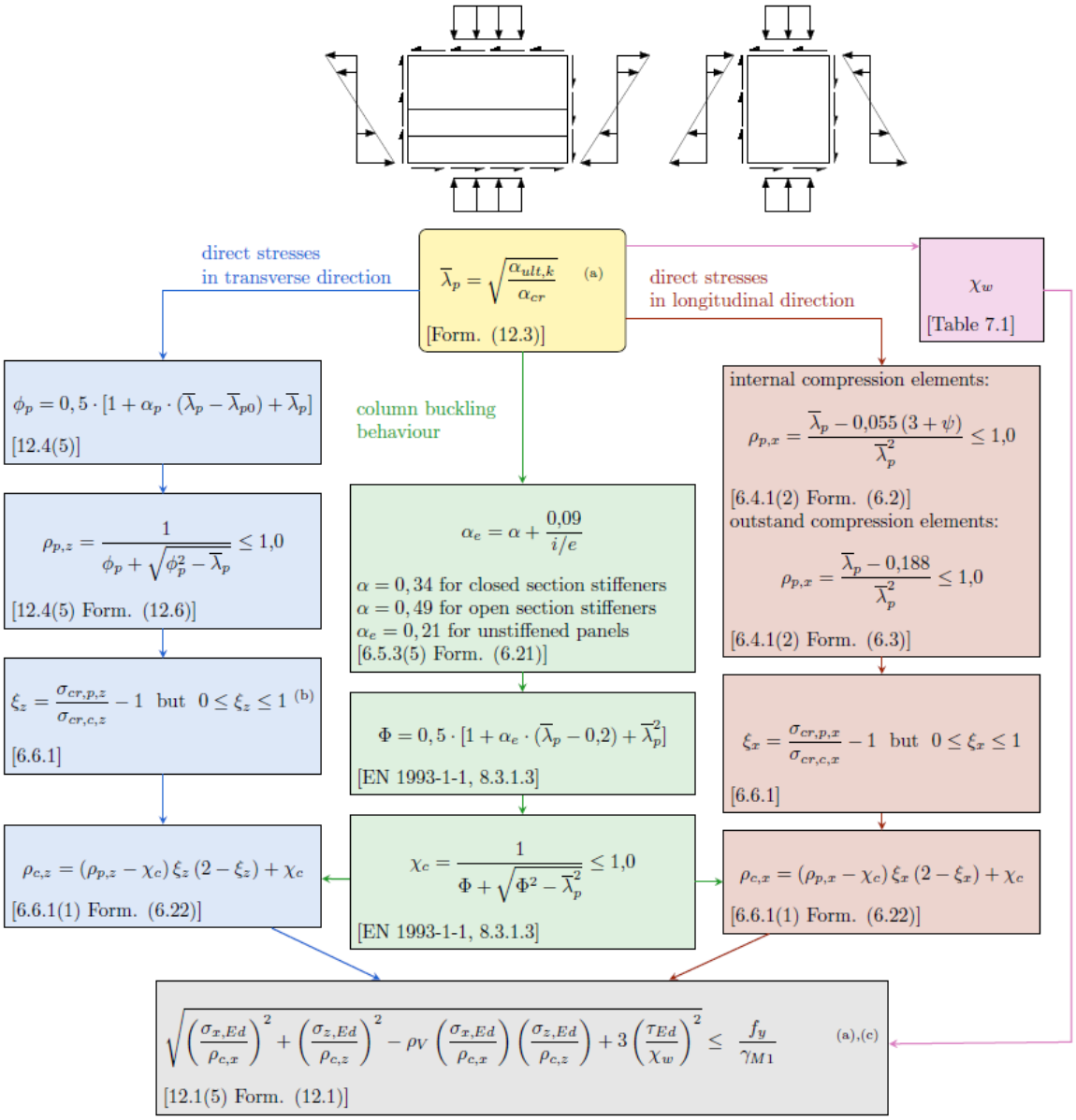

Figure 3.11: Flowchart for the application of the RSM according to the prEN 1993-1-5 [11]

For stiffened plates, global buckling of the stiffened plate and of each individual sub-panel should be verified.

4. Numerical Modelling

This chapter presents the numerical models that best represent the behaviour of the structure when subjected to certain loads, and therefore gives good estimates of the value of the ultimate strength of the plate girder with longitudinal stiffeners. Hereupon, it was necessary to perform a physical and geometrically non-linear analysis.

Several numerical models were built up using the multi-purpose code Abaqus-Python [26] interpreter and Matlab [27] subroutines. The analysis is conducted using the Modified Riks Method [28] and includes the equivalent geometric imperfections and material non-linearity (GMNIA). Modified Riks Method is chosen as it allows the convergence problems associated with solving non-linear systems of equations to be overcome, by using an iterative procedure of variation of the applied load, also known as the arc-length method, with the value of the load at each step given by:

$$P_{Total} = LPF \times P_{Ref}$$

where P_{Ref} is the input of the model (initial reference load) and LPF is the output of the model (load proportionality factor also known by load parameter amplifier). Some models can present convergence issues, known as “back tracking”, being treated in a special manner to avoid numerical “bad results”.

4.1. Plate girder geometry and material properties

Several models were studied, as shown in Figure 4.1, to identify the model that allows to reproduce the structural behaviour with enough accuracy.

A 3-panel model of Figure 4.1 c) was finally adopted. It was concluded that the best compromise between the simplified but accurate model is achieved by having two short panels to give the proper boundary conditions and some distance between the applied loads and the analysed central panel. This was also concluded in a recent investigation on the post-buckling mechanics in slender steel plates under pure shear [29]. For this numerical model, shell elements type S4R were adopted. Regarding the mesh density, recent studies were carried out in order to find a solution that allows an accurate simulation of the structural behaviour, reaching to the conclusion that for a square panel (α = 1), 30 square elements along the edges were sufficiently accurate with an acceptable running time of approximately one minute and a half [12].

Regarding the boundary conditions, studies have shown that longitudinally stiffened plates should be designed as simply supported along all 4 edges [12,29]. In the side panels, support and loading conditions were introduced, minimizing their influence in the results of the interior panel of the beam.

To investigate the structural behaviour and identify the optimal position of the longitudinal stiffener, five plate-girder designs are chosen.

The investigated plate girder geometries consider the following parameters:

- $h_w/t_w = 80;\ \alpha = h_w/a = 1; A_f/A_w = [0\ ; 1.0]$
- $h_w = 1000$ mm; $b_{si} = 100$ mm; $b_{ss} = 50$ mm;
- One close stiffener with $\gamma = 50$, and
- placed at $[0.50\ h_w; 0.60\ h_w; 0.67\ h_w; 0.75\ h_w; 0.80\ h_w]$ from the tension flange; or
- without the longitudinal stiffener (in that case the h_w level is assumed for the stiffener).

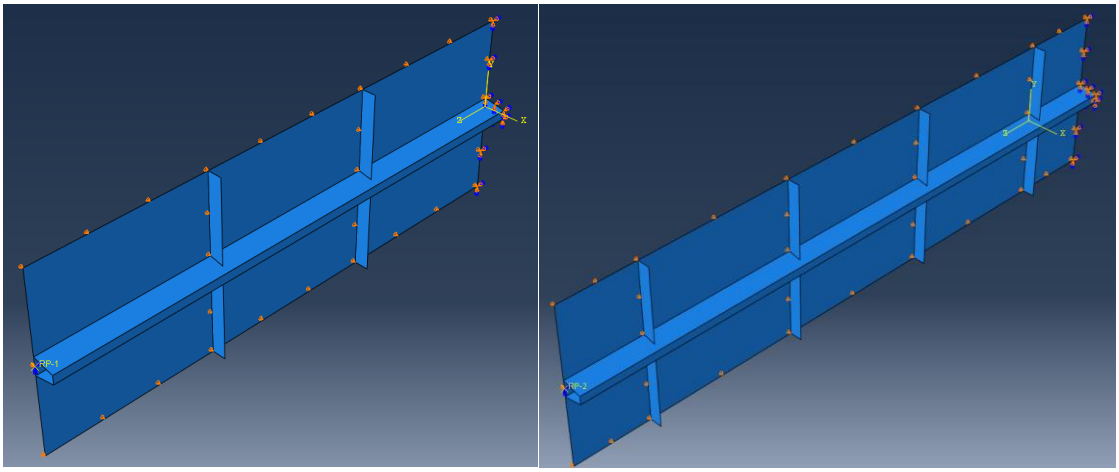

a) First FE model studied

b) Second FE model studied

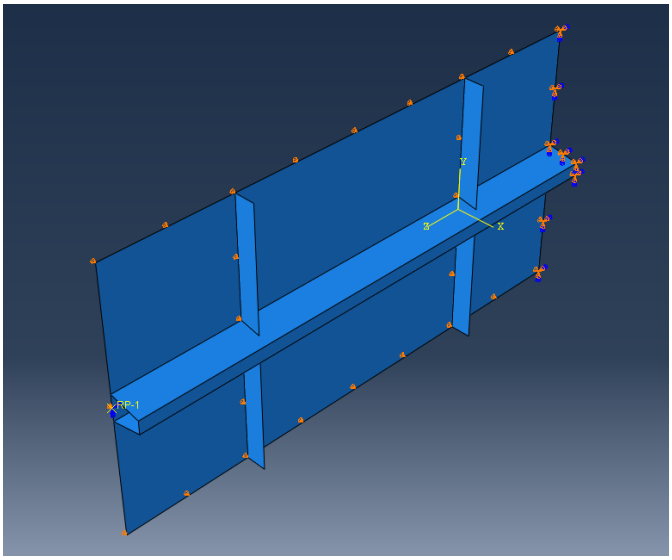

c) Retained FE model

Figure 4.1: Numerical models a), b) and c) investigated

The material model used behaves elastically until it reaches the yield stress f_y=690 MPa, with a Young's modulus equal to 210 GPa. Once the elastic properties of the material are fully utilised, a nominal hardening phase takes place until it reaches the ultimate resistance of the structure, f_u (Figure 4.2). The properties used to define the material model are listed in Table 4.1, according to the prEN 1993-1-14 [30].

Table 4.1: Parameters used in the material model

E [GPa]	E_{sh} [GPa]	f_y [MPa]	$f_{C1\varepsilon u}$ [MPa]	f_u [MPa]	C_1
210	6.185	690	740	770	0.61
ε_y [%]	ε_{sh} [%]	$C_1\varepsilon_u$ [%]	$C_2\varepsilon_u$ [%]	ε_u [%]	C_2
0.33	3	3.81	4.29	6.23	0.69

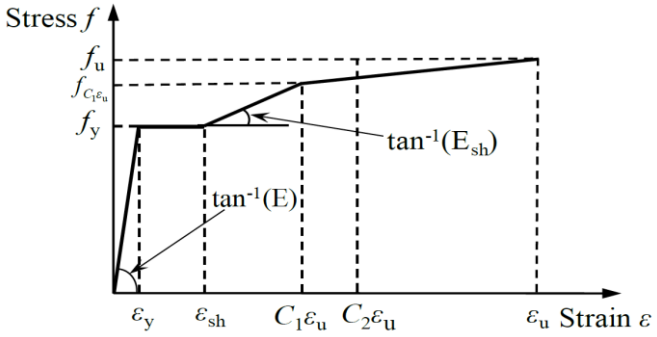

Figure 4.2: Stress-strain law of the steel used in the numerical models

4.2. Geometric imperfections

The geometric imperfections play an important role in the structural strength, especially when using slender plate elements, due to the fact that failure is commonly governed by plate buckling. In addition to these imperfections, it should also be accounted the contribution of residual stresses associated to the cutting and welding of the different plates. In that regard, it is essential to perform the modelling of the numerical models considering an equivalent geometric imperfection, as given in prEN 1993-1-5 and prEN 1993-1-14 [11,31].

4.2.1. Equivalent geometric imperfections

Two sets of equivalent geometric imperfections are analysed in order to assess which one returns the lowest ultimate strength. For this aim, six plate girder geometries are used, as shown in Figure 4.3.

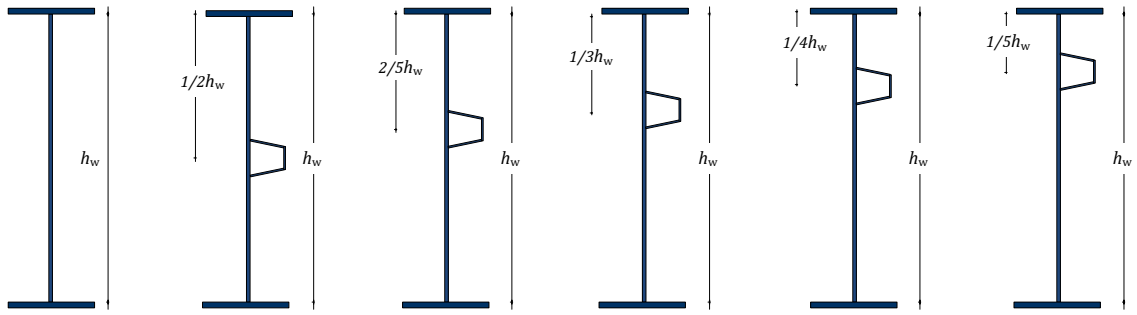

Figure 4.3: Geometry of the plate girders - positions of the longitudinal stiffener

i. Equivalent geometric imperfection 1 (IMP1)

The first imperfection type includes: i) a global imperfection of the stiffened panel with a sine wave shape and an amplitude of $\frac{hw}{400}$, coupled with ii) a local imperfection between sub-panels given by the shape of the first plate buckling mode with an amplitude of $\frac{b_i}{200}$.

Researchers generally prefer to adopt the first buckling mode shape since it has usually a relevant failure mode that is dependent on the applied loading.

ii. Equivalent geometric imperfection 2 (IMP2)

The second imperfection type is obtained by the combination of: i) a stiffened panel global imperfection with a sine wave shape and an amplitude of $\frac{hw}{400}$, coupled with ii) a local sub-panel imperfection between stiffeners, also defined by a sine wave shape with an amplitude of $\frac{b_i}{200}$, and considering the number of semi-waves equivalent to the first buckling mode, symmetrical in relation to the longitudinal stiffener (note that several studies have shown that a symmetrical local imperfection produced the lowest resistance [12,31].

For both IMP1 and IMP2, the local imperfection curves have the same sign as the global imperfection (Figure 4.4), so that it can obtain the lowest resistance, and it is only applied in the central panel to ensure buckling of this panel.

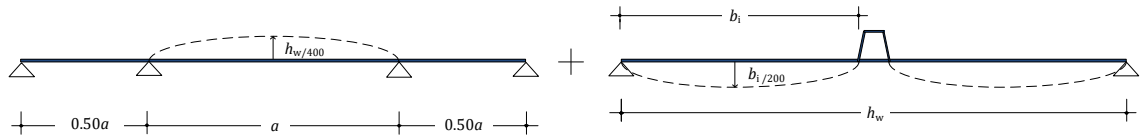

a) panel global imperfection b) local sub-panel imperfection

Figure 4.4: a) Equivalent global geometric imperfection; b) Equivalent local imperfection

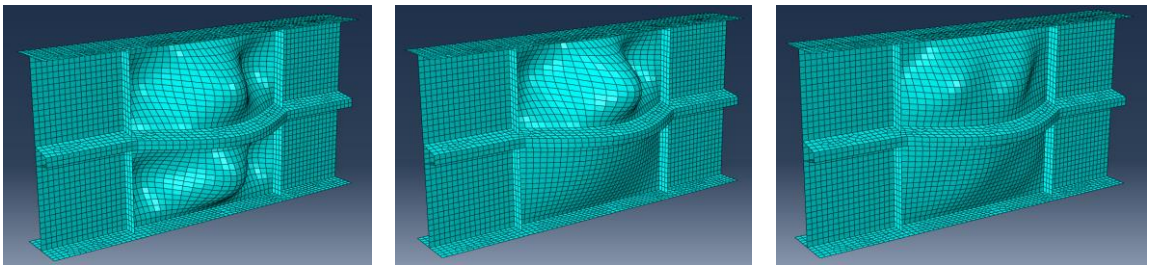

a) b) c)

Figure 4.5: Geometric imperfection based on 1st buckling modes due to a) axial force; b) bending moment; c) shear force

4.2.2. Analysis of equivalent geometric imperfections

As geometrical imperfections are more important for N and M buckling modes, the ultimate resistance of a plate girder with six different stiffener positions subjected to compression and bending moment, simultaneously, was obtained using the numerical analysis software Abaqus [26].

The results obtained for the N-M interaction for the six geometries previously described in Figure 4.3 are presented in Figure 4.6, where the values are normalised by the ultimate resistances obtained for panels with IMP1 and one stiffener located at $0.50h_w$.

From Figure 4.6 it can be concluded that the results match very well, which was expected given that both shapes are comparable. The slight differences between the results are given by the fact that in IMP1, the first buckling mode normally appears in one of the sub-panels whilst in IMP2, the local imperfection is always applied on both sub-panels as shown in Figure 4.4 b).

Moreover, IMP2 is the one that generally gives the lowest resistances for each geometry. This occurs since the number of semi-waves used is based on the shape of the buckling mode, which means that the buckling mode always need to be assessed. Table 4.2 shows a case where the buckling mode presented 3 semi-waves and for IMP2, only 2 semi-waves were applied. In this case, IMP1 gives the lowest results therefore is the preferred one to pursue the study, as it gives the most reliable results.

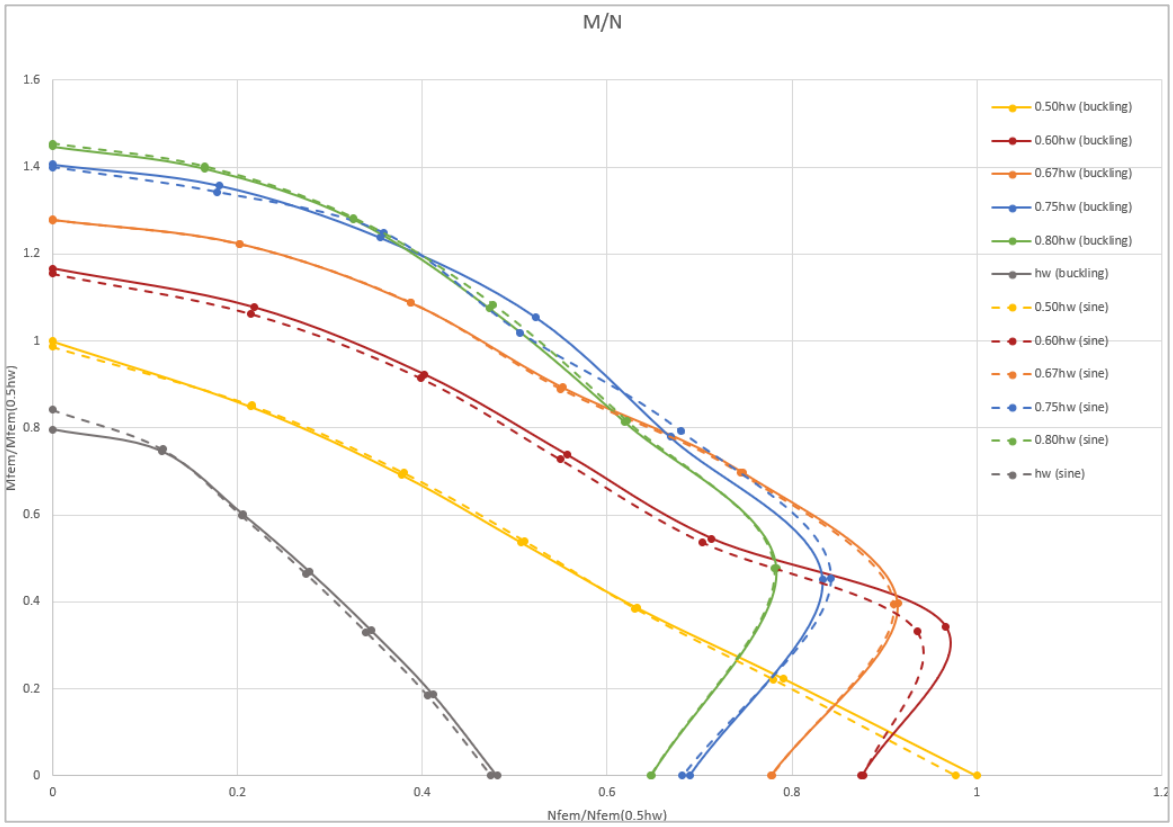

Figure 4.6: Results obtained from the interaction N-M regarding the two cases of equivalent geometric imperfections and six plate girder geometries

Table 4.2: Comparison of results (LPF) given by imperfections IMP 1 and IMP 2 for a longitudinal stiffener at $0.50h_w$

$0.50h_w$				
Θ [º]	N [kN]	M [kNm]	LPF (IMP1)	LPF(IMP2)
0	0.00	1634.85	1.02537	1.06046
15	1901.92	1579.14	0.901427	0.918837
30	3674.22	1415.82	0.820046	0.831519
45	5196.13	1156.01	0.778723	0.793151
60	6363.94	817.42	0.792867	0.828473
75	7098.05	423.13	0.88827	0.935635
90	7348.44	0.00	1.0854	1.137581

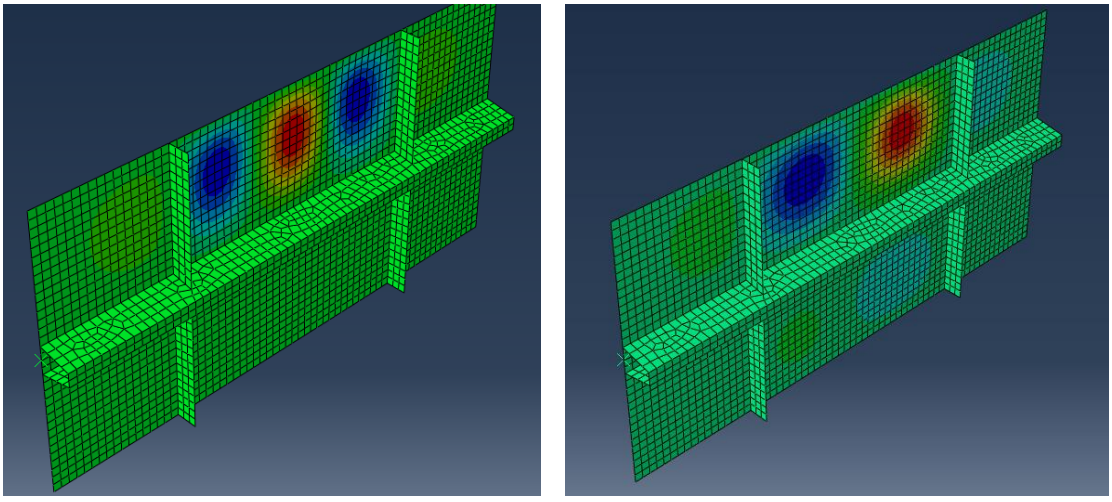

a) b)

Figure 4.7: Ultimate plate girder buckling shape for maximum LPF (Θ = 90º) using a) IMP1 and b) IMP2

On account of IMP1, the same buckling modes were also studied but with a negative amplitude (–IMP1). However, this was not the worst case compared to +IMP1.

However, modelling initial imperfections using eigenmode shapes can be quite demanding, so in this investigation, for pure loads the correspondent first buckling modes were used (as shown in Figure 4.8 a), b) and c)).

But, for the case of a load combination, N+V or N+M, a superposition of the eigen values of two different modes - Figure 4.8 a) and b) - was used as in Figure 4.8 c), with the amplitudes referred previously, to deliver the lowest plate girder resistance.

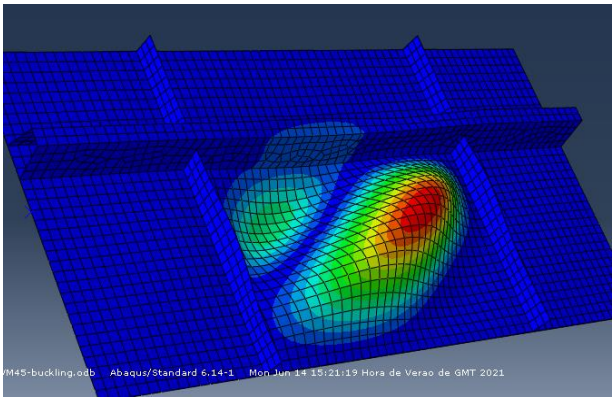

a) 1st buckling mode for pure shear (V)

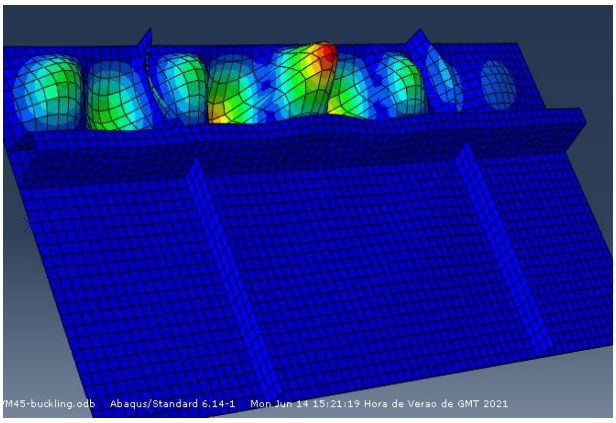

b) 1st buckling mode for pure bending (M)

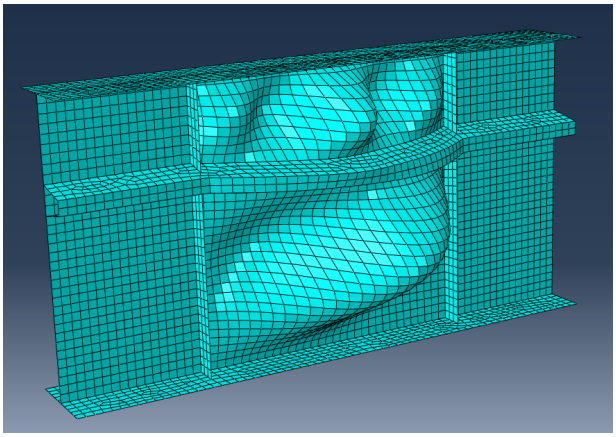

c) Superposition of the 1st buckling modes a)+b) (for M+V)

Figure 4.8: a) 1st shear-type buckling mode; b) 1st bending-type buckling mode; c) Geometric imperfection based on the couple of both 1st buckling modes

5. Parametric Study of Plate Girders with Longitudinal Stiffeners

This chapter evaluates the ultimate resistances obtained by the numerical models of longitudinally stiffened plates with the six geometries described in Figure 4.3, with $\frac{A_f}{A_w} = 0$ and $\frac{A_f}{A_w} = 1$. Firstly, the beams subjected to axial load, bending moment and shear, acting separately, will be evaluated and only then the combined loads N-M-V will be considered.

5.1. Ultimate Resistances for N, M and V loadings

The analysis is based on the numerical models developed for each geometry of longitudinally stiffened slender plates, subjected to individually N, M, V loadings. Figure 5.1 presents the numerical model's resistances and the ones obtained using the prEN 1993-1-5 [11] formulation for each loading.

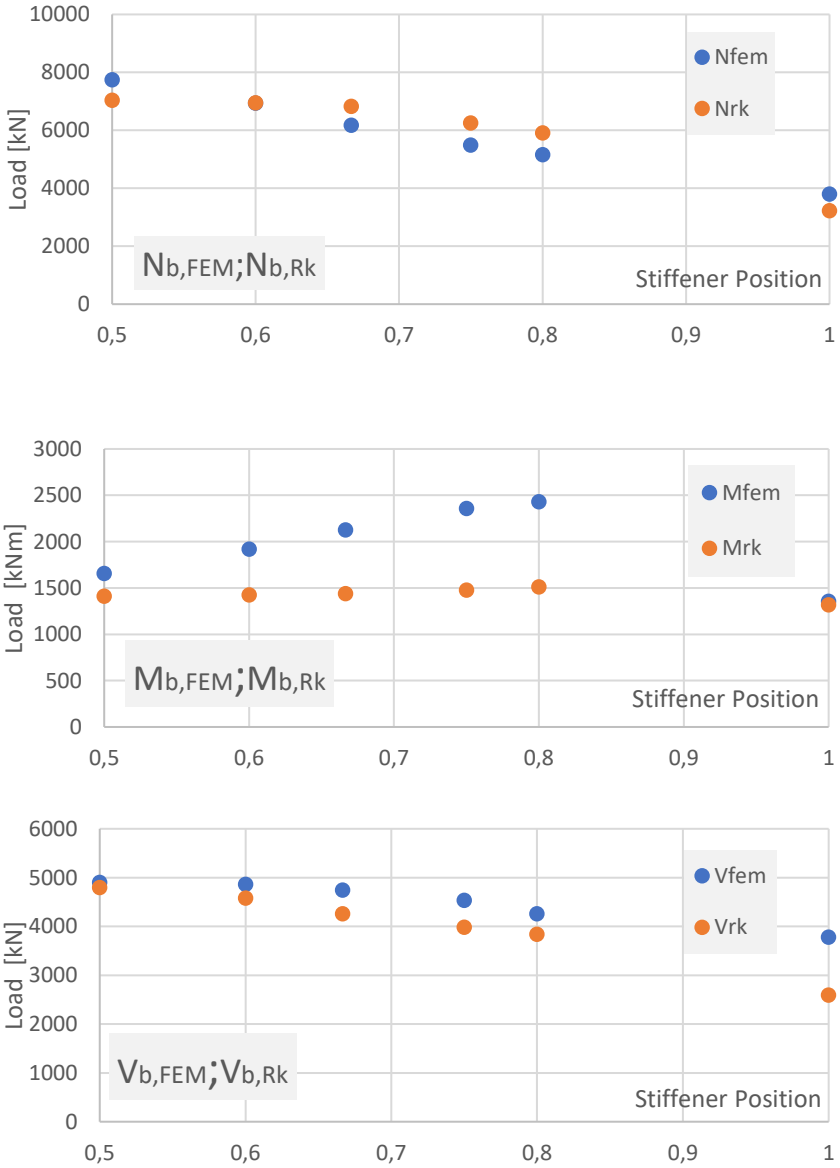

Figure 5.1: Comparison of the resistances a) $N_{b,FEM}/N_{b,Rk}$; b) $M_{b,FEM}/M_{b,Rk}$; c) $V_{b,FEM}/V_{b,Rk}$ for a longitudinally stiffened web

Table 5.1: Statistical study of the ratios $N_{b,FEM}/N_{b,Rk}$, $M_{b,FEM}/M_{b,Rk}$ and $V_{b,FEM}/V_{b,Rk}$ for the 6 geometries

	avg	***std***	$N^{o}_{cases} < 1.0$	$N^{o}_{cases} < 0.9$	***Min***	***Max***
$N_{b,FEM}/N_{b,Rk}$	0.989	0.127	4	2	0.874	1.177
$M_{b,FEM}/M_{b,Rk}$	1.373	0.234	0	0	1.030	1.608
$V_{b,FEM}/V_{b,Rk}$	1.151	0.157	0	0	1.022	1.460

Looking at the results obtained in the Table 5.1, it can be observed that Plate girders with longitudinal stiffeners in the compression part of the web have $N_{b,FEM}/N_{b,Rk} < 1.0$ meaning that, for these geometries, the numerical ultimate resistance is inferior to the one obtained according to the standard being against the structural safety of the element. However, the dispersion of the obtained values is small if compared to the M and V loadings.

For the relation $M_{b,FEM}/M_{b,Rk}$, it presents more conservative results but with greater dispersion, which is clear in the mean and standard deviation obtained, meaning that the numerical models provide resistances that are always much higher than those obtained according to the standard formulation. This is directly related to the possibility of almost total yielding of the tensioned sub-panel in the calculation of $M_{eff,y,FEM}$, which is registered in the numerical calculation, something that is not allowed when obtaining $M_{eff,y,Rk}$ using the standard formulation. This is all the more noticeable if the stiffener is moved up as it better protects the compressed panel and therefore practically does not buckle until it reaches yielding, even on the compression side. The greater the redistribution, as shown in Figure 5.2, the greater the difference between the results given by EN 1993-1-5 and ABAQUS.

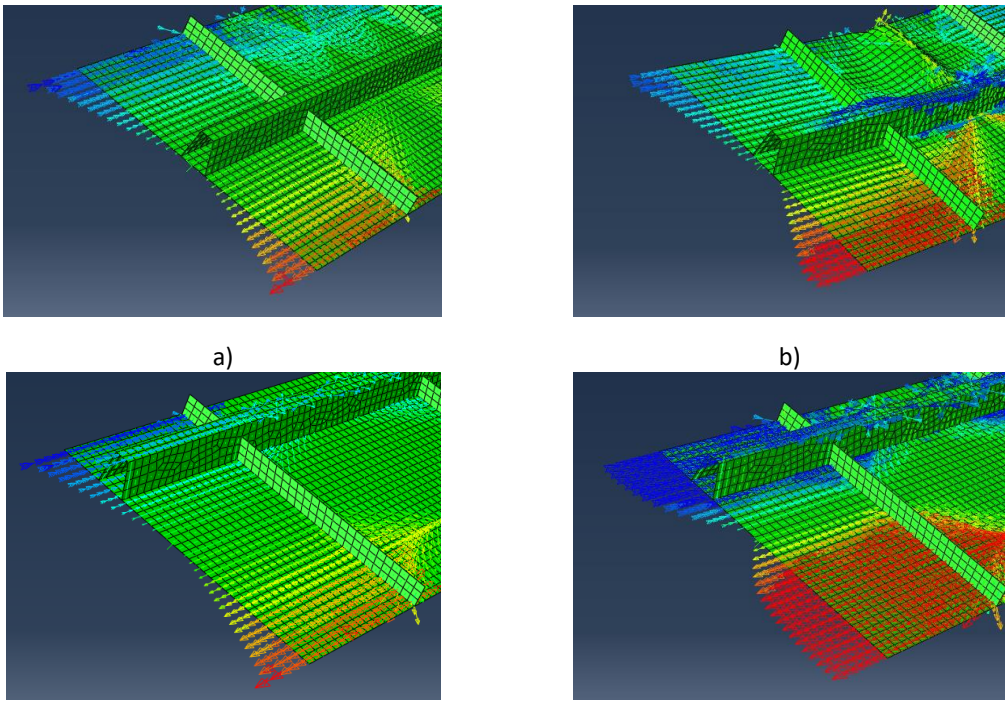

Figure 5.2: Effect of longitudinal stiffener on the evolution of compressive stresses along a stiffened metal plate subjected to pure bending a), b) 0.50h_w and c), d) 0.8h_w

For $V_{b,FEM}/V_{b,Rk}$, the safety of the structure is always guaranteed, having good values of mean and standard deviation. If the stiffener is moved up, the lower sub-panel becomes increasingly slenderer, decreasing the resistance to shear, confirmed by the values obtained both by the standard formulation, as well as the numerical model. To evaluate the influence of the flanges in the ultimate resistance, plate girders with a ratio $A_f/A_w = 1.0$ were analysed. The ultimate resistances obtained are shown in Figure 5.3.

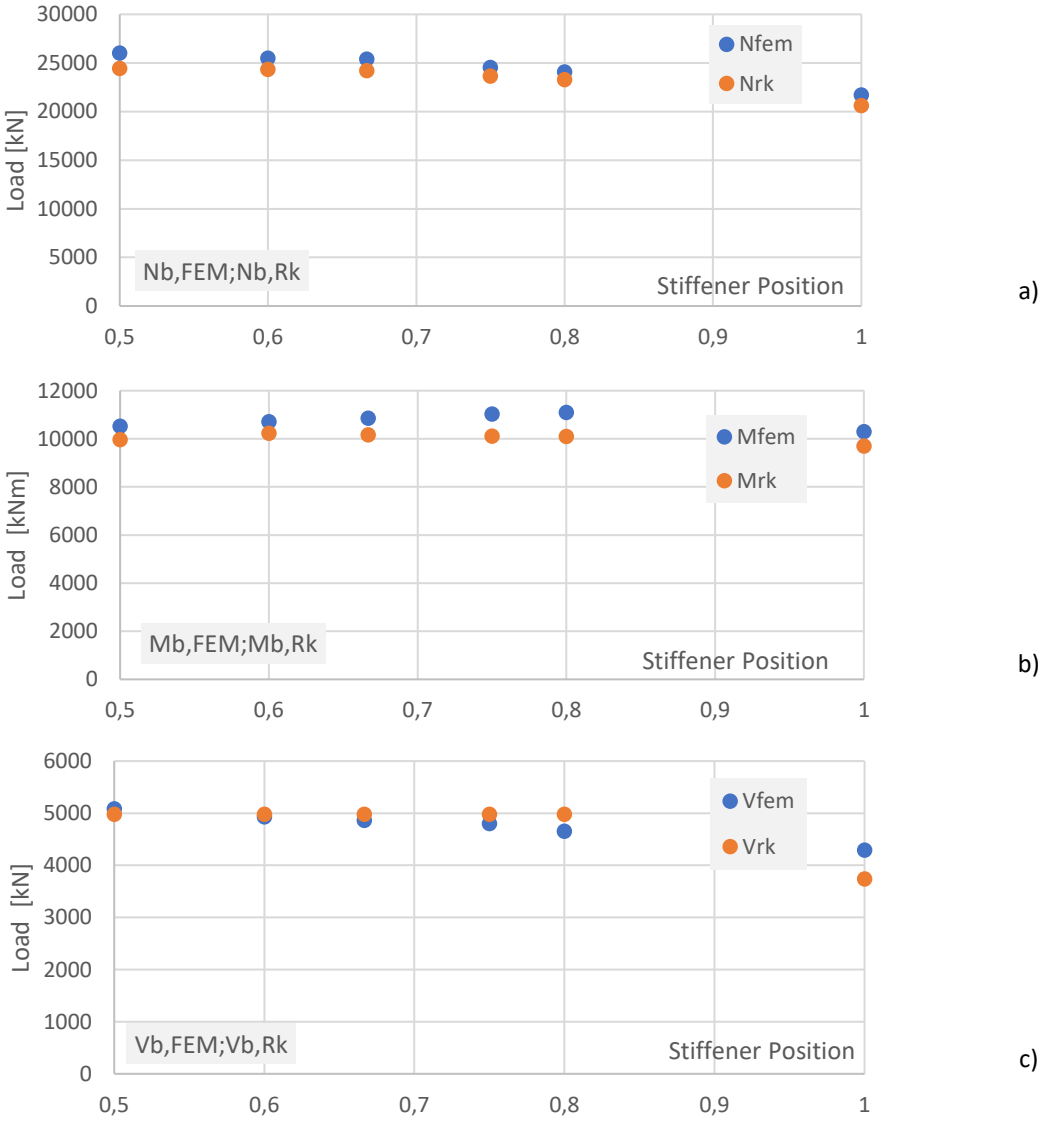

Figure 5.3: Comparison of the resistances a) $N_{b,FEM}/N_{b,Rk}$; b) $M_{b,FEM}/M_{b,Rk}$; c) $V_{b,FEM}/V_{b,Rk}$ for a plate girder with $A_f/A_w = 1.0$

Table 5.2: Statistical study of the ratios $N_{b,FEM}/N_{b,Rk}$, $M_{b,FEM}/M_{b,Rk}$ and $V_{b,FEM}/V_{b,Rk}$ for the 6 geometries and $\frac{A_f}{A_w} = 1.0$

	avg	***std***	$N^{o}_{cases} < 1.0$	$N^{o}_{cases} < 0.9$	***Min***	***Max***
$N_{b,FEM}/N_{b,Rk}$	1.048	0.011	0	0	1.033	1.065
$M_{b,FEM}/M_{b,Rk}$	1.022	0.028	1	0	0.982	1.057
$V_{b,FEM}/V_{b,Rk}$	0.958	0.055	5	1	0.862	1.020

The flanges make the plate girder behaviour much more stable and in turn there is also a huge gain in resistance for compression ($N_{f,Rk}$) and bending moment ($M_{f,Rk}$).

In the presence of strong flanges, prEN 1993-1-5 [11] greatly overestimates the flange resistance to shear ($V_{f,Rk}$), as already referred by Jáger and Kövesdi [8,10]. These values are based on the calculation of the distance between the plastic hinges, *c*. Therefore, André Reis and Biscaya [12] proposed different c values that lead to better estimates of the shear resistances in relation to the numerical model results., shown in

Table 5.3 and Table 5.4.

Table 5.3: Values of c $[mm]$ based on different proposals

λ_w	EN 1993-1-5	Reis	Biscaya
0.862	317.74	725.33	1002.27
0.904	317.74	717.32	956.64
0.971	317.74	704.55	892.01
1.0387	317.74	691.64	835.17
1.077	317.74	684.34	806.18

Table 5.4: Values of $V_{bf,Rd}$ $[kN]$ based on different proposals

λ_w	EN 1993-1-5	Reis	Biscaya
0.862	1149.21	503.42	364.32
0.904	1149.21	509.04	381.70
0.971	1149.21	518.27	409.35
1.0387	1149.21	527.94	437.21
1.077	1149.21	533.57	452.93

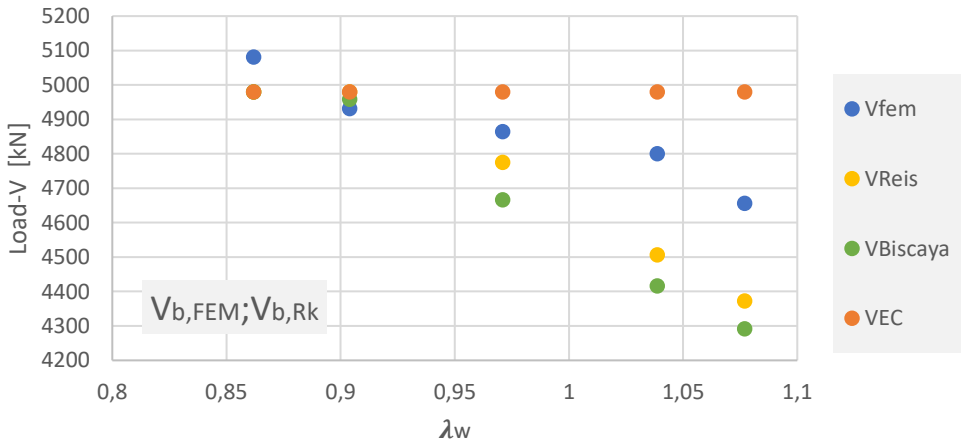

Figure 5.4: Resistance to shear as a function of the web slenderness

Analysing Figure 5.4, for the new proposals of Reis and Biscaya [12], there is a practically horizontal line in the beginning meaning that the plastic resistance governs and as we raise the stiffener, we increase the slenderness of the sub-panel and, consequently, lower the contribution of the flange to the resistance to shear, whilst the Eurocode is not influenced the slenderness of the web. The formulation based on the prEN 1993-1-5 [11] overestimates the value of V_{bf}, as said before, consequently overestimating the total shear resistance. On the other hand, the other two proposals are better adjusted.

5.2. Ultimate Resistances for Combined Loads

First, it is important to explain how the differences between the numerical strengths and those obtained in prEN 1993-1-5 [11] are evaluated, when the N-M-V forces are applied simultaneously. For this, a spherical coordinate system is used, as shown in Figure 5.6: Spherical coordinate system, and the coordinates are obtained as follows:

- $\frac{N_{FEM}}{N_{Rk}} = LPF \times \cos\theta_1 \times \cos\theta_2$
- $\frac{M_{FEM}}{M_{Rk}} = LPF \times \text{sen}\,\theta_1 \times \cos\theta_2$
- $\frac{V_{FEM}}{V_{Rk}} = LPF \times \text{sen}\,\theta_2$

(5.1)

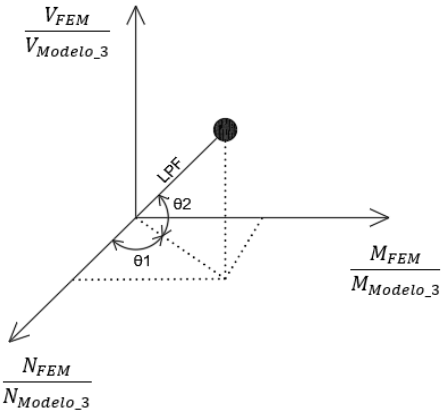

Figure 5.6: Spherical coordinate system

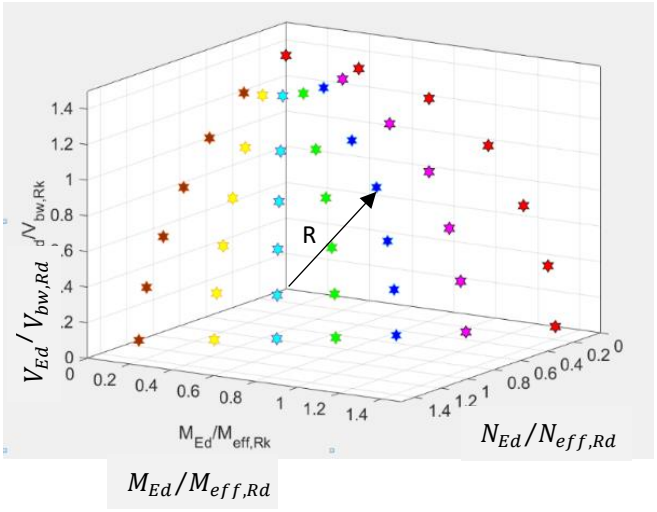

Figure 5.5: 49 points obtained by the numerical model for the N-M-V interaction for a given geometry

For this study, seven values of angles were adopted [0º, 15º, 30º, 45º, 60º, 75º, 90º], thus obtaining 7x7 points of the N-M-V interaction surface for each geometry considered. The norm R of a point on this surface with acting forces (N_{Ed}, M_{Ed}, V_{Ed}), is given by

$$R = \sqrt{\left(\frac{N_{Ed}}{N_{eff,Rd}}\right)^2 + \left(\frac{M_{Ed}}{M_{eff,Rd}}\right)^2 + \left(\frac{V_{Ed}}{V_{bw,Rd}}\right)^2} \quad (5.2)$$

where ($N_{eff.Rd}$, $M_{eff.Rd}$, $V_{bw.Rd}$) correspond to the ultimate resistances obtained by Biscaya (being that previously it was concluded that the proposed formulas were better adjusted to the study), considering a partial safety factor of $\gamma_{M1} = 1{,}0$ (Figure 5.5). For each of the 6 geometries adopted, 2 ratios of A_f/A_w are

considered ($A_f/A_w = 0$ and $A_f/A_w = 1$) and 49 relations between N-M-V loads, corresponding to a total of $6 \times 2 \times 49 = 588$ finite element models.

5.2.1. N-M and M-V interactions

Figure 5.7 to Figure 5.12 show the tendency of the N-M and M-V interactions, for the different positions of the stiffeners, with and without flanges ($A_f/A_w = 0$ and $A_f/A_w = 1$). The graphs are normalised for the case where we have the stiffener located at $0.50h_w$ for a better understanding of the gain or loss of resistance when we change its position.

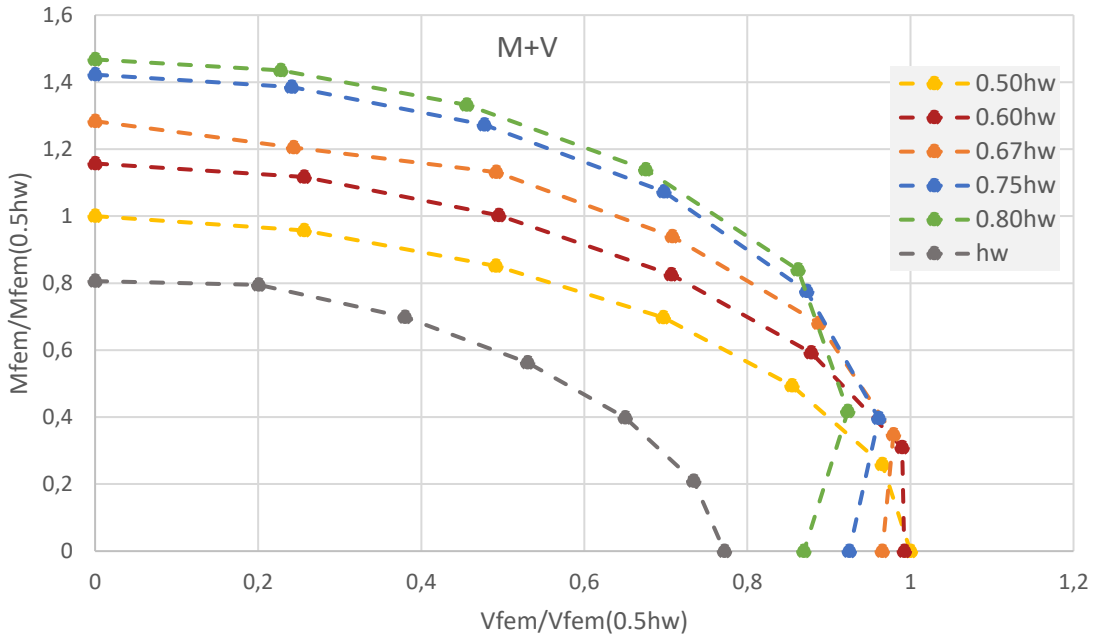

Figure 5.7: M-V interaction for $A_f/A_w = 0$

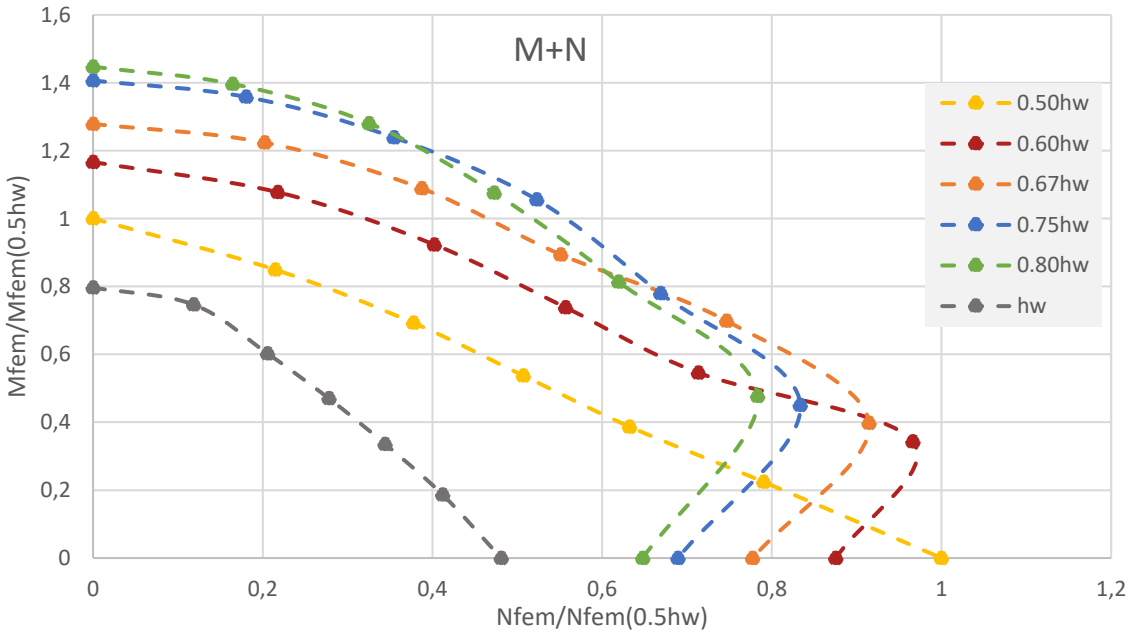

Figure 5.8: N-M interaction for $A_f/A_w = 0$

For the M-V interaction (Figure 5.7) it can be observed that there is an interest in raising the stiffener upwards, because for a higher shear load there is a gain in resistance when we pull the stiffener up to let the bottom sub-panel resist to shear and the top sub-panel to the bending moment, protecting the compressed part of the web more. This happens mainly for $\frac{V_{fem}}{V_{fem}(0.5h_w)} < 0.80$.

Regarding the N-M interaction (Figure 5.8) there is an interaction zone where a change in behaviour can be observed ($\frac{N_{fem}}{N_{fem}(0.5h_w)} < 0.70$). For a better understanding of this behaviour, the following graphics were made where it is possible to observe the buckling mode of the panels for the various load cases.

In the case where we do not have the stiffener in the middle, Figure 5.10, there is a change in the buckling mode when the axial load is increased, and the bending moment is decreased. We now have the buckling of the lower sub-panel since the bending moment gives a compression on the top sub-panel and with the stiffener higher up it protects it because there is a greater amount of working area resisting to the introduced compression. In the case of stiffener positioned in mid span, Figure 5.9, there is no effect of gain in resistance, but in the case of having only axial load, it turns out to be the best situation, thus there is buckling in the two sub-panels.

When adding the flanges, the model becomes much more predictable. The flanges resist to the compression and therefore we do not have this favourable effect as in the previous case, thus having a much better-behaved graphic. Therefore, the position of the stiffener ends up not having as much relevance in this situation.

For the M-V interaction (Figure 5.12), there is practically no interaction between the bending moment and shear, which is basically the Eurocode formulation that was retained.

In conclusion, using the stiffener in the middle turns out to be the compromise, working well for positive and negative moments and in case where we have N and V acting separately, it is always the best option. The other positions must be optimized depending on the load. In the situation without flanges, it would be interesting to raise the stiffener because there is a huge gain in terms of resistance, as said before, however this result turns out to be misleading because beams normally have flanges, and for plate-girders with strong flanges, $A_f/A_w = 1.0$, the stiffener position becomes irrelevant.

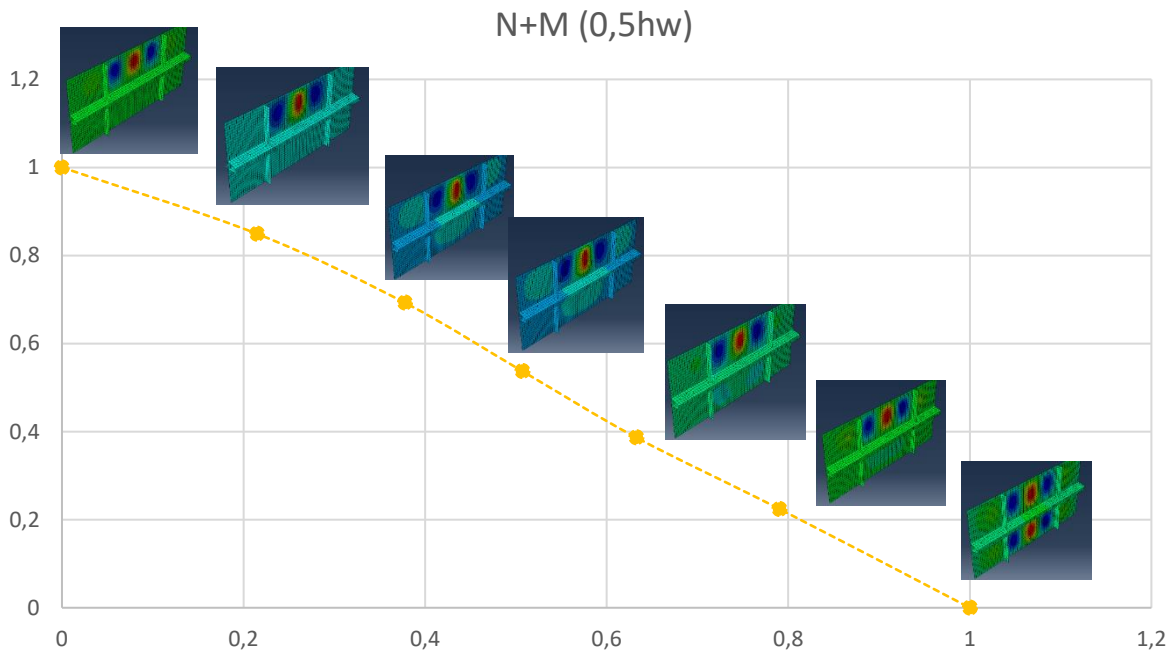

Figure 5.9: N-M interaction for $A_f / A_w = 0$, stiffener position 0.50hw

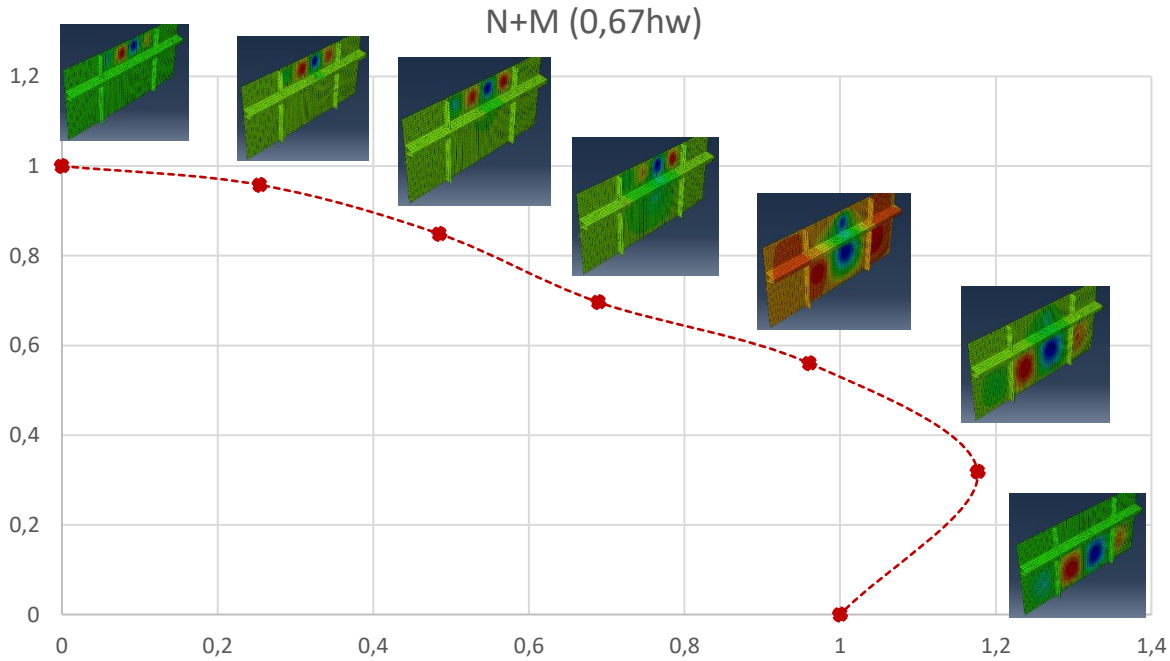

Figure 5.10: N-M interaction for $A_f / A_w = 0$, stiffener position 0.60hw

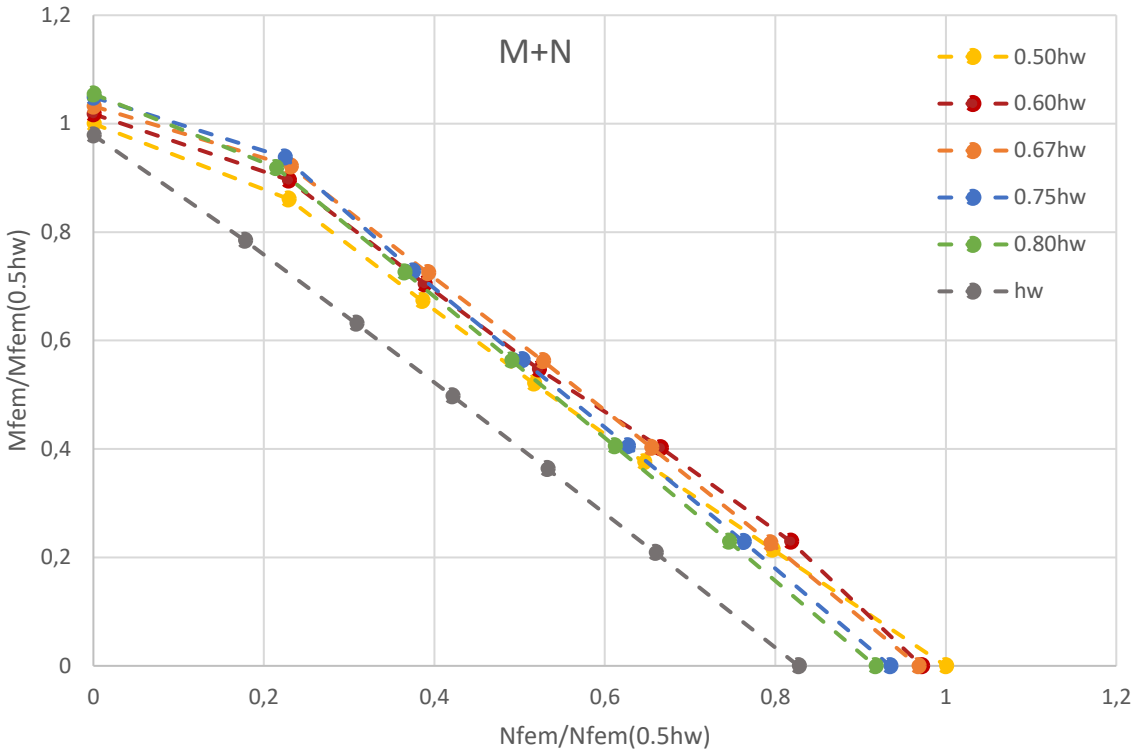

Figure 5.11: N-M interaction for $A_f/A_w = 1.0$

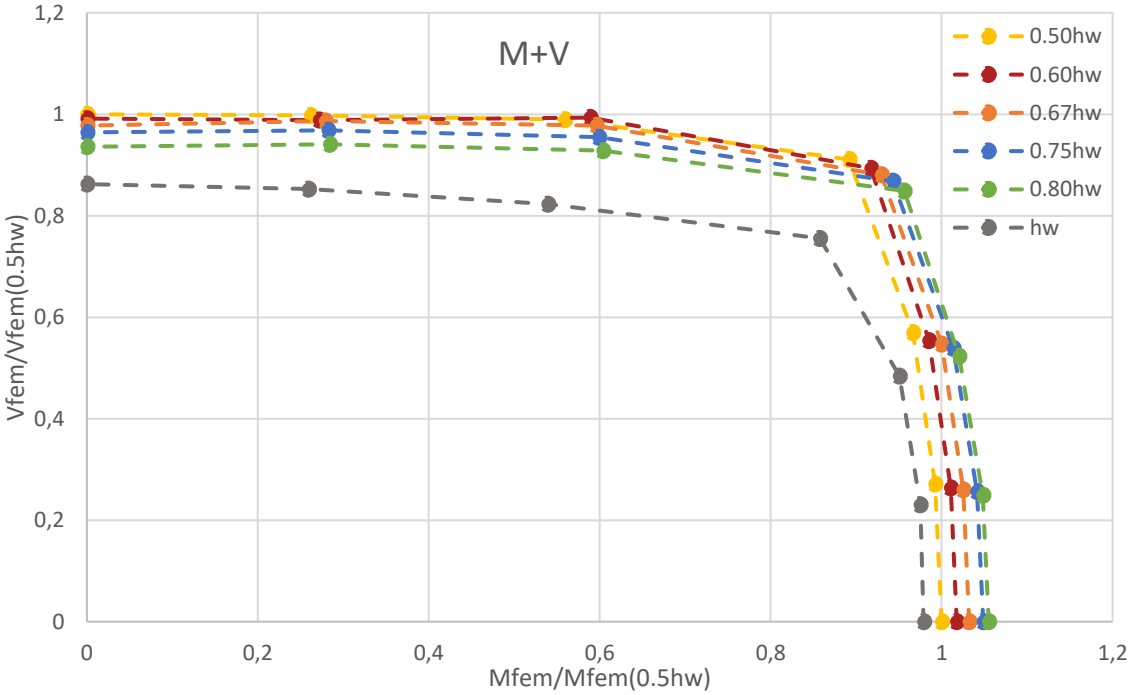

Figure 5.12: M-V interaction for $A_f/A_w = 1.0$

5.2.1. N-M-V interaction

Finally, Table 5.5 summarises the results of the 588 numerical models analysed, where the values are normalised to the effective axial load N_{eff}, in the case of axial load, to the effective bending moment (y direction) $M_{eff,y}$, for the bending moment, and to the design resistance to shear $V_{b,Rd}$, for the case of shear, and logically, these values vary with the geometry of the cross section.

Table 5.5: Statistical study of the N-M-V interaction resistances following Biscaya´s proposal

R_{FEM}/R_{PROP}	$A_f/A_w = 0$					
	avg	***std***	$N^{o}_{cases} < 1.0$	$N^{o}_{cases} < 0.9$	***Min***	***Max***
$0.50h_w$	1.093	0.065	1	0	0.954	1.261
$0.60h_w$	1.247	0.164	5	0	0.974	1.563
$0.67h_w$	1.360	0.249	5	0	0.905	1.829
$0.75h_w$	1.445	0.304	3	2	0.878	2.036
$0.80h_w$	1.452	0.312	3	1	0.874	2.050
h_w	1.280	0.154	0	0	1.000	1.547
R_{FEM}/R_{PROP}	$A_f/A_w = 1.0$					
	avg	***std***	$N^{o}_{cases} < 1.0$	$N^{o}_{cases} < 0.9$	***Min***	***Max***
$0.50h_w$	1.040	0.045	16	0	0.968	1.121
$0.60h_w$	1.055	0.059	12	0	0.980	1.158
$0.67h_w$	1.089	0.055	0	0	1.020	1.218
$0.75h_w$	1.113	0.051	0	0	1.047	1.244
$0.80h_w$	1.110	0.047	1	0	0.993	1.229
h_w	1.227	0.125	1	0	0.993	1.388

For $A_f/A_w = 0$, the geometry that obtained the best results was the one with the mid-span stiffener, which was expected since the bases of this formulation (N, M and V applied separately) tend to become more conservative as we raise the stiffener up, concluded in Section 5.1.

As the stiffeners are moved up along the web compressive part, it becomes more conservative (increase in the mean) and there is also an increase in the dispersion of results (higher standard deviation). Only three points are outside the safety zone, that is, below the 10% margin that is somehow considered in the reduction of resistance when using the partial safety factor of $\gamma_{M1} = 1{,}10$ ($^{R_{FEM}}/_{R_{PROP}} < 0.9$), thus giving a good calibration of resistances by Biscaya´s proposal.

When adding the flanges, which in this case are considered strong flanges, the average in general is much closer to the unit, obtaining less conservative results but always on the safety side (although it becomes more conservative as we rise up the stiffener) and there is also a decrease in the standard deviation as the flanges make the model much more stable.

In Figure 5.13, the final graphics associated with the results shown in Table 5.5 are presented, showing the behaviour observed for the two different ratios of A_f/A_w for the proposal of Biscaya regarding the N-M-V interaction.

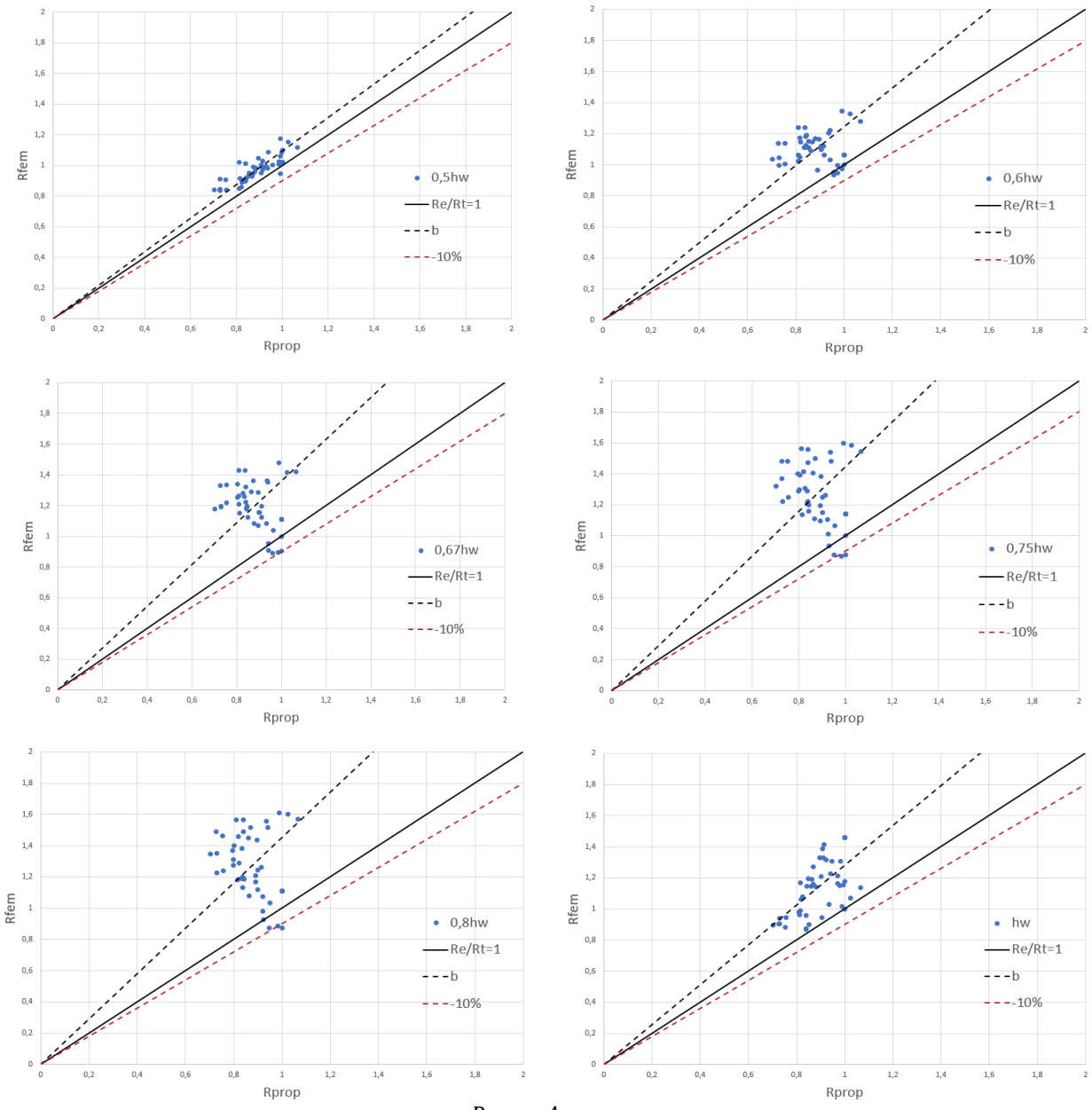

$$\frac{R_{FEM}}{R_{PROP}}\left(\frac{A_f}{A_w}=0\right)$$

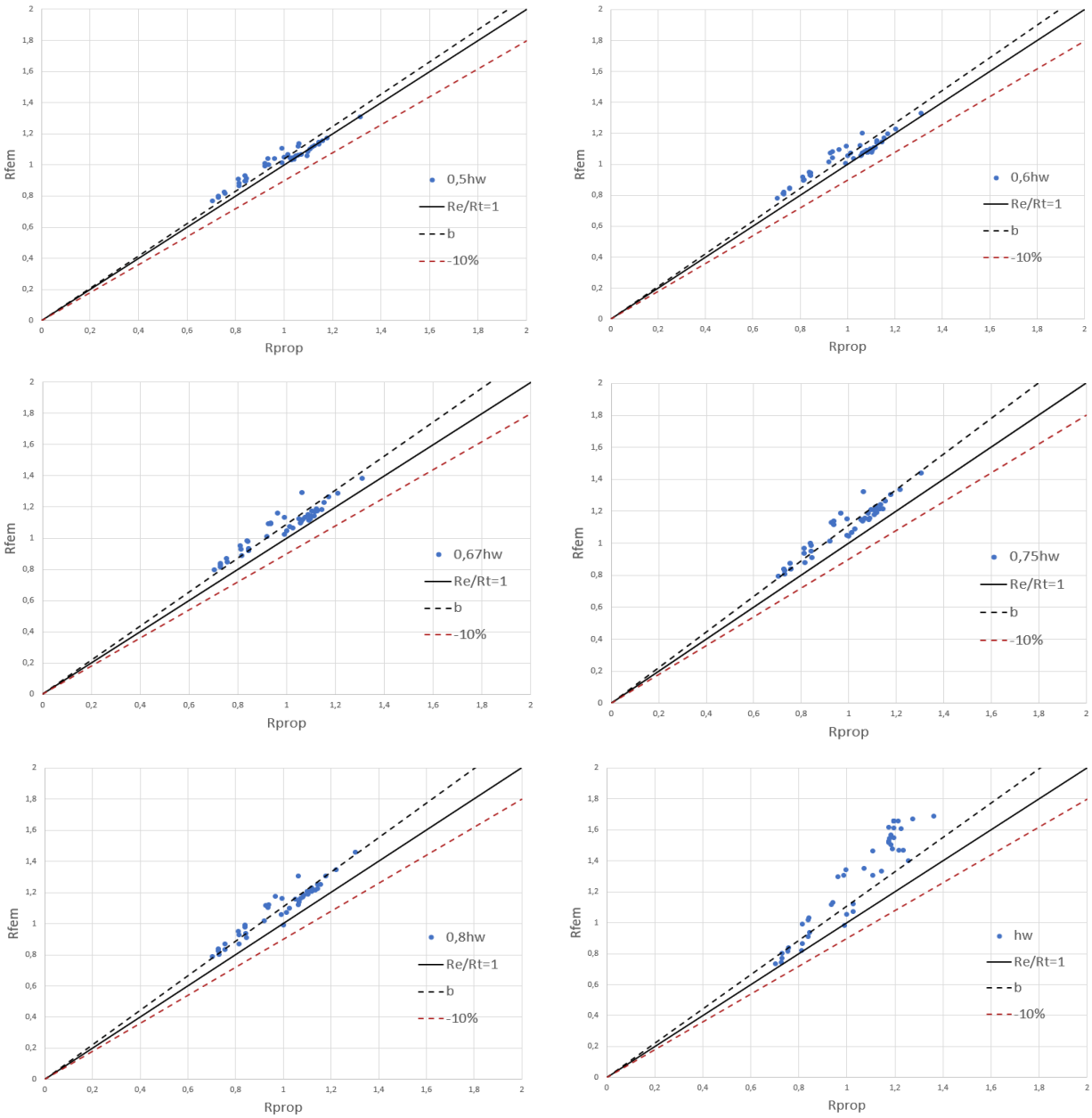

$$\frac{R_{FEM}}{R_{PROP}}\left(\frac{A_f}{A_w} = 1.0\right)$$

Figure 5.13 : R_{FEM}/R_{PROP} for plate girders with six longitudinal stiffener positions and $\frac{A_f}{A_w} = 0$ or 1.0

In addition, Figure 5.14 present some N-M-V interaction surfaces according to Biscaya´s interaction proposal so that it is possible to evaluate the relevance of the position of the stiffener.

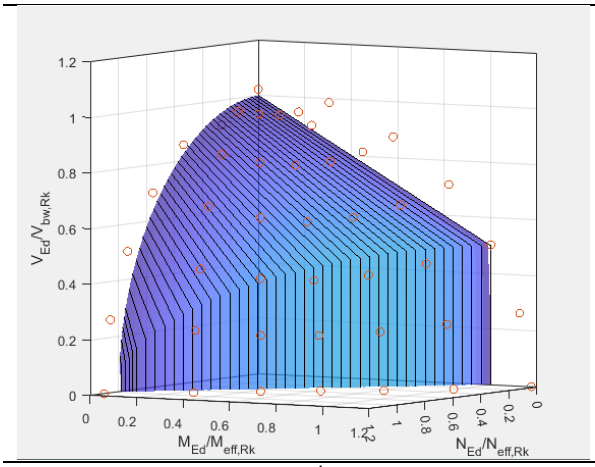

$0.50h_w \; // \frac{A_f}{A_w} = 0$

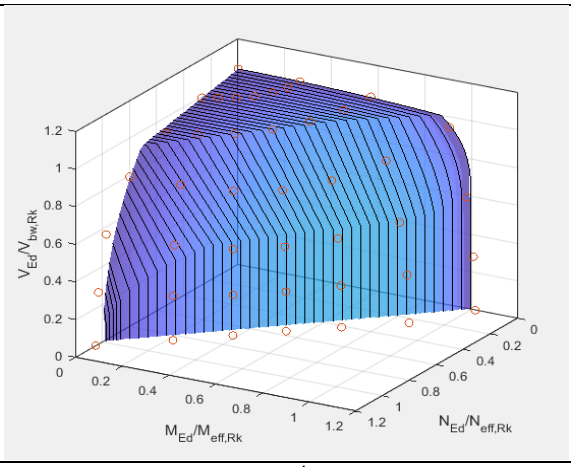

$0.50h_w \; // \frac{A_f}{A_w} = 1$

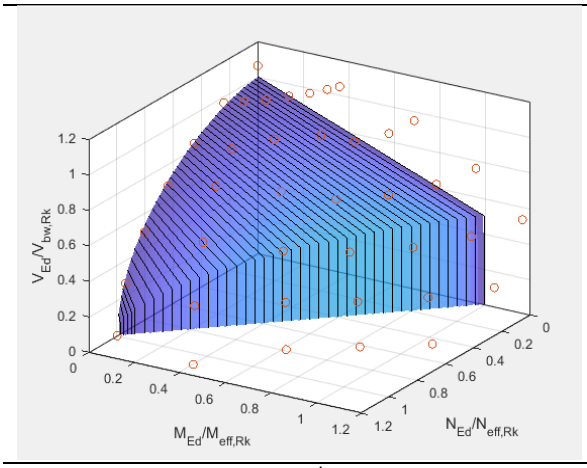

$0.60h_w \; // \frac{A_f}{A_w} = 0$

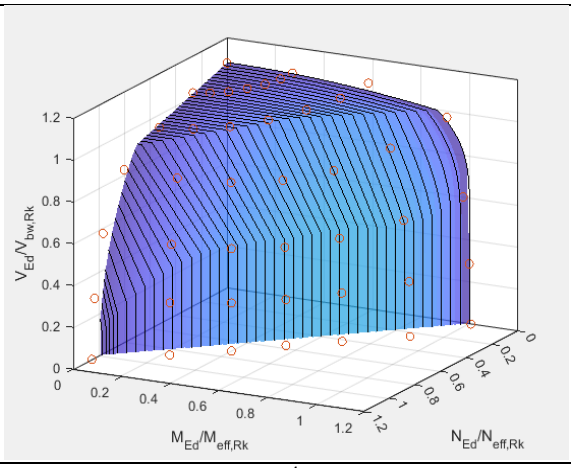

$0.60h_w \; // \frac{A_f}{A_w} = 1.0$

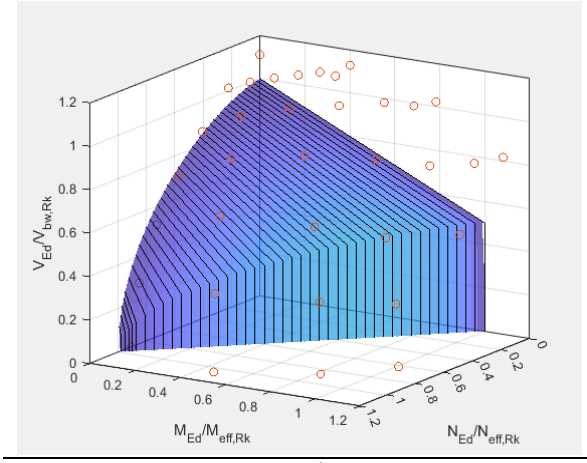

$0.67h_w \; // \frac{A_f}{A_w} = 0$

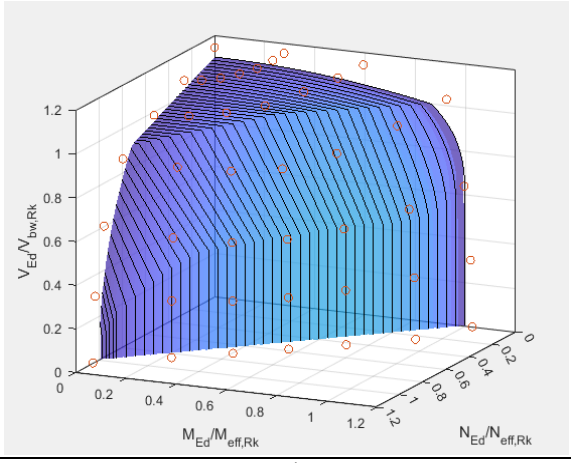

$0.67h_w \; // \frac{A_f}{A_w} = 1.0$

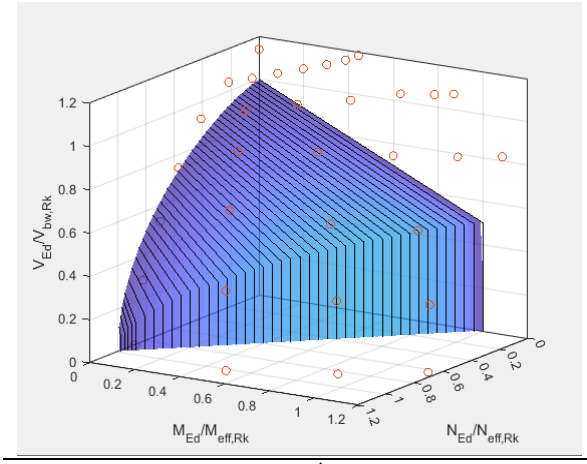

$0.75h_w$ // $\frac{A_f}{A_w} = 0$

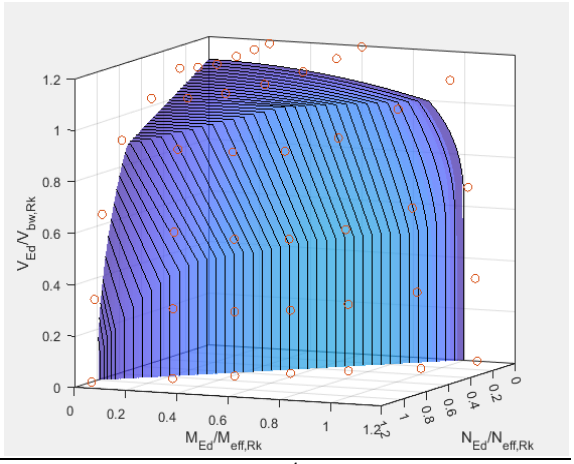

$0.75h_w$ // $\frac{A_f}{A_w} = 1.0$

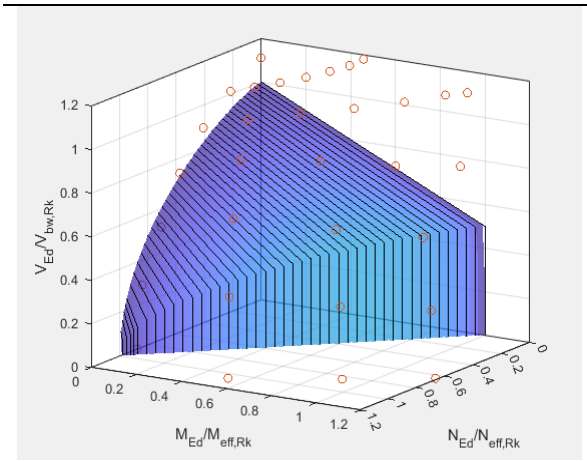

$0.80h_w$ // $\frac{A_f}{A_w} = 0$

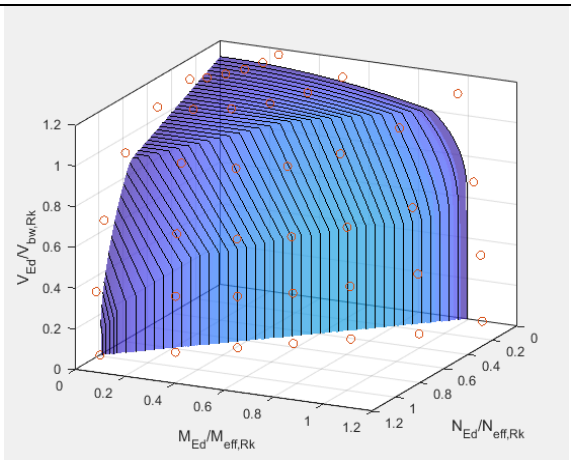

$0.80h_w$ // $\frac{A_f}{A_w} = 1.0$

Figure 5.14: R_{FEM}/R_{PROP} for plate girders with a longitudinal stiffener

5.3. Post maximum load behaviour

It is also of interest to evaluate the behaviour of the plate girder after reaching its maximum capacity. That depends on the type of loading and failure mode, as well as, on the plate girder slenderness and its capacity to redistribute the stresses after reaching the maximum load capacity.

To evaluate the post maximum load capacity of the plate girder, the arc-length parameter used in the GMNIA analysis is assumed to be a good parameter to have an overall view of the plate girder behaviour during the process of loading. It should be noted that the same plots were put together using the axial displacement of the web for the axial load, and overall rotation of the loaded sections for the case of applying a bending moment. It was concluded that these plots present the same layout, differing only in the units used in the horizontal axis. It was decided that the arch-length parameter was a good form of evaluating the global behaviour of the plate girder for very high load-levels, and after the maximum load capacity.

Therefore, for the N, M and V loadings, applied separately in the plate girder, the load parameter LPF is plotted as a function of the the Arch-length parameter. These plots are presented in Figures 5.15 (for N

loadings); 5.16 (for M loadings) and 5.17 (for V loadings) and considering the stiffened web without flanges $\frac{A_f}{A_w} = 0$ (dash lines) and with strong flanges $\frac{A_f}{A_w} = 1$ (solid lines). These figures also present the buckling modes reported in each loading type for the case where the longitudinal stiffener is placed at $0.50h_w$, at $0.80h_w$, or in the case no stiffener is used.

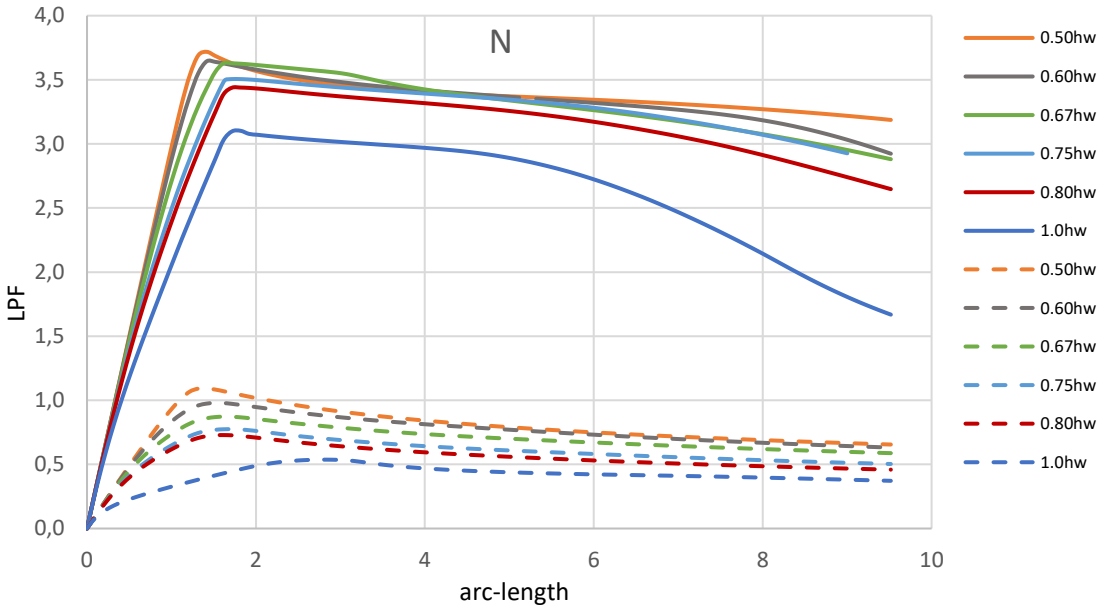

Load	Stiffener Position		
	$0.50h_w$	$0.80h_w$	–
N	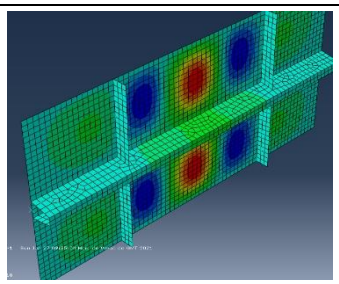	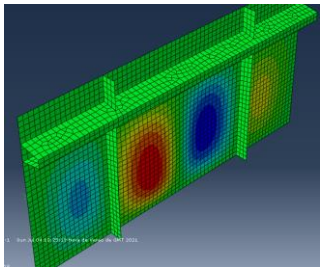	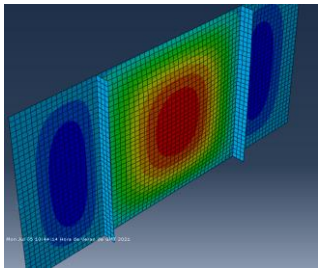
	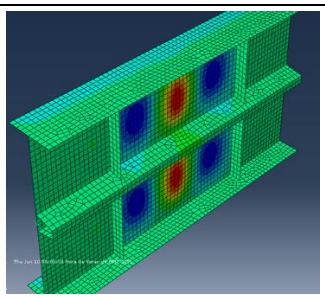	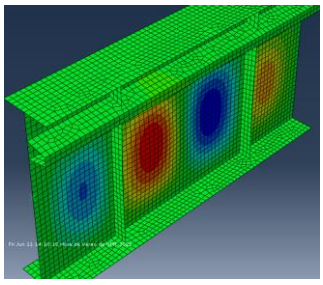	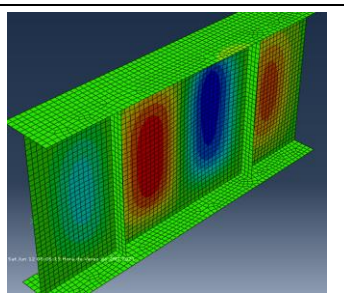

Figure 5.15: LPF/arc-length plot when plate-girder subjected to pure compression

When the plate-girder is subjected to the axial load, and no flanges are adopted, the maximum resistance is much lower than when strong flanges are adopted. The increase of resistance when the flanges are added is even higher than the factor of 3 of the increased area, due to the fact that the flanges do not buckle at the same time of the web. In all cases a local plate buckling mode was reported, as can be seen in Figure 5.15.

This fact explains why after reaching the maximum plate girder capacity, very high loads can still be equilibrated with increasing deformations. This behaviour is more noticeable if the longitudinal stiffener is placed at mid-height of the web, dividing the web into two sub-panels with the same buckling behaviour to the pure compression loading. The worst-case scenario is if no stiffener is used. In that case, the maximum capacity is lower and the web cannot maintain the load capacity so well after reaching the maximum resistance.

For the case of a bending moment (Figure 5.16), a single stiffened web has a much lower bending resistance than the plate girder with strong flanges, as it would be expected.

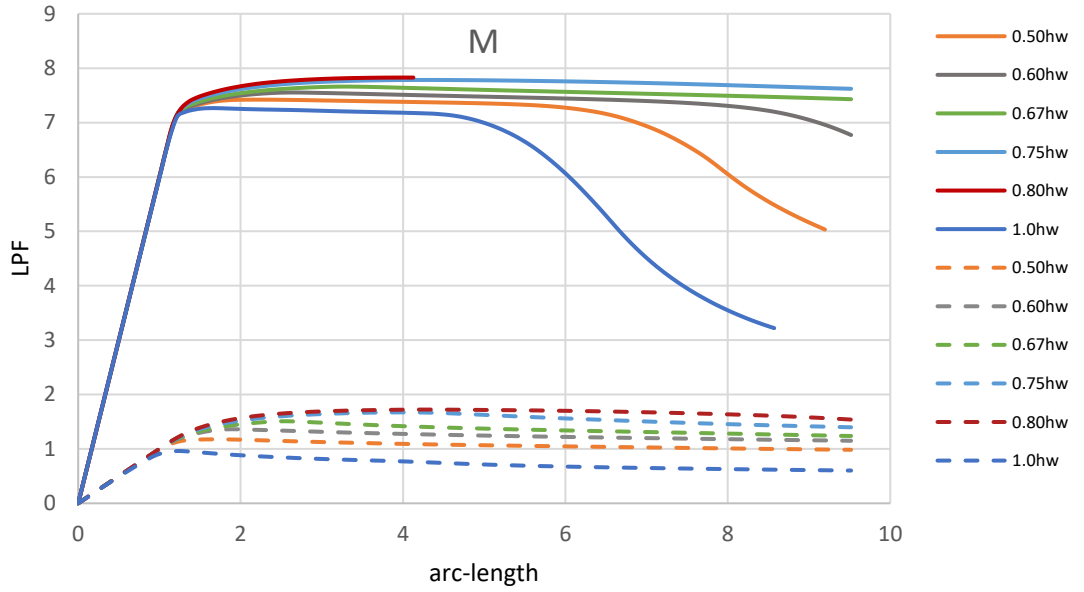

Load	Stiffener Position		
	$0.50h_w$	$0.80h_w$	–
M	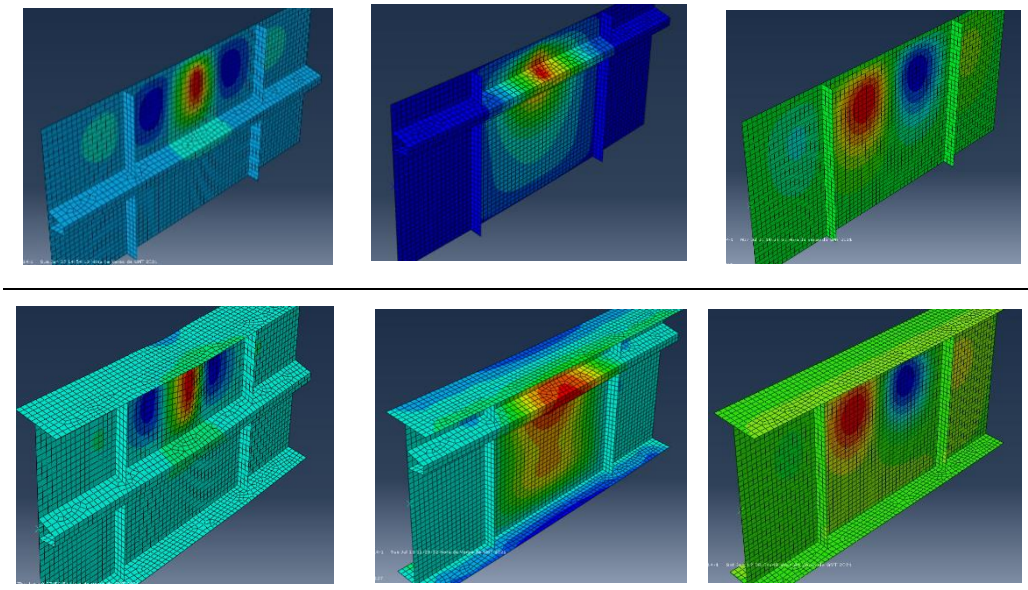		

Figure 5.16: LPF/arc-length plot when plate-girder subjected to pure bending

When the flange is added, the load capacity of the plate girder is much reduced after reaching the maximum resistance. This is due to the fact that the buckling mode of the plate girder also involves the buckling of the top compressed flange into the web, usually known as flange induced buckling. However, if the longitudinal stiffener is near the top compressed flange, like at $0.80h_w$, the web is prevented from buckling, and the bending capacity is preserved. In this situation, the failure mode also involves the buckling of the longitudinal stiffener placed in the compressed part of the web. If no flanges are used, the resistant capacity is kept almost constant after reaching the maximum, since no buckling occurs in the top sub-plate until reaching the complete yielding of the cross-section, except for the case where there is no stiffener.

Finally, for the case of plate girders subjected to shear forces, as presented in Figure 5.17 a local plate buckling mode was reported in all cases.

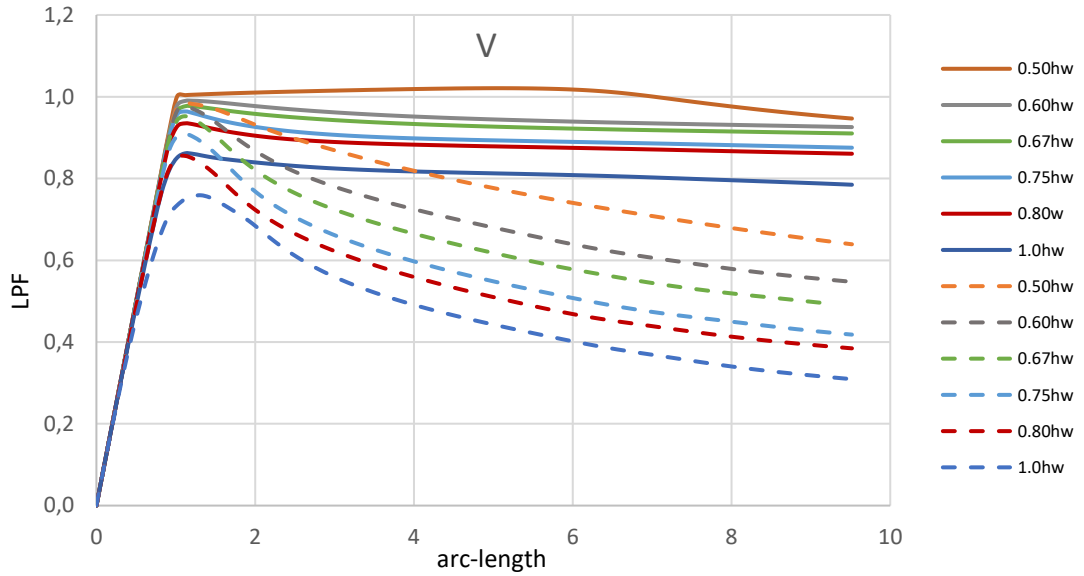

Load	Stiffener Position		
	$0.50h_w$	$0.80h_w$	–
V	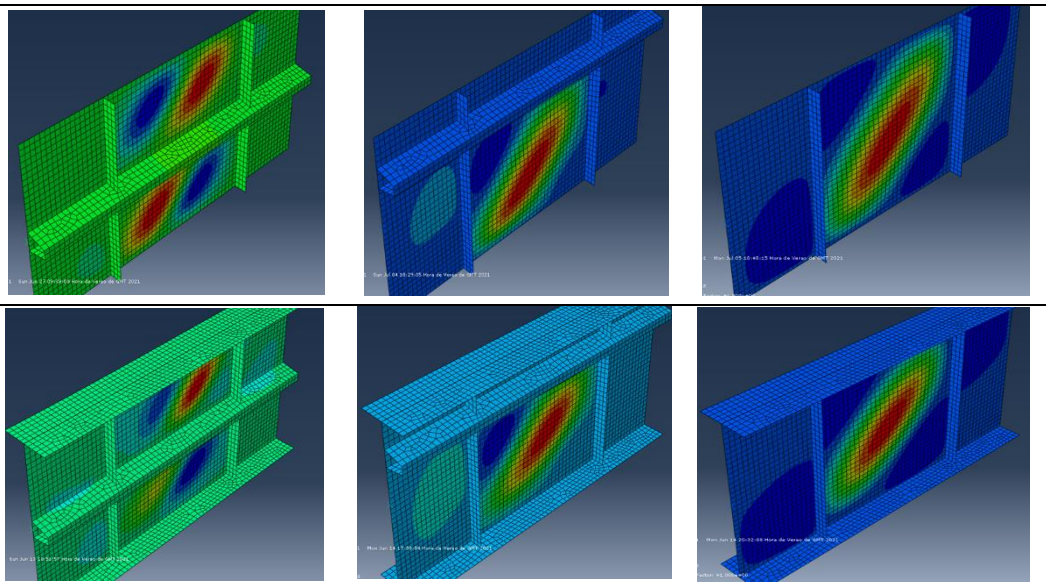		

Figure 5.17: LPF/arc-length plot when plate-girder subjected to pure shear

First, it is interesting to notice that the gains of using a longitudinal stiffener are significant, dividing the web into two sub-panels, but the difference of adding flanges is not so pronounced. In all cases the buckling mode that leads to failure is a typical shear plate buckling mode. And, since the longitudinal stiffener is very stiff, it perfectly divides the web into two sub-panels, sometimes even with two buckling semi-waves.

The second interesting aspect is that the maximum shear resistance is higher if the stiffener is placed at mid-height of the web. Some reduction of this maximum shear resistance is noticeable if the stiffener is moved up or suppressed.

The third aspect that should be noticed is the fact that without flanges the stiffened plate loses significant shear capacity after reaching the maximum load. That is more visible for slender sub-panels obtained when the stiffener is moved up on the web. More significant than that is that when adding the flanges, although the maximum plate girder shear capacity is not much increased, it remains practically unchanged with increase deformations, due to the fact that the edges of the buckle web can be remained supported by the flanges when they are submitted to higher distortions.

Even for the case of a longitudinal stiffener placed at mid-height of the web, the maximum shear capacity is reached for very high distortions, and much after the web has buckled. It seems as a second failure mechanics of a frame composed by the flanges and the vertical transverse stiffeners reaches yielding in a second moment with very high distortions, and that compensates the loss of shear resistance of the web. This plate girder behaviour loaded to shear was very recently reported in ref. [29].

6. Application of the Reduced Stress Method with Stress Shedding

As an option, pr EN 1993-1-5 allows the design of plated girder structures using the Reduced Stress Method as introduced in 3.4. When applying this method, the plate critical stresses need to be obtained for the complete stress field applied to the stiffened plate. For complex stress fields, this task was not so straightforward to do with analytical solutions, and numerical approximated solutions were often adopted. The software EBPlate (EBP) was a step forward to support this task [25].

6.1. Plate Girder Geometry and Critical Stresses using EBPlate

The geometry of the stiffened plate is first introduced in the software, as well as the elasticity modulus and Poisson´s coefficient, $E = 210\ GPa$ and $\nu = 0.30$, respectfully (Figure 6.1). After that, the longitudinal stiffener with its respective characteristics is introduced, as shown in Figure 6.2.

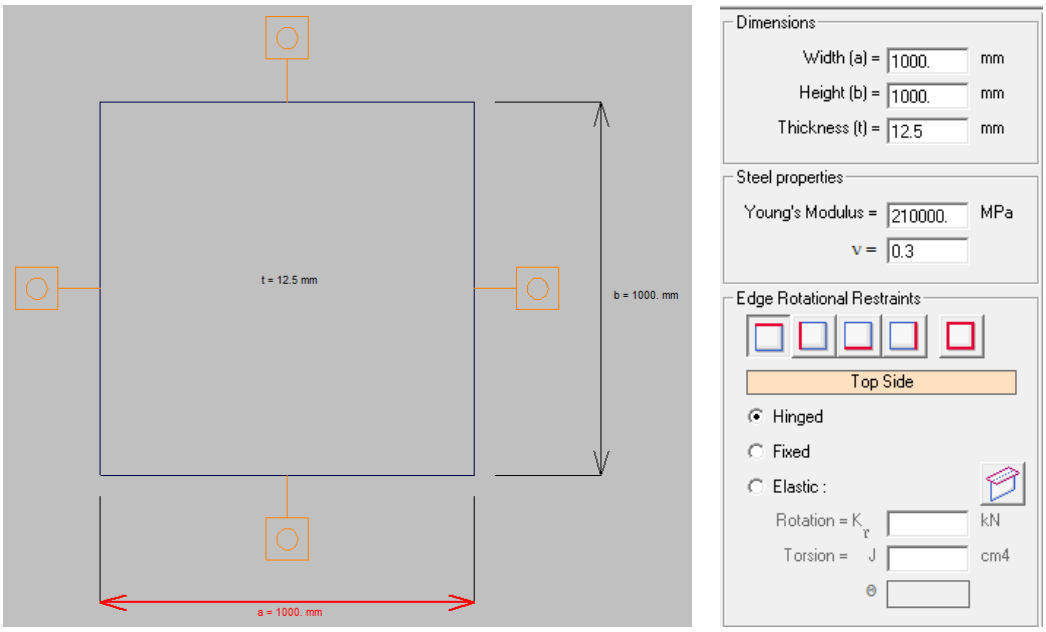

Figure 6.1: Geometry of the stiffened plate introduced in EBP

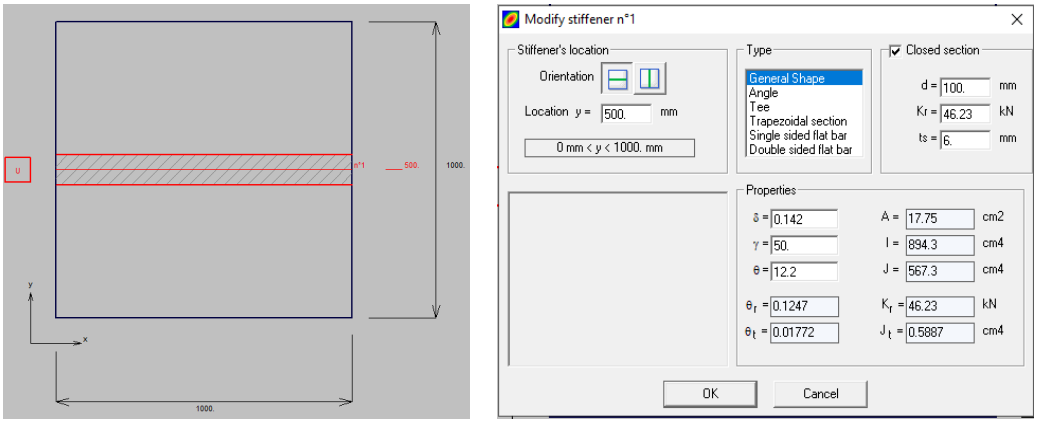

Figure 6.2: Properties of the longitudinal stiffener introduced in EBP

To determine the critical stresses for the axial force, bending moment and shear loadings, for each of the plate girder geometries, it is necessary to consider the two types of plate failure mode, global and local, modes (Figure 6.3 a) and b)), and consider the governing buckling mode. In order to avoid local buckling of the plate and stiffened sub-panels (equivalent to the global buckling), the stiffened plate is modelled as an orthotropic plate. Thus, the option "Orthotropic plate" must be activated and the coefficient η_x is equalled to –1, preventing the local plate modes.

Having these values of the critical stresses regarding both buckling modes, the lowest value is then used to determine the plate girder ultimate resistance for a specific loading that can considers the axial force, bending moment and shear force applied together or separately.

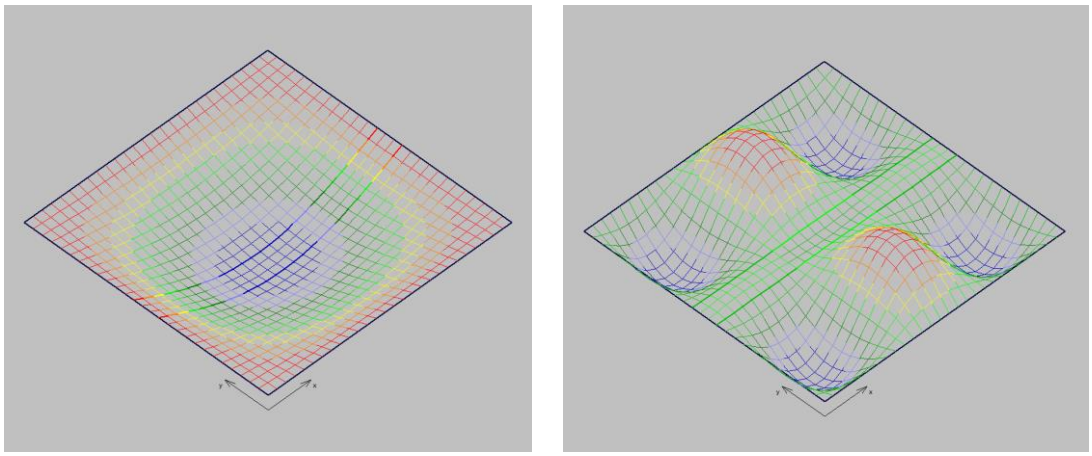

a) b)

Figure 6.3: Buckling modes a) global and b) local of a stiffened plate-girder subjected to an axial force using EBP

6.2. Ultimate Resistances for N, M and V loadings

The analysis is based on the comparison of both calculation methods (RSM and EWM), when plate girders are loaded with N, M, V loadings, applied separately, as shown in Figure 6.4. For a simple stiffened plate (without flanges), the main conclusions from these results are:

1) Conclusions on the $\mathbf{N_{RSM}/N_{EWM}}$ analysis:

- In the EWM, the effective widths for the compressed web panels produce a certain stress redistribution to the web part under tension and to the compressed flange; for relatively narrow compressed sub-panels this stress redistribution is small.
- However, the larger the sub-panels are (if the stiffener is moved up in the web), the greater the stress redistribution reported using the EWM, which corresponds to having a more noticeable plastic redistribution of stresses, thus moving away from the elastic behaviour as it is assumed when using the RSM and justifying a higher ultimate resistance to an axial compressed force.

- For the RSM points, there is a linear variation when shifting the stiffener up caused by the reduction of the local critical load, due to the fact that the most slender of the two sub-panels will govern the plate girder resistance.

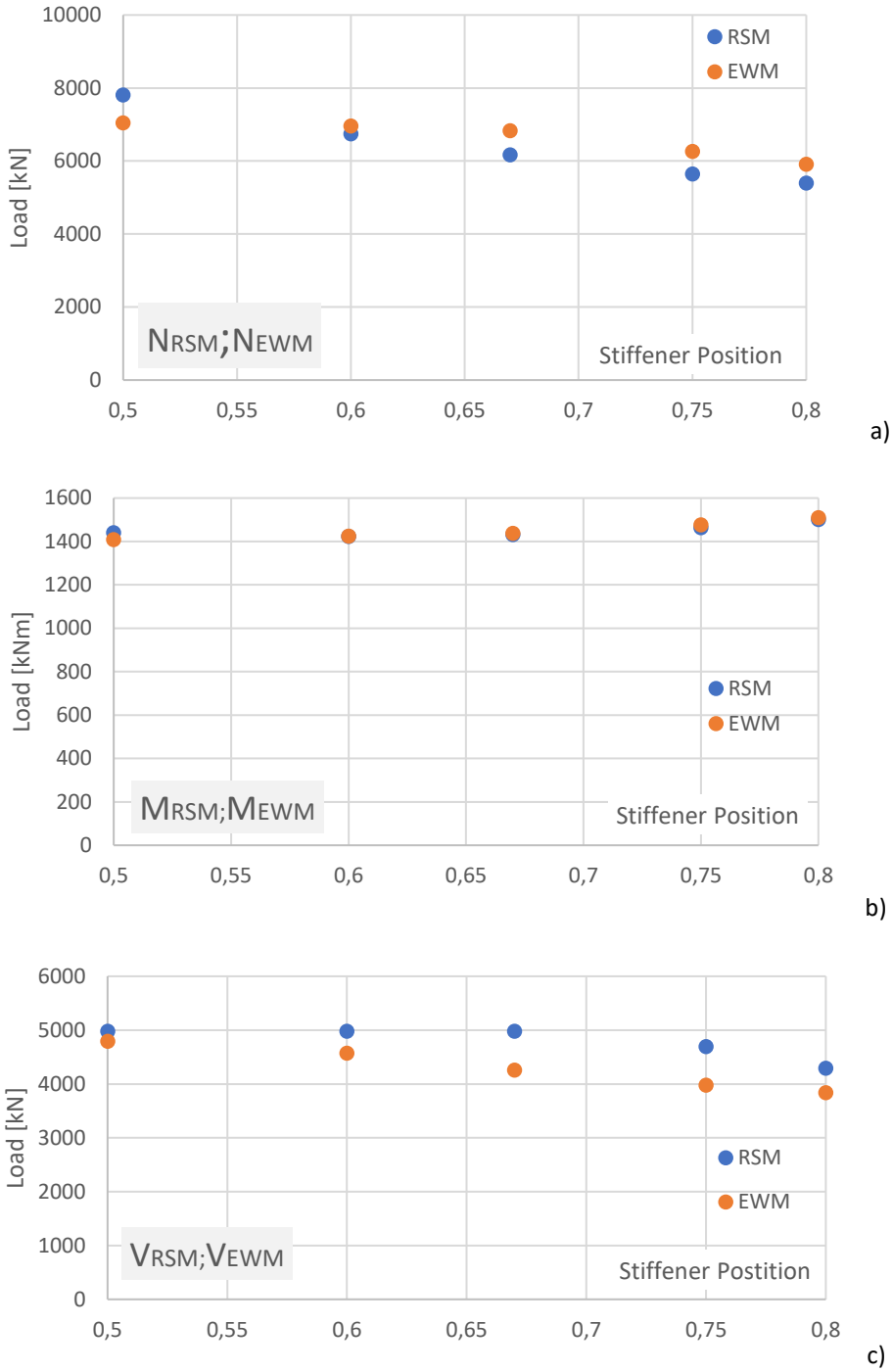

Figure 6.4: : Comparison of the resistances a) N_{RSM}/N_{EWM}; b) M_{RSM}/M_{EWM}; c) V_{RSM}/V_{EWM} for a plate girder with $A_f/A_w = 0$

2) Conclusions on the $\mathbf{M_{RSM}/M_{EWM}}$ analysis:

- For the present plate girder, the bending resistances are the same irrespective of the method used; This occurs due to the fact that, when a bending moment is applied, there is no web local buckling up to reaching the yielding of the flange.

- Hence even for the EWM there is no possible redistribution of stresses (the elastic stress distribution is maintained) and the ultimate resistance corresponds to the yielding bending moment for both methods.

3) Conclusions on the V_{RSM}/V_{EWM} analysis:

- The shear resistance given by the RSM is always higher than that of the EWM because the critical stresses obtained using the EBP are higher than the ones obtained by the approximate formulations given in the Annex A3 of prEN 1993-1-5 [11], as shown in Figure 6.5.

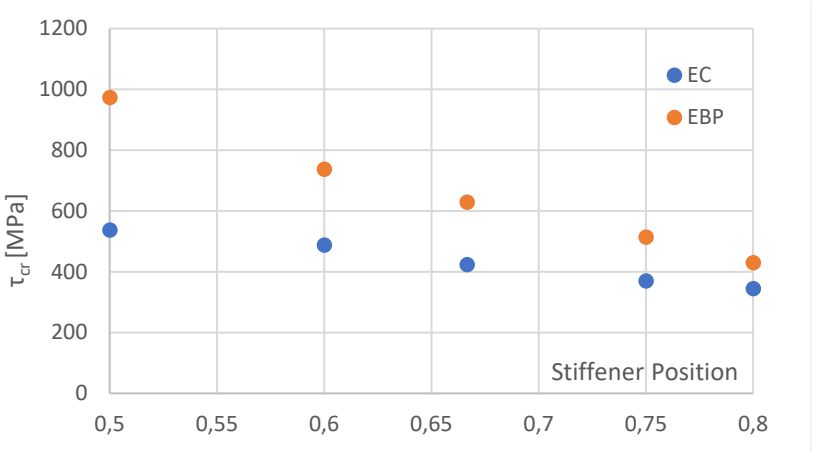

Figure 6.5: Comparison of critical stresses obtained by prEN 1993-1-5 and EBP

To evaluate the influence of the flanges in the ultimate resistance of the stiffened plate girder when using the RSM, plate girders with a ratio $A_f/A_w = 1.0$ were analysed. The ultimate resistances obtained are shown in Figure 6.6.

As previously mentioned, the RSM neglects the contribution of the flanges to the resistance, therefore, as it was expected, the resistances obtained for the axial force obtained by the EWM are always higher when adding the flanges to the plate girder cross-section.

For the bending resistance, as explained previously, there is no web local buckling up to reaching the yielding of the flange. Hence even for the EWM there is no possible redistribution of stresses (the elastic stress distribution is maintained) and the ultimate resistance corresponds to the yielding bending moment for both methods.

For the case of the plate-girder loaded by the shear force, there are no differences on the resistances obtained by the RSM whether in the presence of flanges or not, because the resisting area, A_w, is kept constant. Again, this happens due to the fact that the RSM does not consider the shear resistance contribution of the flanges.

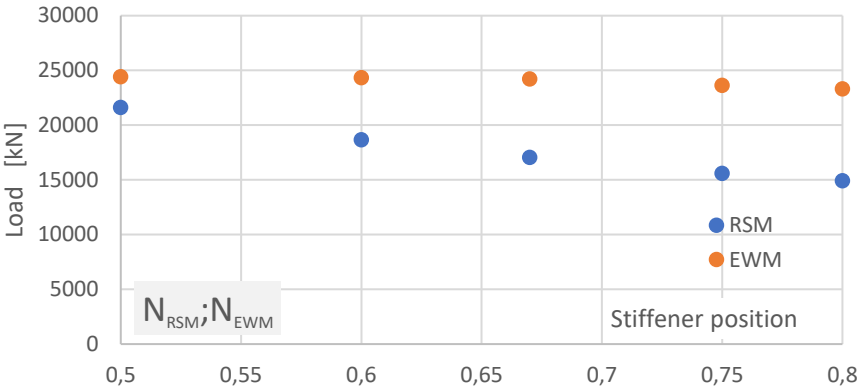

a)

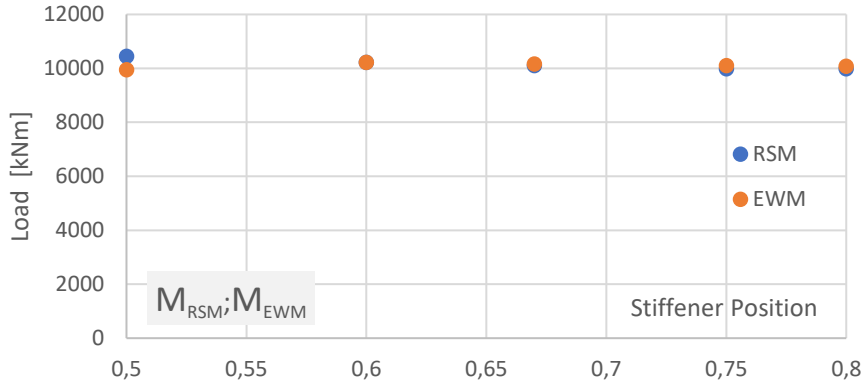

b)

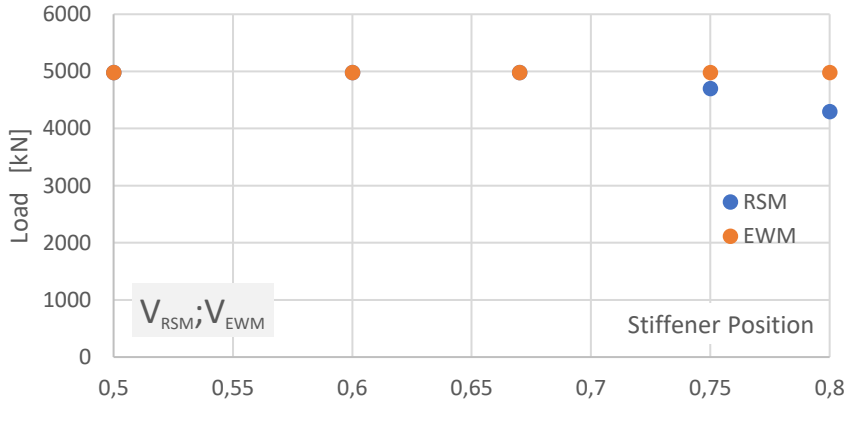

c)

Figure 6.6: Comparison of the resistances a) N_{RSM}/N_{EWM}; b) M_{RSM}/M_{EWM}; c) V_{RSM}/V_{EWM} for a plate girder with $A_f/A_w = 1.0$

6.3. Formulation of the Reduced Stress Method with Stress Shedding – RSM + S

To allow stress shedding in the RSM, Biscaya [12] proposed a formulation for the RSM based on the approach from the old BS 5400 – Part 3 - Code of practice for the design of steel bridges. The applied internal forces can be written as a function of the factor k , which represents the fraction of the direct stress that remains in the web:

$$N_{Ed} = \alpha\,[A_w k + (2A_f + (1-k)A_w)]c_{\theta,N} \tag{6.1}$$

$$M_{Ed} = \alpha\,[\frac{A_w h_w}{6} k + (A_f h_w + (1-k)\frac{A_w h_w}{6})]c_{\theta,M} \tag{6.2}$$

$$V_{Ed} = \alpha\, A_w c_{\theta,V} \tag{6.3}$$

Considering the RSM, the load amplifiers can be rewritten as function of the k factor and $c_{\theta,N}$, $c_{\theta,M}$, and $c_{\theta,V}$ factors, as follows:

$$\alpha_{ult,k} = f_y \sqrt{\frac{1}{3(c_{\theta,V})^2 + (kc_{\theta,N} + kc_{\theta,M})^2}} \tag{6.4}$$

$$\alpha_{cr} = \frac{\sqrt{4\left(\left(\frac{c_{\theta,V}}{\tau_{cr,V}}\right)^2 + \left(k\frac{c_{\theta,M}}{\sigma_{cr,M}}\right)^2\right) + \left(k\frac{c_{\theta,N}}{\sigma_{cr,N}}\right)^2 - \left(k\frac{c_{\theta,N}}{\sigma_{cr,N}}\right)}}{2\left(\left(\frac{c_{\theta,V}}{\tau_{cr,V}}\right)^2 + \left(k\frac{c_{\theta,M}}{\sigma_{cr,M}}\right)^2\right)} \tag{6.5}$$

$$\alpha_{rk} = f_y \sqrt{\frac{1}{3(\frac{c_{\theta,V}}{\chi_w})^2 + (k\frac{c_{\theta,N}+c_{\theta,M}}{\rho})^2}} \tag{6.6}$$

To better understand these equations, an example is presented in Figure 6.7.

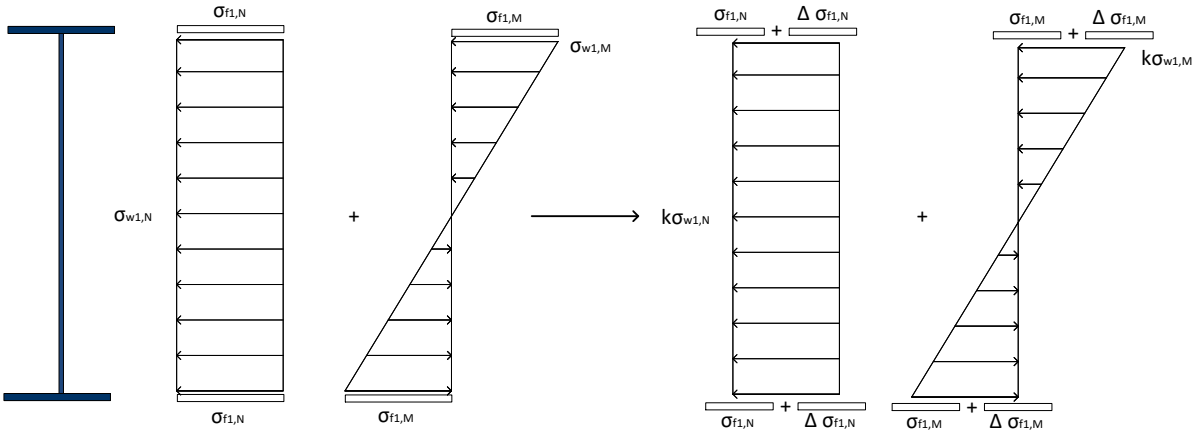

Figure 6.7: Example of RSM+S applied on a plate girder cross-section

where each stress is given by:

- $\sigma_{f,N} = \alpha_{Rk} \cdot c_{\theta,N}$, $\sigma_{f,M} = \alpha_{Rk} \cdot c_{\theta,M}$
- $\sigma_{w,N} = \alpha_{Rk} \cdot c_{\theta,N}$, $\sigma_{w,M} = \alpha_{Rk} \cdot c_{\theta,M}$
- $\Delta\sigma_{f,N} = (1-k)\sigma_{w,N} \cdot \frac{A_w}{2A_f}$
- $\Delta\sigma_{f,M} = (1-k)\sigma_{w,M} \cdot \frac{W_w}{h_w} \cdot \frac{1}{A_f}$
- $\sigma_{f,N} + \Delta\sigma_{f,N} + \sigma_{w,N} + \Delta\sigma_{f,M} \leq f_y \rightarrow k_{min}$

(6.7)

Because the flanges have a maximum capacity due to yielding ($F_f = F_{f,sup,N} + F_{f,sup,M} \leq A_f f_y$), α is a function of the stress distribution, as well as the ratio of flange to web gross section. When a stiffener is added, Figure 6.8 shows the shedding portion of the bending moment.

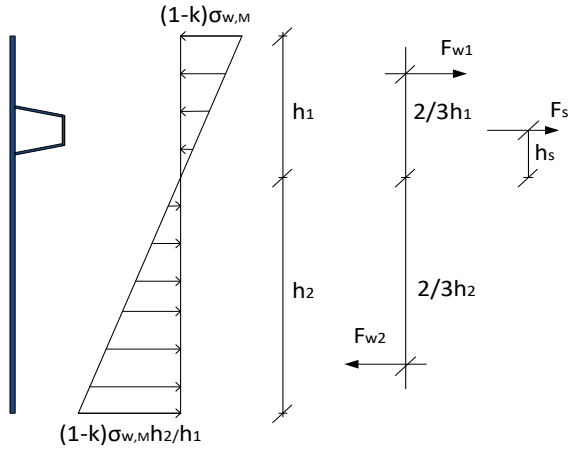

Figure 6.8: Shedding portion of bending moment

which, it terms of the internal forces required to assure the equilibrium of the cross-section, are given by

- $\Delta M_w = F_{w1} \cdot \frac{2}{3}h_1 + F_{w2} \cdot \frac{2}{3}h_2 + F_s \cdot h_s$
- $F_{w1} = (1-k)\sigma_{w,M} \cdot \frac{h_1}{2} \cdot t_w$
- $F_{w2} = (1-k)\sigma_{w,M} \cdot \frac{h_2}{h_1} \cdot \frac{h_2}{2} \cdot t_w$
- $F_s = (1-k)\sigma_{w,M} \cdot \frac{h_s}{h_1} \cdot h_s \cdot A_S$

(6.8)

Moreover, to be in equilibrium, the forces of the flanges must produce the same bending moment:

- $\Delta M_w = \Delta F_{f,sup} \cdot h_1 + \Delta F_{f,inf} \cdot h_2$
- $\Delta F_{f,inf} = \Delta F_{f,sup} \cdot \frac{h_2}{h_1}$
- $\Delta M_w = \Delta F_{f,sup} \cdot h_1 + \Delta F_{f,sup} \cdot \frac{h_2}{h_1} \cdot h_2 \rightarrow \Delta F_{f,sup} = \Delta M_w / (h_1 + \frac{h_2}{h_1} \cdot h_2)$
- $\Delta\sigma_{f,M} = \Delta F_{f,sup} / A_f$

(6.9)

6.4. N-M-V interaction using the RSM

The N-M-V interaction resistance for different load cases can be evaluated using both proposals according to the prEN 1993-1-5 [11] (RSM and EWM) and the numerical models previously presented. Figure 6.9 presents the ratios R_{RSM}/R_{FEM} for plate girders with five longitudinal stiffener positions and $A_f/A_w = 0$ or 1.0. Both resistances obtained from the EWM (in green) and RSM without stress shedding (in orange). Figure 6.10 compares the RSM resistance surface (in blue) with the FEM resistances (points in orange). As these results are not very easy to compare, Table 6.1 gives the statistical evaluation of the resistances of the interaction of N-M-V loads according to the RSM.

According with these results the following main conclusions can be drawn for the N-M-V interaction:

$A_f/A_w = 0$ – Stiffened plate girders without flanges

- Although the differences are not higher than 10%, the RSM provides resistances greater than those obtained by the numerical models for several cases, namely when N and V have high values (see Figure 6.9 for $A_f/A_w = 0$), this is due to the fact that a quadratic iteration between the N+M normal stresses and V shear stresses is always adopted, whereas the shape of the N-V interaction graphic has not always an exact quadratic shape.
- The RSM has a quadratic shape (see Figure 6.10 for $A_f/A_w = 0$) because the bases come from a von Mises formula while the N-V interaction proposed for the EWM does not (see Figure 5.14 for $A_f/A_w = 0$), especially for slenderer plates, which is the case; thus, a bigger difference between the two results is observed, with the RSM providing resistances that are not on the safety side.
- In fact, it can be seen in Figure 6.10 that in the N-V plane the RSM resistances are overestimated compared to the numerical model results; on the contrary, the actual resistance shape along the plane M-V for the two methods is approximately an ellipse thus both methods match with the numerical resistances much better.
- The RSM provides overall higher resistances than the EWM for the cases without flanges because it applies the concept of a global slenderness of the web, as well as, a reduction factor based on the von Mises formula; this can be concluded by the lower ratio R_{FEM}/R_{RSM} averages obtained in Table 6.1 if compared with the ratios R_{FEM}/R_{EWM} averages from Table 5.5 for the EWM.

$A_f/A_w = 1.0$ – Stiffened plate girders with strong flanges

- When adding flanges to the cross-section, the resistances obtained by the RSM have a much better match with the numerical results (see Figure 6.9 for $A_f/A_w = 1$); this can also be concluded by Table 6.1 ratio R_{FEM}/R_{RSM} averages (below 1.2) and dispersions (below 0.15).
- Because the RSM neglects the stress shedding of the normal stresses from the web to the strong flanges, the normal force design resistances are very much on the conservative side, as can be clearly concluded from the resistance surfaces provided in Figure 6.10 for $A_f/A_w = 1$).

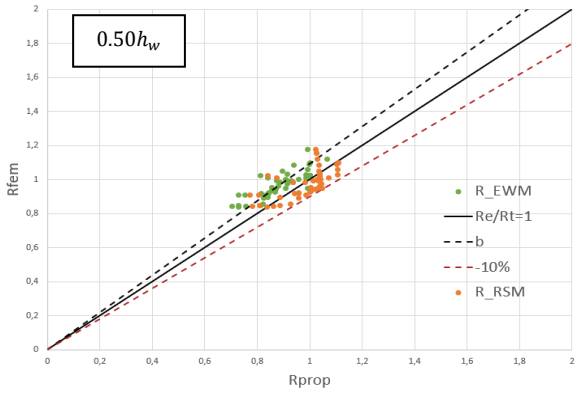

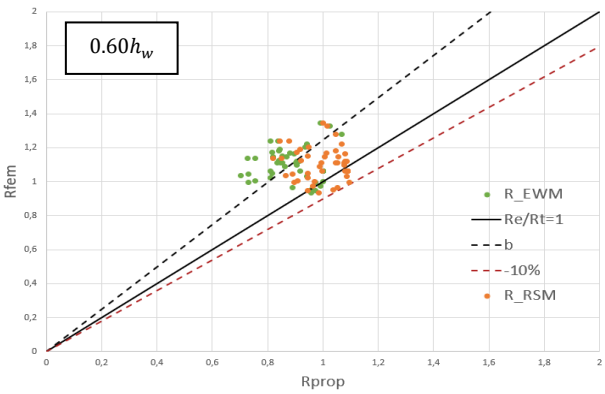

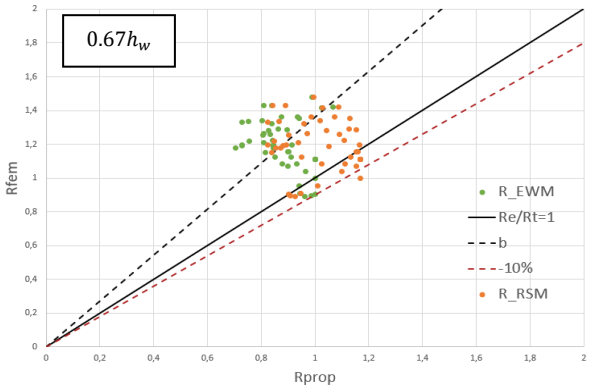

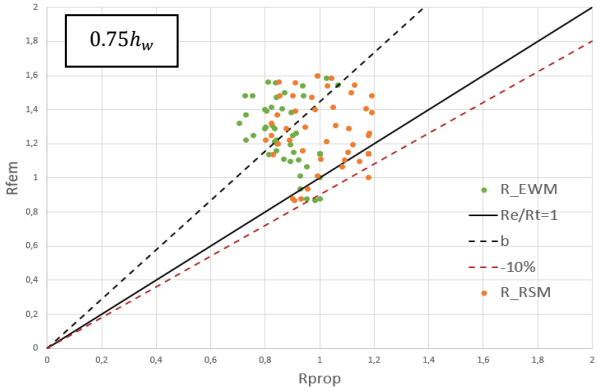

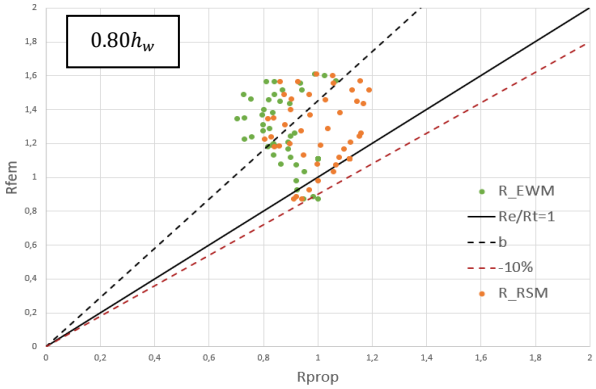

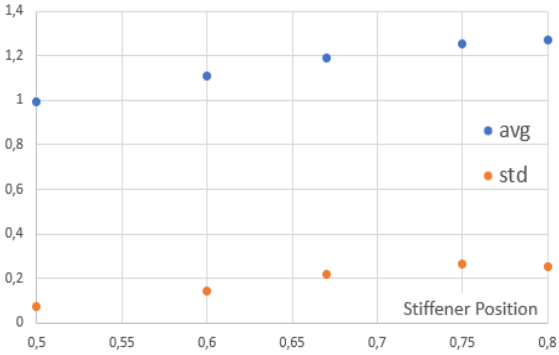

R_{RSM}/R_{EWM} $(A_f/A_w = 0)$

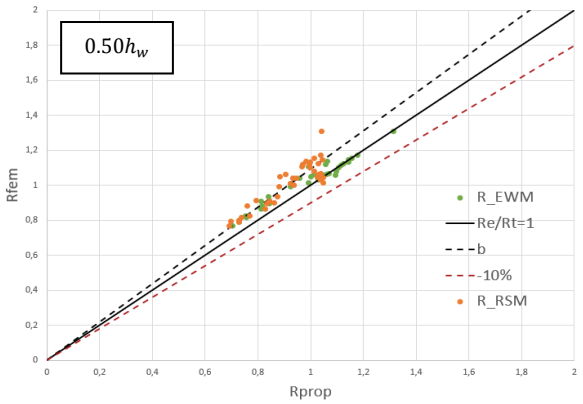

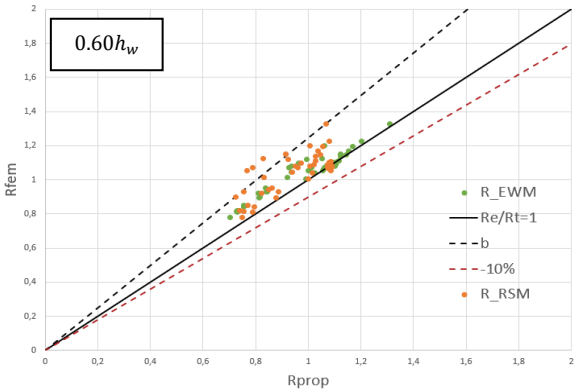

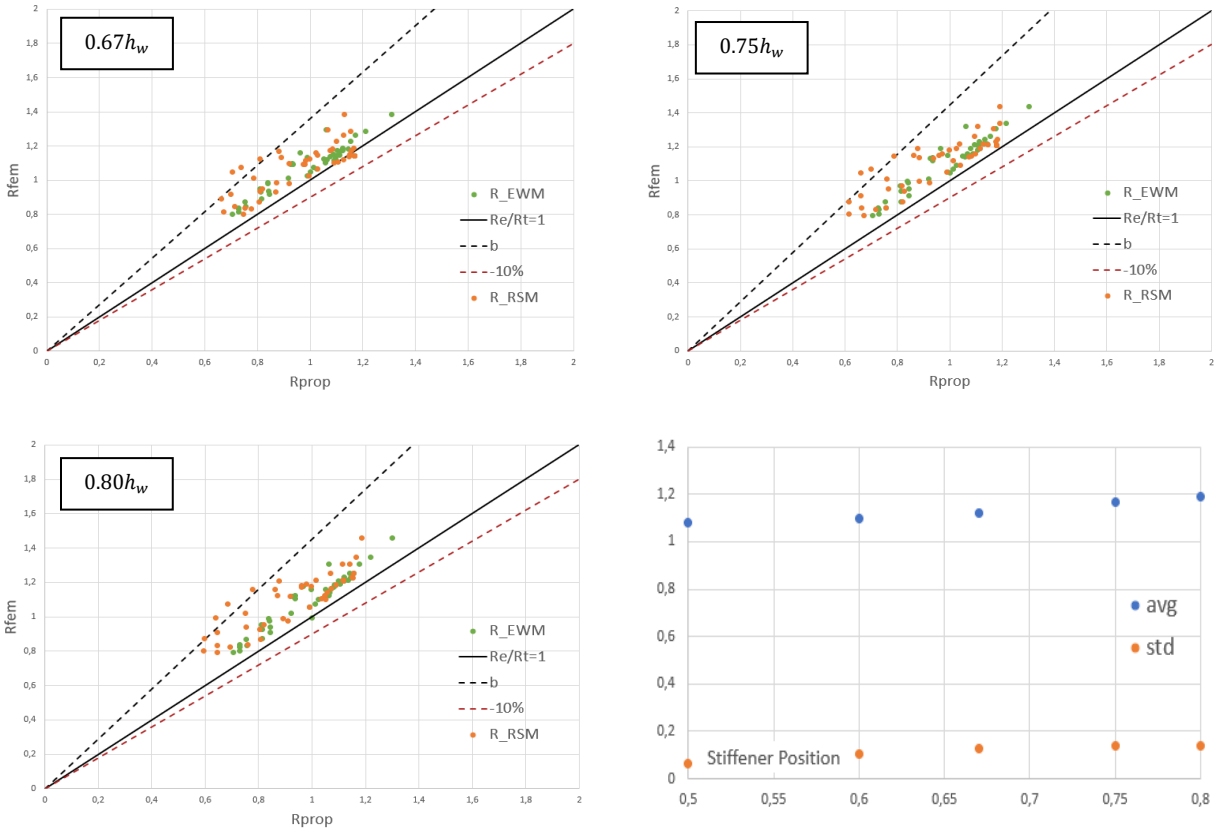

R_{FEM}/R_{PROP} $(A_f/A_w = 1.0)$

Figure 6.9: R_{RSM}/R_{FEM} for plate girders with five longitudinal stiffener positions and $A_f/A_w = 0$ or 1.0

Table 6.1: Statistical study of the N-M-V interaction resistances according to the RSM

R_{FEM}/R_{RSM}	$A_f/A_w = 0$					
	avg	***std***	$N^{o}_{cases} < 1.0$	$N^{o}_{cases} < 0.9$	***Min***	***Max***
$0.50h_w$	0.996	0.074	34	0	0.904	1.215
$0.60h_w$	1.108	0.142	14	0	0.909	1.472
$0.67h_w$	1.188	0.221	16	0	0.853	1.698
$0.75h_w$	1.256	0.266	13	0	0.848	1.837
$0.80h_w$	1.269	0.256	13	0	0.917	1.824
R_{FEM}/R_{RSM}	$A_f/A_w = 1.0$					
	avg	***std***	$N^{o}_{cases} < 1.0$	$N^{o}_{cases} < 0.9$	***Min***	***Max***
$0.50h_w$	1.078	0.064	10	0	0.968	1.258
$0.60h_w$	1.098	0.105	10	0	0.971	1.377
$0.67h_w$	1.123	0.130	10	0	0.977	1.491
$0.75h_w$	1.169	0.141	0	0	1.022	1.587
$0.80h_w$	1.191	0.138	0	0	1.047	1.571

RSM	FEM
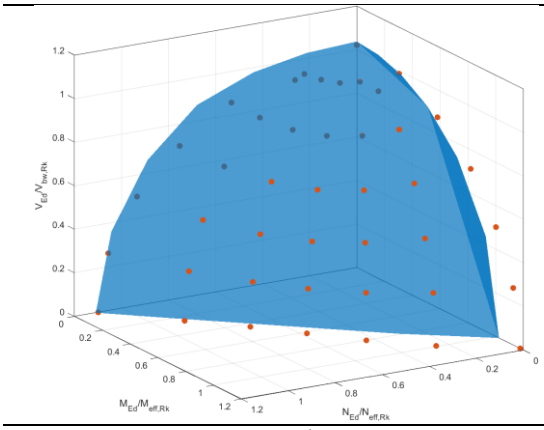	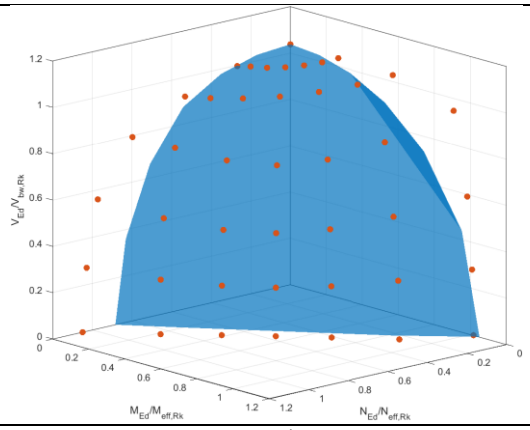
$0.50h_w$ // $\frac{A_f}{A_w} = 0$	$0.50h_w$ // $\frac{A_f}{A_w} = 1$
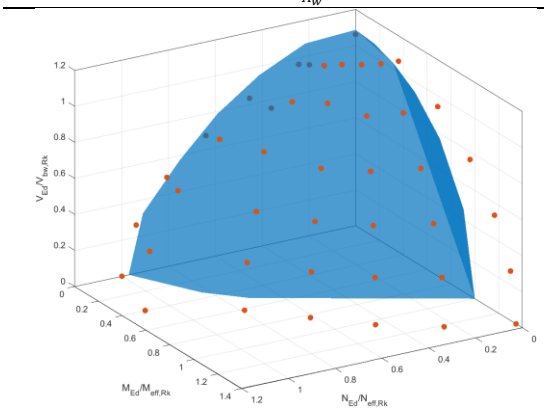	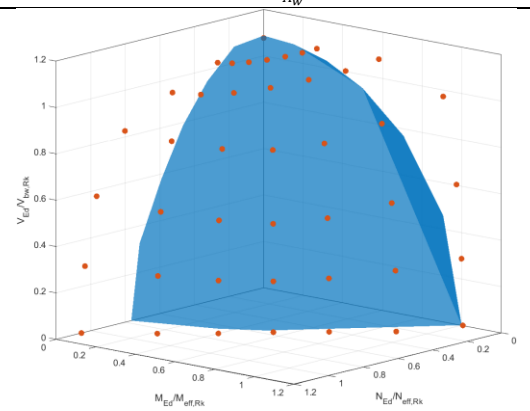
$0.60h_w$ // $\frac{A_f}{A_w} = 0$	$0.60h_w$ // $\frac{A_f}{A_w} = 1.0$
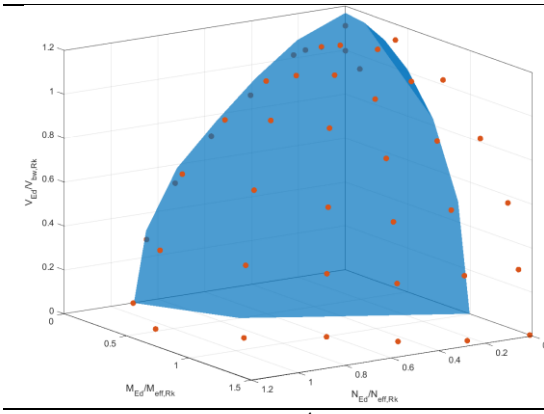	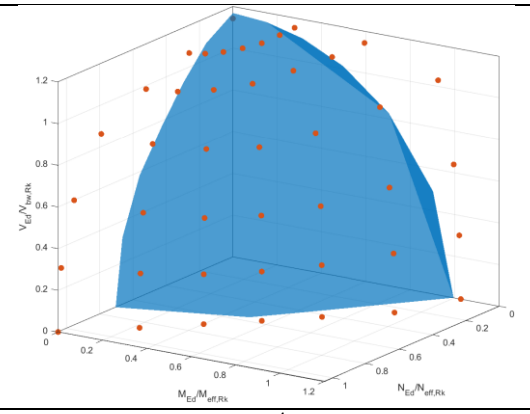
$0.67h_w$ // $\frac{A_f}{A_w} = 0$	$0.67h_w$ // $\frac{A_f}{A_w} = 1.0$
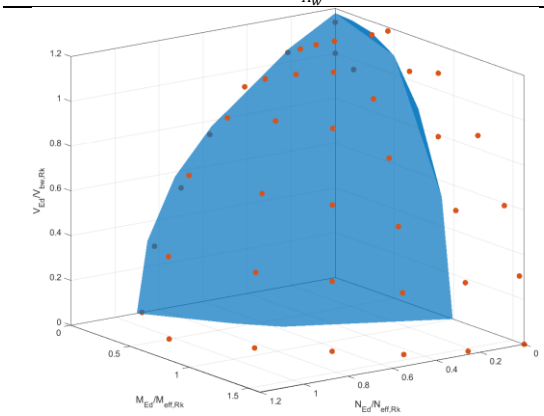	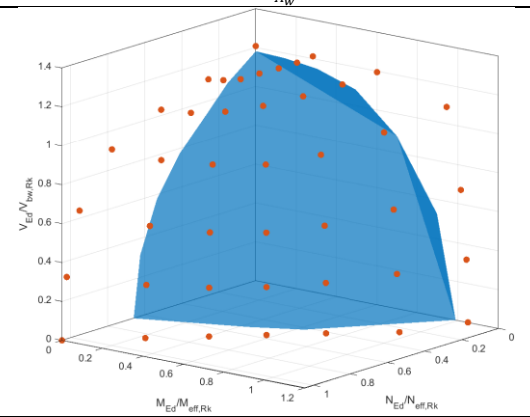
$0.75h_w$ // $\frac{A_f}{A_w} = 0$	$0.75h_w$ // $\frac{A_f}{A_w} = 1.0$

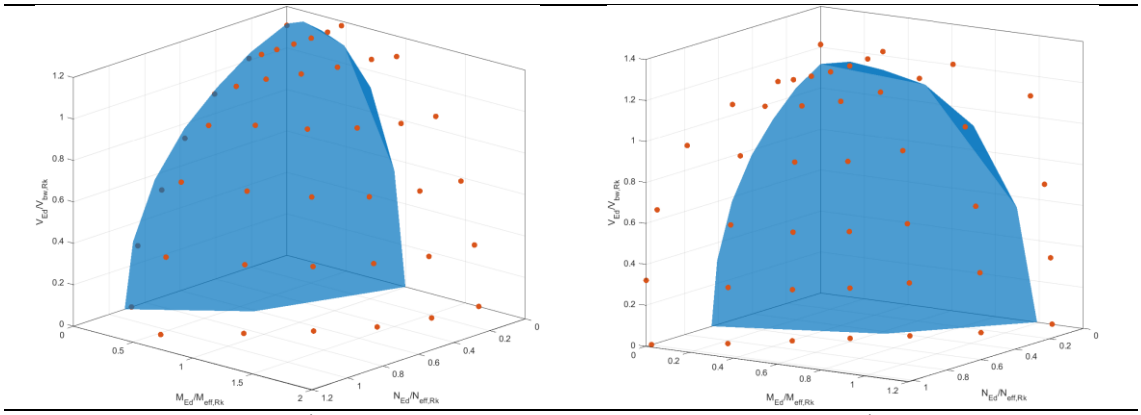

$0.80h_w$ // $\frac{A_f}{A_w} = 0$	$0.80h_w$ // $\frac{A_f}{A_w} = 1.0$

Figure 6.10: N-M-V interaction surface from the RSM and FEM resistance points

6.4.1. RSM+S for N and M loadings

After evaluating the ultimate resistance of the plate-girders when subjected to compression, bending moment and shear using the RSM as proposed in the prEN 1993-1-5 [11], it is intended to use the RSM+S to assess what can be improved when compared with the numerical resistances.

As mentioned before, for the plate-girders under study, when a bending moment is applied, the resistance is equal to the yielding bending moment, so no stress shedding can be done from the web to the flanges; thus, no improvement can be archived for this case.

But, for pure compression, the ultimate resistances obtained with the possibility of shedding tend to be much more similar to the ones obtained by the numerical models, as well as those of the EWM (Figure 6.11).

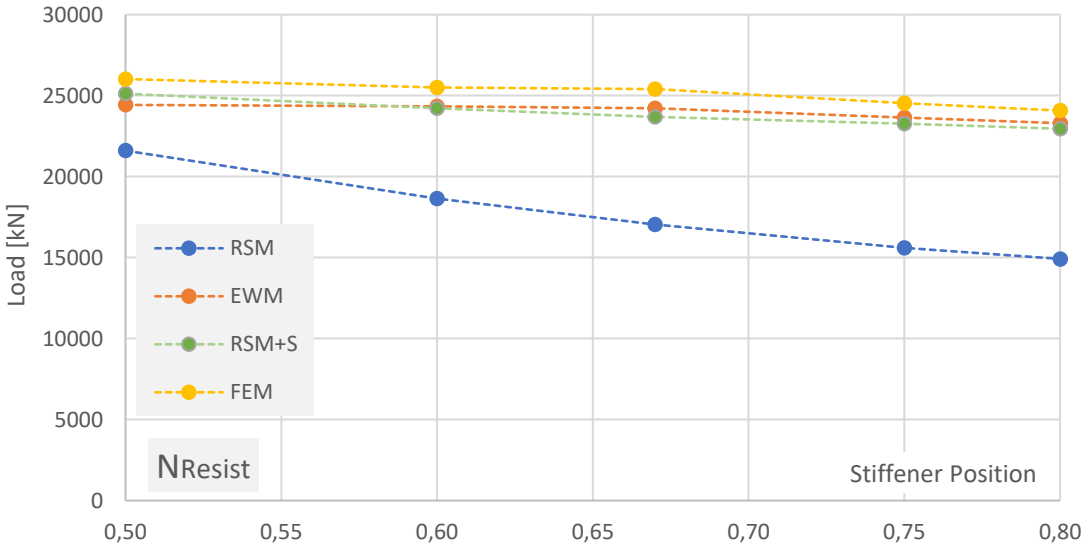

Figure 6.11: Comparison of the pure compression resistance to between the 3 methods (RSM, RSM+S and EWM) and the FEM results

Therefore, the RSM with stress shedding gives much better results than when neglecting the flanges contribution. As the stiffener is shifted up, the coefficient k applied to the normal stresses that remain in the web tends to become smaller (Figure 6.12), indicating that there is a greater possibility of redistribution even if most of the normal stresses remain in the web (between 0.65 and 0.85). To get to lower values of k, flanges with more area were required.

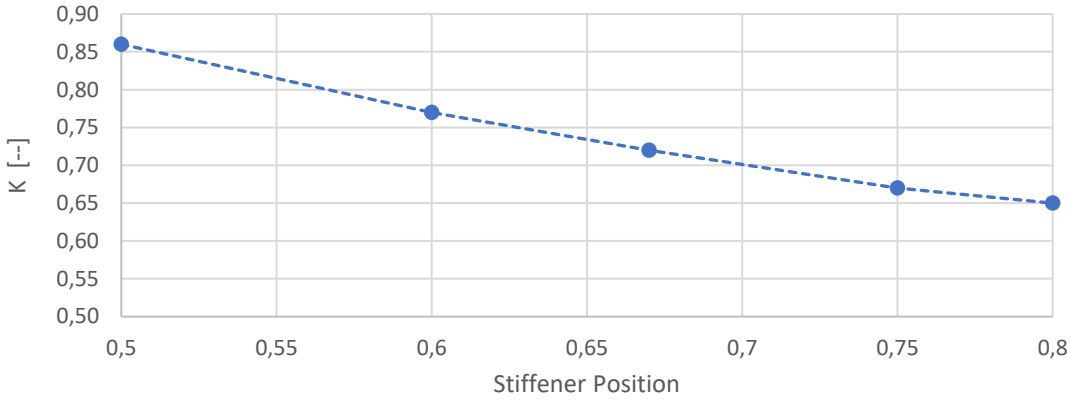

Figure 6.12: Values of k for the different stiffener positions

6.4.2. RSM+S for N-M interaction

Finally, the influence of shedding on the N-M interaction is analysed for the plate girder with the stiffener at mid height of the section ($0.50h_w$) and flanges with $A_f/A_w = 1.0$. Figure 6.3 presents the comparison between the N-M interaction for the different load cases (with $\theta_1 = [0, 15, 30, 45, 60{,}75, 90]$ and $\theta_2 = 0$).

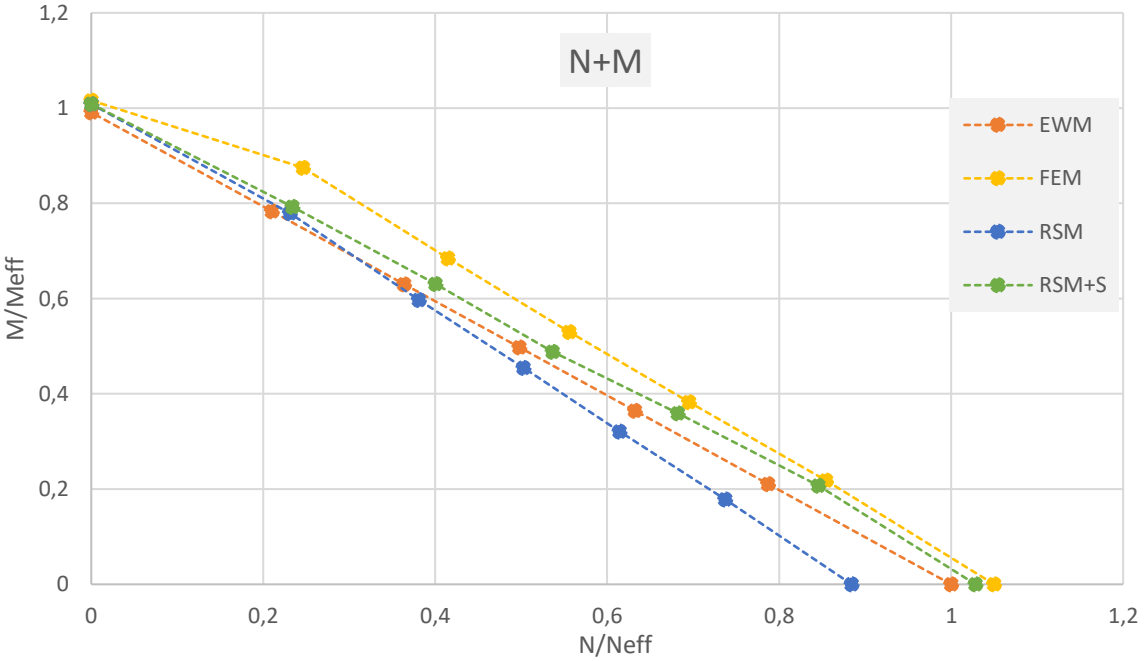

Figure 6.13: Comparison of the interaction graphic of N-M between the 3 methods (RSM, RSM+S and EWM) and the FEM results

The RSM+S presents the N-M interaction surface closest to those obtained through the numerical models (FEM). Both the EWM and RSM+S produce an approximate linear form when the stiffener is located at mid height, however, the N and M resistances obtained by the EWM are more conservative.

The resistance benefits of considering the stress shedding are higher for smaller the θ_1, that is, the smaller the bending moment is. This is observed in Figure 6.14, where values of k are increasing, thus decreasing the allowed maximum redistribution. In general, it can be concluded that the RSM+S provides very reliable results for the slender HSS plate girders under study.

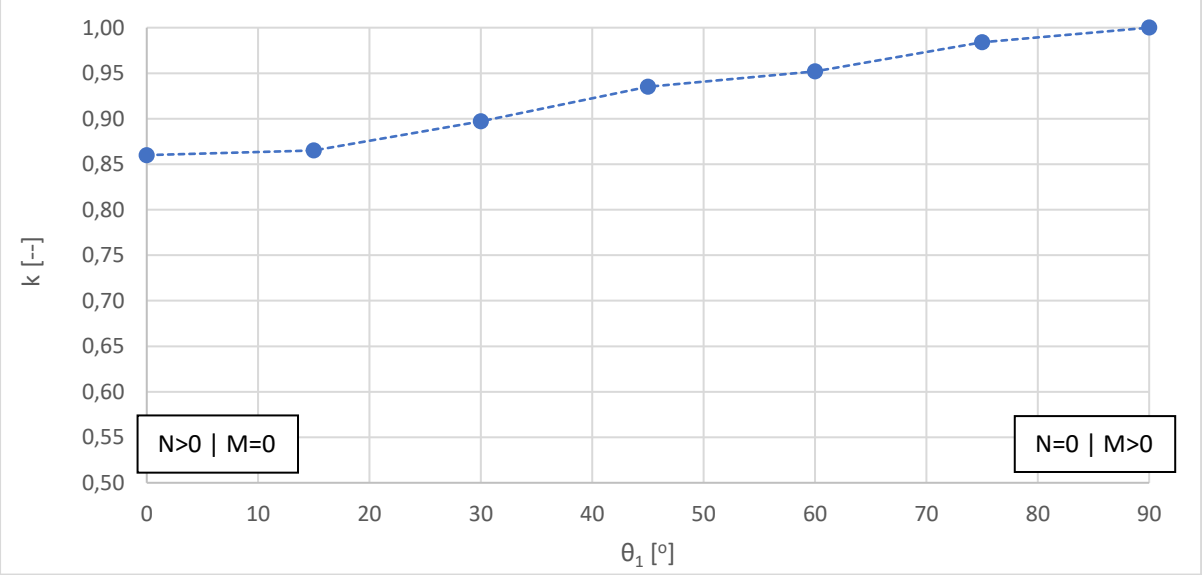

Figure 6.14: Values of k as a function of θ_1

7. Conclusions and Further Research Works

7.1. Main Conclusions

In the initial phase of the study of S690 stander steel plates with one longitudinal stiffener, it was discussed in Chapter 4 that the three panel FE models should be adopted with the applied loads at the edge of the lateral panels to minimize the effect on the middle one that is being analysed. It was also studied which geometric equivalent imperfection attained the more precise ultimate resistances for the case studies. It was concluded that IMP1, based on the first buckling modes is the most appropriate. Thus, the shape of the equivalent imperfection based on the first buckling N, M, V modes was adopted in the study, but it was necessary to combine these modes to analyse the combined N-M-V loadings.

In Chapter 5 it was concluded that the standard calculation methodology does not consider the stress redistribution that occurs on the web with a longitudinal stiffener when the plate is subjected to bending moments, something that is noticeable in the high results of Figure 5.1 b), which correspond to a great reserve of resistance of the standard formulas for this specific case, being increasingly conservative as the longitudinal stiffener is moved up to the compressed part of the web. Through the results obtained when the plate girder is subjected to pure forces (N, M and V separately), it was concluded that the best option would be to keep the stiffener at mid height of the web for the compression or shear loadings, while if the plate girder is subjected to bending moment only, the higher the stiffener is, the better. For the combination of N-M and M-V loadings, it was concluded the stiffener in the middle of the web turns out to be the best commitment.

The comparative analysis and discussion of the ultimate resistances to the N-M-V interaction obtained using the interaction formulas proposed by Biscaya [12, 13, 15] proved they are well calibrated for high strength steel S690 plate girders with various positions of the longitudinal stiffener.

In Chapter 6, a more detailed study of the application of the RSM was performed, with the possibility of having some stress shedding from the web to the flanges. It was found that when no shedding is assumed, the RSM gives, in general, for plate girders without flanges and submitted to N, M and V separately, higher resistances than those obtained with the EWM. This is mainly since the buckling critical stresses obtained using the EBP are higher than the ones obtained by the approximate formulations given in the prEN 1993-1-5 - Annex A. When adding the flanges, the results reverse since the RSM neglects the possibility of the flanges receiving some part of the normal stresses applied at the webs. Therefore, this method provides for a general plate girder, with a longitudinal stiffener at mid high of the web, lower resistances than the ones obtained by the EWM. Regarding the N-M-V interaction study, as the RSM has a quadratic shape, it ends up providing results against safety specially for N-V high loadings applied to slender plates.

Finally, using stress shedding RSM + S (Chapter 6.3) as proposed by Biscaya, it was concluded that this new proposal provides very consistent results, being the closest ones to the ultimate resistances obtained by the numerical models.

7.2. Further Research Works

During the execution of the present work, several aspects were identified, that deserve further research. Some of them are listed in the sequence:

- Evaluation of the differences in the resistances obtained using the equivalent geometric imperfections and the real geometric imperfections with residual stresses, in order to confirm that the use of the former is always a conservative an adjusted assumption.
- Analysis of plate girders with asymmetric flanges subjected to the interaction of N-M-V stresses according to the new proposal by Biscaya.
- Obtain an N-M-V interaction expression that is applicable to cases where one longitudinal stiffener is located in the tensioned or compressed diagonal.
- Development of an expression or graphic figure that can provide the value of k as function of the web slenderness and ratio between the area of the flanges and the web.
- Further extend the application of the RSM+S method to plate girders with other geometries and submitted to combined loads of bending moment with normal and shear forces.

References

[1] J. O. Pedro; A. J. Reis – Composite cable-stayed bridges: state of the art, Proceedings of the ICE - Bridge Engineering, Vol. 169 (2016), Issue 1, pp. 13-38, doi: 10.1680/bren.14.00005

[2] J. O. Pedro; A. Reis – Nonlinear analysis of composite steel-concrete cable-stayed bridges, Engineering Structures 32 (9), Sep. 2010, pp. 2702-2716, doi: 10.1016/j.engstruct.2010.04.041

[3] A. Biscaya; J. O. Pedro; U. Kuhlmann – Strength of transversally stiffened I-girders under combined shear and compression, Journal of Construction Steel Research 178 (2021), doi: 10.1016/j.jcsr.2020.106500

[4] J. O. Pedro; A. Reis; C. Baptista – High strength steel (HSS) S690 in highway bridges: General guidelines for design – Stahlbau vol. 87 (2018), Issue 6, pp. 555-564, doi: 10.1002/stab.2018106

[5] EN 1993-1-5 – *Eurocode 3 – Design of Steel Structures* – Part 1-5: Plated Structural elements, CEN, 2006

[6] F. Sinur – Behaviour of longitudinally stiffened plate girders subjected to bending-shear interaction, University of Ljubljana, PhD Thesis, 2011

[7] F. Sinur; D. Beg – Moment-shear interaction of stiffened plate girders Numerical study and reliability analysis, J. Constr. Steel Res. 88, pags. 231-243, 2013

[8] B. Jáger; B. Kövesdi; L. Dunai – I-girders with unstiffened slender webs subjected by bending and shear interaction, J. Constr. Steel Res. 131, 2017

[9] B. Jáger; B. Kövesdi; L. Dunai – Numerical investigations on bending and shear buckling interaction of I-Girders with slender web, Thin-Walled Structures, 143, 2018

[10] B. Jáger; B. Kövesdi; L. Dunai – Bending and shear buckling interaction behaviour of I-girders with longitudinally stiffened webs, J. Constr. Steel Res. 145, 2018

[11] prEN 1993-1-5 – Eurocode 3 – Design of steel structures – Part 1-5: Plated structural elements, CEN, 2021

[12] A. Biscaya – Buckling resistance of steel plated girders considering M-V interaction with high compression forces, PhD Thesis, Univ. de Lisboa, IST, 2021

[13] A. Biscaya, H. Afonso, J. O. Pedro – New proposal for the N-M-V design interaction of steel plate girders Application to S690 high-strength steel, Congresso CMM, 2021

[14] H. Afonso – Dimensionamento de Vigas de Secção Soldada com Aço S690 Sujeitas a Esforços Combinados de Flexão, Corte e Compressão, MSc Dissertation, Univ. de Lisboa, IST, 2021

[15] Pedro Martins Mendes, José J. Oliveira Pedro – Dimensionamento de Estruturas de Edifícios e Estruturas Especiais – Vol. 2. Ed. IST PRESS, Maio de 2020 (576 pags). ISBN: 9789898481740

[16] Yuan, H. X., Chen, X. W., Theofanous, M., Cao, T. Y., Du, X. X. (2019), "Shear behaviour and design of diagonally stiffened stainless-steel plate girders", Journal of Constructional Steel Research 153, pp. 588-602

[17] J. Martins, H. Cardoso – Comportamento crítico de painéis de alma reforçados diagonalmente, Congresso CMM, 2021

[18] EN 1993-1-1 – *Eurocode 3 – Design of Steel Structures* – Parte 1-1: Plated Structural elements, CEN, 2006.

[19] B. Johansson, R. Maquoi, G. Sedlacek, C. Müller, D. Beg – "Commentary and worked examples to EN 1993-1-5 'Plated Structural Elements', ECCS, 2007

[20] D. Beg, U. Kuhlmann, L. Davaine, B. Braun – Design of Plated Structures, ECCS Eurocode Design Manuals, Ernst & Sohn, 2010

[21] T. von Karman; E. E. Sechler; L. H. Donnell – *"The Strength of Thin Plates in Compression", Transactions of the American Society of Mechanical Engineers* (ASME), vol. 54, p.53, 1932.

[22] A. Biscaya; J. O. Pedro; U. Kuhlmann – Experimental behaviour of longitudinally stiffened steel plate girders under combined bending, shear and compression – Engineering Structures 238 (2021) 112139, doi: org/10.1016/j.engstruct.2021. 112139

[23] J. Scheer e H. Nölke, "Neuer Vorschlag zum Nachweis der Beulsicherheit von Platten unter mehreren Randspannungen," *Festschrift G. Valtinat,* pp. 261–274, 2001.

[24] J. Scheer e H. Nölke, "Zum Nachweis der Beulsicherheit von Platten bei gleichzeitiger Wirkung mehrerer Randspannungen," *Stahlbau,* vol. 70, nº 9, p. 718–729, 2001

[25] EBPlate, *"Elastic Buckling of Plates"*, Software Developed by CTICM in the Frame of the ComBri Project, RFCS Contract n RFS-CR-03018, 2006.

[26] SIMULIA, Abaqus Scripting User´s Manual. Dassault Systems, 2011

[27] Matlab, Matlab R2018. MathWorks, 2018

[28] B. G. Falzon; M. H. Aliabadi – *BUCKLING AND POSTBUCKLING STRUCTURES, Experimental, Analytical and Numerical Studies*, Computational and Experimental Methods in Structures – vol. 1, Imperial College Press, London, 2008.

[29] P. Y. Wang; P. M. Masungi; M. E.M. Garlock; S. E. Quiel - *Postbuckling mechanics in slender steel plates under pure shear: A focus on boundary conditions and load path,* Thin-Walled Structures, 108448, 2021

[30] prEN 1993-1-14 – Eurocode 3, "Design of Steel Structures – Part 1-14: Design assisted by finite element analysis," no. August, 2020.

[31] S. Piculin – *STABILITY OF STIFFENED CURVED STEEL PLATES IN BRIDGE GIRDERS*, PhD Thesis, Univerzav Ljubljani, 2020